MICROELECTRODE ARRAYS FOR NEURONAL RECORDINGS:
DEVELOPING NOVEL TECHNOLOGY AND APPLICATIONS

by

Hamid Charkhkar
A Dissertation
Submitted to the
Graduate Faculty
of
George Mason University
In Partial fulfillment of
The Requirements for the Degree
of
Doctor of Philosophy
Electrical and Computer Engineering

Committee:

_____   Dr. Joseph Pancrazio, Dissertation Director

_____   Dr. Nathalia Peixoto, Committee Member

_____   Dr. Qiliang Li, Committee Member

_____   Dr. Parag Chitnis, Committee Member

_____   Dr. Monson Hayes, Department Chair

_____   Dr. Kenneth Ball, Dean, The Volgenau School
                                          of Engineering

Date: _____   Summer Semester 2015
                                    George Mason University
                                    Fairfax, VA

Microelectrode Arrays for Neuronal Recordings: Developing Novel Technology and
Applications

A dissertation submitted in partial fulfillment of the requirements for the degree of
Doctor of Philosophy at George Mason University

By

Hamid Charkhkar
Bachelor of Science
Ferdowsi University of Mashhad, 2005

Director: Dr. Joseph Pancrazio, Professor
Department of Electrical and Computer Engineering

Summer Semester 2015
George Mason University
Fairfax, VA

Dedication

I dedicate this dissertation to my wife, Fatemeh, for being there for me during my entire graduate studies. I also dedicate this dissertation to my parents and my sister, Farideh, for their unconditional love and support throughout my life.

Acknowledgments

My most sincere gratitude goes to my advisor, Dr. Joseph J. Pancrazio, who trusted my abilities and provided invaluable help and guidance during my graduate studies. Not only he has been my mentor in my graduate studies, but also he generously exposed me to new areas and directions in my research, and has offered me invaluable advice to refine my professional development. I feel very fortunate to have had the opportunity to do my research under his guidance.

My sincere thanks also go to the Dr. Nathalia Peixoto who introduced me to the field of Neuroengineering and effortlessly supported me throughout my PhD studies. I am thankful to her for shaping my prospective toward my future goals and showing me how to become a life-time learner.

I would also like to thank my friends and colleagues in Neural Engineering Lab at George Mason University who have helped me completing my research and provided me with their constructive inputs to improve this work.

Table of Contents

v

List of Tables

List of Figures

xiii

xv

Abstract

MICROELECTRODE ARRAYS FOR NEURONAL RECORDINGS: DEVELOPING NOVEL TECHNOLOGY AND APPLICATIONS

Hamid Charkhkar, PhD

George Mason University, 2015

Dissertation Director: Dr. Joseph Pancrazio

Over the last few decades, there has been a large growth in developing the technology for use in brain sciences. The advancement in such technology has found applications in neuroscience research as well as emergence of novel diagnostic and therapeutic devices for neurological diseases. The majority of these techniques relies on monitoring or modulating the bioelectric activity of the excitable brain cells, neurons. To record the bioelectrical activity of network of neurons, microelectrode arrays (MEAs) patterned and fabricated by photolithography have been widely utilized. Despite the extensive use of MEAs for neural applications, major constraints have limited the utility of the MEAs. The extracellular potentials detected by MEAs are typically in the range of 40 to 500 microvolts and the signal magnitude decreases proportionally to the inverse of the distance between the neuronal source and the electrode. To achieve high spatial resolution and selective recordings in the brain, designing microscale MEAs seems necessary. However, with the reduction in the electrode size, the impedance increases for the conventional metal electrodes resulting in high thermal noise and potentially lower signal-to-noise ratios (SNRs). For *in vitro* applications, compared to disposable plastic chambers and cultured dishes, the MEAs are typically reused in experiments since they are expensive.

In this thesis, we present new techniques to overcome some of the challenges with the current MEA technology to 1) make MEAs more suitable for large-scale cell-based testing experiments and 2) establish a stable interface for *in vivo* chronic recordings. Moreover, we demonstrate the utility of the *in vitro* MEA-based approach as an emergent platform for new applications in brain research such as assessing the functional toxicity of novel material for brain implants and determining the response of neuronal populations to a biomarker of Alzheimers disease, amyloid beta ($A\beta$).

Chapter 1: Introduction

Over the last few decades, there has been a large growth in developing the technology for use in brain sciences. The advancement in such technology has found applications in neuroscience research as well as emergence of diagnostic and therapeutic devices for neurological diseases. Electroencephalogram (EEG), cochlear implants, and deep-brain stimulation are among the most known examples. The majority of such techniques relies on monitoring or modulating the bioelectric activity of the brain cells, neurons.

Neurons are the excitable cells in our nervous system that communicate with each other through all-or-nothing bioelectric potentials known as action potentials. The action potentials generated by neurons are small signals (~ 100 mV$_{p-p}$) with short duration in time (~ 1 ms). The membrane potential transient behavior observed with action potentials is due to voltage and time dependent changes in membrane conductances. Traditionally, recordings of action potentials from single cells have been demonstrated for both *in vivo* and *in vitro* experimental paradigms. These methods include the use of tungsten or stainless-steel wires for *in vivo* applications [1, 2] or pipette electrodes in patch clamp, a laboratory technique that allows measuring the electrical activity of single ion channels [3]. However, the brain consists of networks of neurons, and therefore, there is value in monitoring the electrophysiological activity of population of neurons rather than relying on only single-cell measurements. To achieve this goal, arrays of microelectrodes patterned and fabricated by photolithography have been widely utilized and shown to be suitable for recording neuronal network activity [4].

Microelectrode arrays (MEAs) have been used to record extracellular action potentials from network of neurons *in vitro* for applications in toxicology and biosensing [5–7] and *in vivo* from brain regions associated with movement control or planning [8–10].

1

Despite the extensive use of MEAs for neural applications, there exists major limitations for these devices. In general, the extracellular potentials detected by MEAs are typically in the range of 10 to 500 microvolts. The signal magnitude decreases proportionally to the inverse of the distance between the neuronal source and the electrode. It is beneficial to design low-impedance MEAs that allow effective coupling between neurons and the electrodes and consequently maximizing the signal-to-noise ratio (SNR) in the recordings. To achieve high spatial resolution and selective recordings in the brain, designing microscale MEAs is important. However, with the reduction in the electrode size, the impedance increases for the conventional metal electrodes resulting in high thermal noise and potentially lower SNRs [11].

For *in vitro* applications, compared to disposable plastic chambers and cultured dishes, the MEAs are typically reused in experiments since they are expensive. As such, utilizing the MEA platform for large scale screening applications has remained limited.

In this thesis, we present new techniques to overcome the challenges mentioned above to 1) make MEAs more suitable for large-scale cell-based testing applications and 2) establish a stable interface for *in vivo* chronic recordings. Moreover, we demonstrate the utility of the *in vitro* MEA-based approach as an emergent platform to address some of the challenges in brain research, namely 1) assessing the functional toxicity of novel material for brain implants and 2) determining the response of neuronal populations to a biomarker of Alzheimers disease, amyloid beta ($A\beta$).

In chapter 2, we report the design and demonstration of a low-cost novel *in vitro* MEA using conventional liquid crystal display manufacturing techniques. The resulting MEA is flexible, conducive for neuronal culture, and capable of monitoring extracellular potentials at a SNR comparable to standard commercially available MEAs. The design layout is consistent with results from finite-element modeling. Electrochemical impedance and input referred noise have been measured for the fabricated MEA. Finally, it is demonstrated that spike activity of the cultured cortical neurons on the MEA is sensitive to pharmacological blocker tetrodotoxin (TTX), indicating that cells cultured on these substrates not only

exhibit consistent neural activity, but also show consistent pharmacological responsiveness.

In chapter 3, we show that neuronal cultures on MEAs could be utilized as a functional assay to assess the neurotoxicity of amyloid-β 1-42 ($A\beta_{42}$), a biomolecule implicated in the Alzheimers disease (AD). In this approach, neurons harvested from embryonic mice are seeded on the substrate-integrated microelectrode arrays. The cultured neurons form a spontaneously active network, and the spiking activity as a functional endpoint could be detected via the MEA. $A\beta_{42}$ oligomer, but not monomer, significantly reduced network spike rate. In addition, we demonstrate that the ionotropic glutamate receptors, NMDA and AMPA/kainate, play a role in the effects of $A\beta_{42}$ on neuronal activity *in vitro*. To examine the utility of the MEA-based assay for AD drug discovery, we test two model therapeutics for AD, methylene blue (MB) and memantine. Our results show an almost full recovery in the activity within 24 hours after administration of $A\beta_{42}$ in the cultures pre-treated with either MB or memantine. Our findings suggest that cultured neuronal networks may be a useful platform in screening potential therapeutics for $A\beta$ induced changes in neurological function.

In chapter 4, we first compare the performance of two computational methods, cross correlation and transfer entropy, in detecting the connectivity in a modeled network. We, then, investigate the changes in the functional connectivity in neuronal networks *in vitro* in response to $A\beta_{42}$. Two representative networks that were either treated with $A\beta_{42}$ or memantine + $A\beta_{42}$ are utilized in the analysis. Our findings indicates that for the network exposed to 5 μM $A\beta_{42}$ the connectivity among the units drastically reduces. On the other hand, the memantine treated cultures show minimal connectivity loss after $A\beta_{42}$ treatment.

In chapter 5, we examine the utility of living neuronal networks as functional assays for *in vitro* material biocompatibility, particularly for materials that comprise implantable neural interfaces. Novel implantable neural interfaces increasingly capitalize on novel materials to achieve microscale coupling with the nervous system. Like any biomedical device, neural interfaces should consist of materials that exhibit biocompatibility in accordance with the international standard ISO10993-5, which describes *in vitro* testing involving fibroblasts

where cytotoxicity serves as the main endpoint. Taking advantage of MEA-based platform, we expose established positive and negative control materials to the neuronal networks in a consistent method with ISO 10993-5 guidance. Exposure to the negative controls, gold and polyethylene, does not significantly change the neuronal activity whereas the positive controls, copper and polyvinyl chloride (PVC), result in reduction of network spike rate. We also compare the functional assay with an established cytotoxicity measure using L929 fibroblast cells. Our findings indicate that neuronal networks exhibit enhanced sensitivity to positive control materials. In addition, we assessed functional neurotoxicity of tungsten, a common microelectrode material, and two conducting polymer formulations that have been used to modify microelectrode properties for *in vivo* recording and stimulation. These data suggest that cultured neuronal networks are a useful platform for evaluating the functional toxicity of materials intended for implantation in the nervous system.

In chapter 6, we examine the effects of conductive polymer coated microelectrodes on the spontaneous activity of cultured neuronal networks. Coating the microelectrodes with conductive polymers has been previously reported to improve extracellular recordings presumably via reduction in microelectrode impedance. To examine the basis of such reports, we modified every other microelectrode of *in vitro* MEAs with either conducting polymer, poly-3,4-ethylenedioxythiophene (PEDOT) conjugated with poly-styrenesulfonate (PSS) or a blend of carbon nanotube (CNT) and PEDOT-PSS. Mouse cortical tissue was dissociated and cultured on the MEAs to form functional neuronal networks. The performance of the modified and unmodified microelectrodes was evaluated by activity measures such as spike rate, spike amplitude, burst duration and burst rate. We observed that the yield, defined as percentage of microelectrodes with neuronal activity, was significantly higher by 55% for modified microelectrodes compared to the unmodified sites. However, the spike rate and burst parameters were similar for modified and unmodified microelectrodes suggesting that neuronal networks were not physiologically altered by presence of PEDOT-PSS or PEDOT-PSS-CNT. Our observations from immunocytochemistry indicate that neuronal cells were more abundant in proximity to modified microelectrodes.

4

In chapter 7, we demonstrate stable long-term recordings *in vivo* using microelectrodes modified with a variant of PEDOT. Although PEDOT have been utilized before for *in vivo* recordings, the long term stability and integrity of such coatings for chronic applications remains unclear. Our group has recently demonstrated that use of the smaller counter ion tetrauoroborate (TFB) during electrodeposition increased the stability of the PEDOT coatings *in vitro* compared to the commonly used counter ion PSS. We selectively modified half of the microelectrodes on Neuronexus single shank probes with PEDOT-TFB while the other half of the microelectrodes were modified with gold as a control. The modified probes were then implanted into the primary motor cortex of rats. Single unit recordings were observed on both PEDOT-TFB and gold control electrodes for more than 12 weeks. Compared to the gold coated microelectrodes, the PEDOT-TFB coated microelectrodes exhibited a significantly lower impedance and higher number of units per microelectrode over time. Our equivalent circuit modeling of the impedance data suggests stability in the polymer-related parameters for the duration of the study. Overall, our findings confirm that the PEDOT-TFB is a chronically stable coating for neuronal recordings.

In the last chapter, chapter 8, we present an overall summary of the thesis and discuss possible future directions.

Chapter 2: Development of a disposable low-cost microelectrode array for cultured neuronal network recording

2.1 Introduction

Cultured neuronal networks have emerged as a powerful means of assessing the effects of putative neuroactive compounds. By allowing cells to form intact networks over planar substrates with integrated microelectrodes, physiologically relevant bioelectrical events corresponding to all-or-nothing spikes can be recorded. Often more than one type of spike can be resolved on a single microelectrode contact such that differences in the form and time course of the spike waveforms can be used to distinguish multiple neurons or units. Measurement of spike rate, burst activity, and correlated activity between units can be used as a quantitative basis for neuropharmacological assays [6,12,13], biosensor-based applications [14,15], or fundamental studies of neuronal network dynamics [16–19].

To reproducibly create arrays of microelectrodes on the order of cellular dimensions, fabrication techniques and materials common to the microelectronics industry have been used. Many prior studies have employed microelectrode arrays utilizing glass as a substrate patterned via photolithography with conductors of indium tin oxide (ITO) and passivated with polydimethylsiloxane [20–22]. In fact, this format developed by the University of North Texas has served as the basis for industrial activities surrounding neurological drug testing [23]. In addition, commercially available microelectrode arrays from Multichannel Systems use glass as a substrate with titanium nitride or ITO as a conductor and silicon nitride as an insulator [24]. Recent developments in MEA technology have involved the production of highly integrated devices which incorporate on-chip electronics through

6

CMOS technology [25,26], allowing unprecedented spatial resolution and monitoring of bio-electrical activity. The cost and complexity of the MEAs have significantly impacted how they are used. MEAs are expensive, fragile, and often composed of materials that are not readily conducive to conventional cell biology laboratory handling and disposal. Unlike the common polystyrene and multi-well dishes that are used once and discarded in cell biology laboratories, MEAs are typically re-used and require special handling. We report the development and demonstration of a novel flexible MEA that is readily manufacturable with liquid crystal display fabrication technologies. Parylene C (poly-chloro-p-xylylene), a biocompatible polymer exploited in implantable devices [27,28] was utilized as the insulator for the MEA. Researchers have previously employed parylene-C for *in vivo* applications to develop parylene-based neuronal probes [29–31] or as a surface coating in microwires and silicon arrays [32,33].

Our MEA design is supported through the use of computational modeling. Using finite element analysis and simulation, we show that the distance between microelectrode array contacts is sufficient to resolve potentials associated with current densities typical of mammalian neurons. Finally, we demonstrate that the substrates can be sterilized via autoclave and are capable of supporting long term neuronal cultures. The resulting networks exhibit extracellular potentials and multi-unit spike activity comparable to commercially available structures.

2.2 Methods

2.2.1 Fabrication and characterization

An array of 64 gold microelectrodes 20 μm in diameter was patterned on the substrate with insulation over the leads with parylene-C (Fig . 2.1A,B). As depicted in Fig. 2.1C, the substrate was a layer of polyethylene napthalate (PEN), a polyester material common in the bottling industry [34], with thickness of 125 μm. The gold electrodes were deposited by e-beam evaporation and patterned using standard photolithography and wet etch. Parylene-C
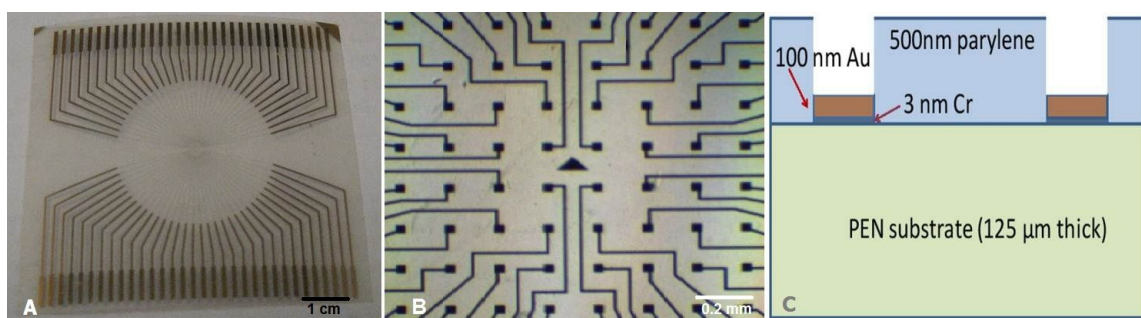
Figure 2.1: (A) The fabricated MEA, (B) Microelectrode area in the center of the MEA, and (C) Cross-section of the MEA. Substrate is polyethylene napthalate (PEN) with thickness of 125 μm; gold electrodes were patterned on top and parylene-C used as an insulator between the electrodes and over the leads.

was deposited by chemical vapor deposition and then exposed to oxygen reactive ion etching. For a lead 10 μm wide and length of approximately 1 cm, the shunt capacitance across the layer of parylene-C layer, with relative permittivity of 3.1 F/m, was estimated to be 270 pF/nm thickness. To minimize effects of shunt capacitance, parylene-C was deposited to a thickness of 500 nm yielding a relatively high shunt impedance of 29 MΩ at 1 KHz.

Electrochemical characterization of the fabricated array, which in this paper we call the PEN array, was performed by electrochemical impedance spectroscopy (EIS) on individual electrodes from a typical array. The measurements were done using a two-electrode setup by a potentiostat/galvanostat (CH 600D, CH Instruments, Texas, US) equipped with an electrochemical analyzer module (CHI Version 9.03, CH Instruments). Measurements were made in the presence of phosphate-buffered saline (PBS) at pH of 7.4 at room temperature by applying a sinusoidal signal with 20 mV amplitude over a range of frequencies from 10 Hz to 100 kHz to characterize the complex impedance of the working electrode and the electrolyte solution.

2.2.2   Cell culture

Similar to preparation of glass MEAs described in [21,22], the PEN MEAs were prepared as follows. Following sterilization by steam autoclave, the microelectrode array was activated

8

by brief exposure to a butane flame to induce a hydrophilic surface conducive to cell adhesion. MEAs were then coated with 50 μg/mL poly-D-lysine (PDL) overnight and washed with sterile water. After drying, the surface was additionally coated with 20 μg/mL laminin for one hour.

Frontal cortex tissue from an embryonic 18 day gestation C57 mouse was received from Brain Bits (Brain Bits, Springfield, IL) in B27/hibernate media. The tissue was dissociated enzymatically with papain/deoxyribonuclease (Worthington Biochemical Corp, Lakewood, NJ) mixture followed by mechanical trituration. Cells were plated on the previously prepared MEAs at a concentration of 500,000 cells per array. All cultures were incubated at 37°C with 10% CO2 and maintained in Dulbeccos minimum essential medium (DMEM, Invitrogen, Carlsbad, CA) supplemented with 5% horse serum (Atlanta Biologicals, Lawrenceville, GA), 5% fetal bovine serum (Invitrogen, Carlsbad, CA), 2% B-27 (Invitrogen, Carlsbad, CA), and 0.2% ascorbic acid for the first week. After one week, glial cells covered the arrays in a single carpet-like layer. At this time, the cultures were transitioned to serum-free media consisting of DMEM supplemented only with B-27 and ascorbic acid. A 50% media exchange occurred twice a week to maintain culture viability.

2.2.3 Experimental setup

MEAs with cultured networks were within a stainless steel perfusion chamber permitting constant temperature at 37°C [6]. Extracellular recordings were conducted in media consisting of DMEM supplemented with 25 mM glucose, 40 mM HEPES, and 26 mM sodium bicarbonate (NaHCO$_3$) adjusted to a pH of 7.4. A total recirculating volume of 40 mL was established and the network was perfused at a constant rate of 1 mL per minute with a peristaltic pump. The data acquisition system was OminPlex (Plexon Inc, Dallas, TX) with 64 channels, sampling frequency of 40 KHz per channel and the bandwidth of 8 KHz. Each of the 64 electrode channels was individually examined for extracellular spikes before being selected for recording and single units were later extracted from each channel by Offline Sorter (Plexon Inc, Dallas, TX). Data were analyzed using Neuroexplorer V.4. (Plexon Inc,

9

Dallas,TX) and a 4-point moving average was applied to the spike rate in order to filter high frequency noise. Baseline activity was established for one hour. To ascertain the biological nature of the recordings, tetrodotoxin (TTX, Sigma-Aldrich, St. Louis, MO) was prepared in 1 μM stock solution and added to the recirculating bath to create a final concentration of 10 nM. The effects of TTX on PEN array networks were examined for 30 minutes, followed by a one hour wash with fresh media that was not re-circulated. '

2.2.4   Modeling

COMSOL version 4.1 was used to develop a 3-D model of the extracellular potentials of a neuron. Due to the symmetry in the MEA layout, only two microelectrodes were used in the model to reduce the computational time and memory resources. For sake of simplicity, a spherical current sink was used to represent a neuronal cell body where a current density value of the sink was set to 450 $\mu A.cm^{-2}$ to simulate the maximum inward sodium (Na) current observed in a typical mammalian neuron with a cell body of 20 μm diameter [35–37]. The extracellular space, shown in Fig. 2.2, was modeled as a large cube ($350 \times 350 \times 200$ μm) and filled with a purely resistive, homogeneous media with conductance of 0.3 S/m [38]. Although the exact chamber used in the extracellular experiment was much greater than the modeled cube, greater values for the cube dimensions had negligible effects on the simulation results. The top surface of the cube was defined to be the ground (V = 0), consistent with the recording chamber architecture and the bottom surface contained gold electrodes embedded in the parylene-C insulator layer. The electrodes had surface area of 930 μm^2 and conductivity of $\sigma = 4.5 \times 10^8$ S/m. The potential of each electrode was allowed to float, consistent with a recording situation where they are connected to a high-input impedance preamplifier. The insulation layer had a conductivity of $\sigma = 1.67 \times 10^{-13}$ S/m, which is a typical value for parylene-C. The underlying physics of the modeling was based on the continuity equation 2.1:

$$\nabla \cdot J = \frac{\partial \rho}{\partial t} \tag{2.1}$$

10
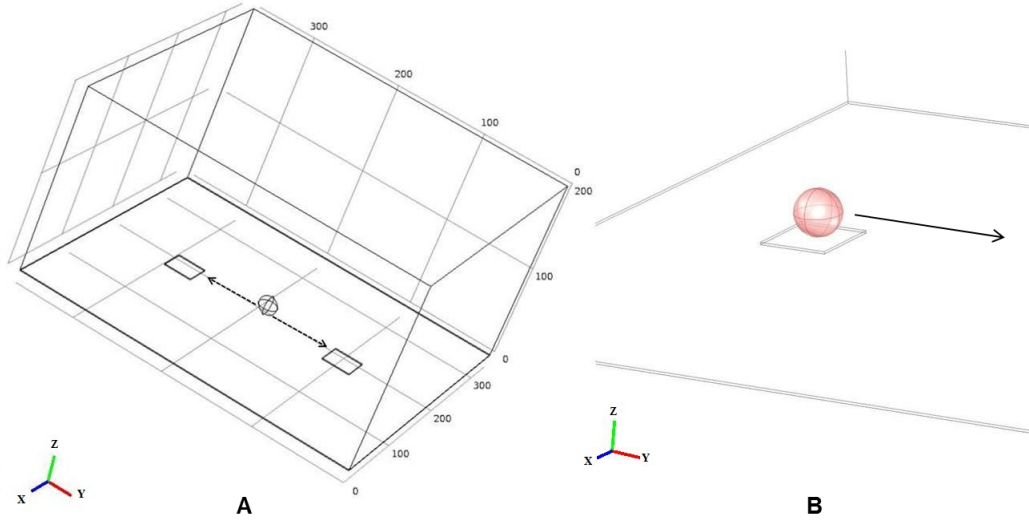
Figure 2.2: (A) The whole geometry including the ball neuron and extracellular space simulated in the finite element model; (B) Magnified view of the modeled neuron over the electrode. Arrows show the directions that the neuron was swept along.

Where $\frac{\partial \rho}{\partial t}$ is the rate of change in charge density (A/m^2) which corresponds to the current density of the model neuron. According to the Ohm's law, the relation between J in equation 2.1 and electrical field E is:

$$J = \sigma E \tag{2.2}$$

Considering the definition of the electrical potential V under static conditions and by substituting equation 2.2 into equation 2.1, we derive the elliptic Poissons equation:

$$\nabla \cdot (\sigma \nabla V) = \frac{\partial \rho}{\partial t} \tag{2.3}$$

The key parameters in equation 2.3 are the conductivity of the materials and current density of the neuron, which were already known. Since under actual recording conditions, the microelectrode sites are connected to a high input impedance amplifier, the double-layer capacitance due to electrode-electrolyte was not considered in the simulation.

11

2.3 Results and discussion

2.3.1 Modeling

To calculate the electrical potential perceived by the electrodes, the spherical current sink was placed 0.5 μm above one of the two electrodes similar to the approach used previously [38]. According to simulation results (Fig. 2.3), by sweeping the current sink along the y-axis from the proximal electrode to a distal electrode, voltage decreases at the proximal electrode while it increases at the distal electrode site. As shown in Fig. 2.4, the maximum extracellular potential from the simulations above the electrode is 173 μV and it reaches 30 μV when the current sink is 90 μm away from each of the electrodes. If the current sink is further moved from the original electrode, the extracellular potential will be detected by the neighboring electrode. By considering a 30 μV potential to be near the threshold for detection, the modeling indicates that a microelectrode pitch of 180 μm is large enough to minimize observation of the same signal source on two adjacent microelectrodes while allowing each source to be detected on at least one nearby microelectrode at a level above noise. Modeling alternative electrode shapes or sizes, ranging from $10^3 \mu m^2$ to $10^4 \mu m^2$, had no appreciable effect on the detected voltage [39].

2.3.2 Impedance measurement

As shown in Fig. 2.5, the measured impedance for representative electrodes paralleled previous observations for metal electrodes in saline solution [40–42]. The magnitude of the impedance (Fig. 2.5A) at 1 KHz was 950 $\pm$ 202 KΩ (mean $\pm$ SD, N = 6) while the phase (Fig. 2.5B) was -80.8 $\pm$ 2.9° which is consistent with previous work with gold microelectrodes [43].

12
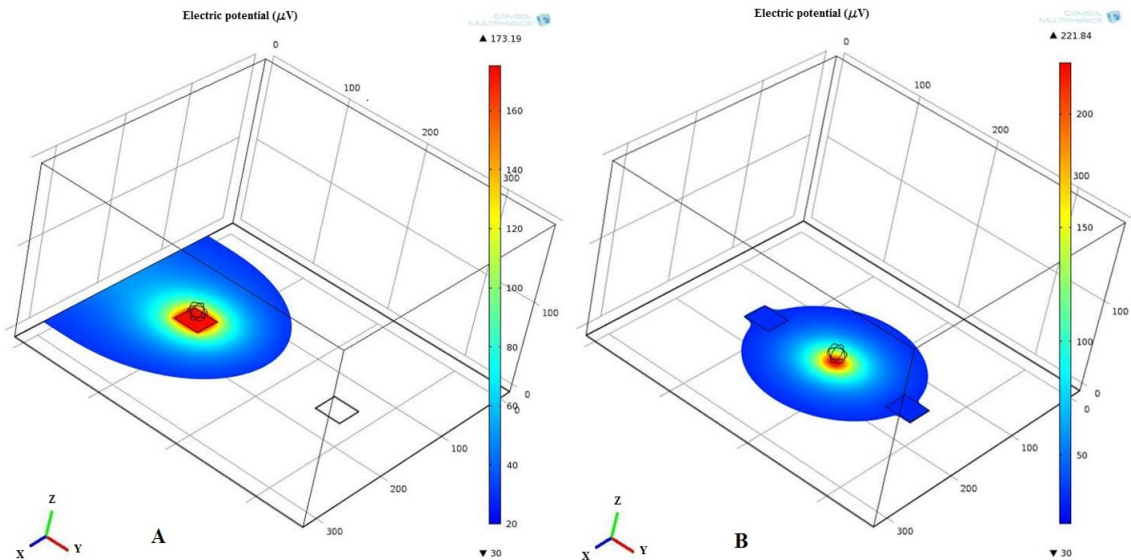
Figure 2.3: Electrical potential distribution on surface of the array obtained using finite-element simulations. (A) The modeled neuron is on top of a microelectrode, (B) the modeled neuron, represented as a spherical current sink, was placed in the middle of two adjacent microelectrodes. Minimum shown data value in both plots is 30 μV.
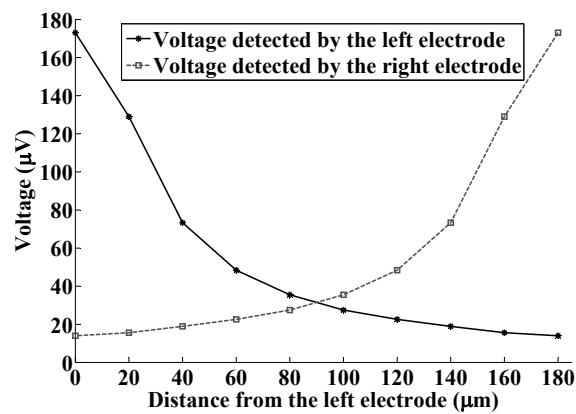
Figure 2.4: Detected voltage by two adjacent electrodes as spherical current sink was swept from one towards the other. By moving the current sink from the original electrode, the detected extracellular potential increases at the neighboring electrode site.

13
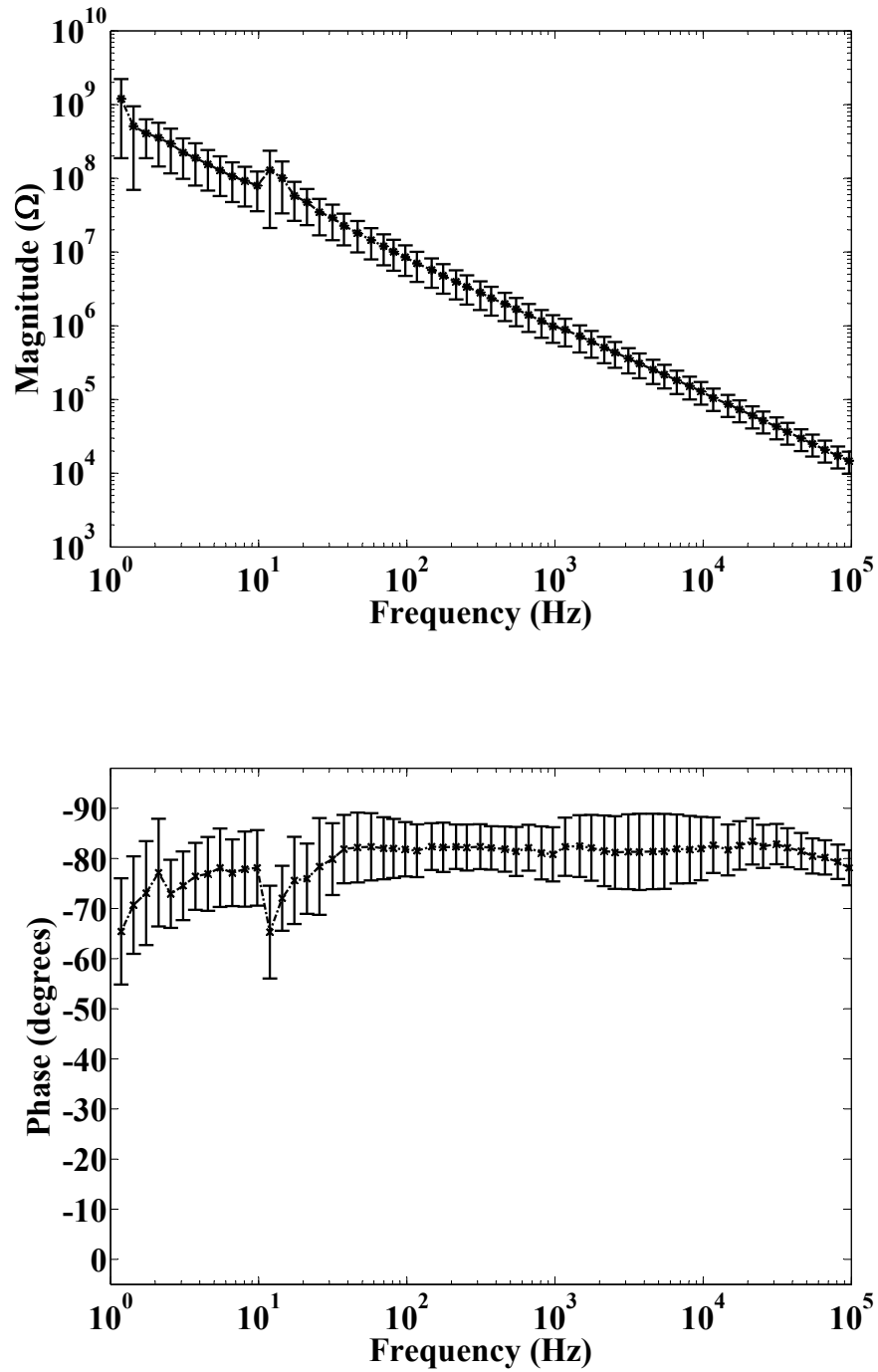
Figure 2.5: Electrochemical impedance spectroscopy on 6 typical electrodes of a PEN array. The magnitude (top) decreased when increasing the frequency and the phase (bottom) was stable around 1 KHz, which is an expected behavior for metallic electrodes in a saline electrolyte. Error bars are ± SD.

14

2.3.3 Neuronal culture

Following surface preparation, the PEN array supported cell body adhesion and neuronal maturation to form active networks. This was denoted by the extension of neuronal processes and a homogenous culture with few cell clumps (Fig. 2.6A), and after 7-10 days *in vitro*, a dense network with an associated cell carpet (Fig. 2.6B).

2.3.4 Neuronal recordings & toxin experiment

Extracellular potentials were observed as early as six days *in vitro*, but pronounced spiking and synchronization, which is typical of cortical networks [19], typically occurred between 25-30 days *in vitro*. Both shape and amplitude of the recorded waveforms were identical to those previously reported for conventional arrays [13]. Fig. 2.7A shows snapshots of the spikes in continuous waveform recorded from a PEN MEA. As illustrated in Fig. 2.7B, networks displayed coordinated bursting activity consistent with prior recordings on MEAs [5]. The measured root-mean-square (RMS) value for the input referred noise at each microelectrode site was 5 ± 1.6 μV (mean $\pm$ SD), which is consistent with the reported value for other MEAs [43]. To verify the physiological basis of the recorded spikes, the conventional sodium channel blocker TTX was administered. After establishing a baseline for 60 min, addition of TTX rapidly and reversibly inhibited spike activity, an observation consistent with prior work [44]. Fig. 2.8 illustrates the changes of mean spike rate after the addition of TTX to a representative frontal cortex culture. The administration of the TTX resulted in $96 \pm 3\%$ (mean $\pm$ SEM) reduction in spike rate, N = 3 experiments comprising 41 single units recordings. Results from network activity on the PEN MEAs parallel previous findings from MEAs [6]. These data suggest that the PEN array can be utilized as a biological assay to detect neurotoxins similarly to the currently available MEAs [6, 12, 13].

15
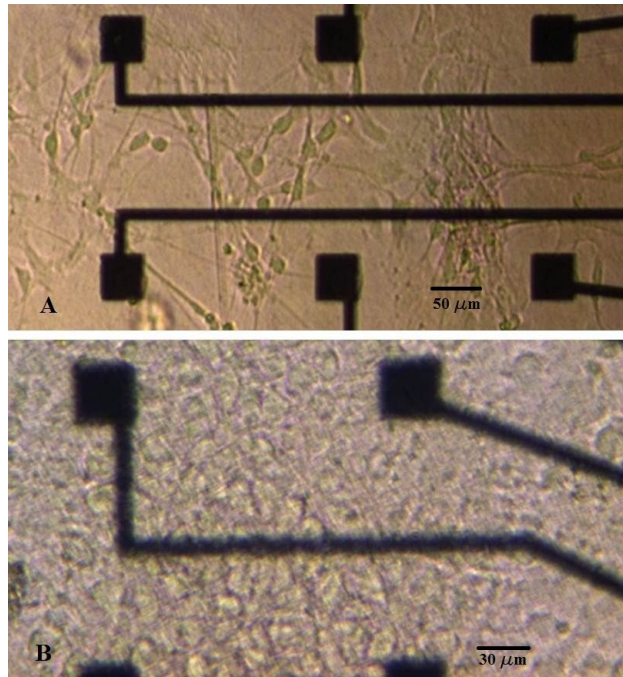
Figure 2.6: Cultured cortical neurons over the MEA. (A) Picture from a 6-day-old network depicting fully extended processes. (B) Picture from a 14-day-old well developed network illustrating a dense cell carpet.
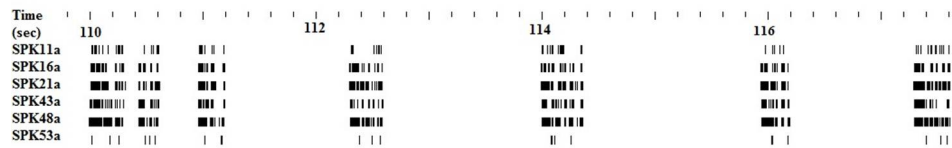
Figure 2.7: (A) Snapshots of individual extracellular potentials recorded using the PEN array; (B) Raster plot for 6 most bursting units. The time stamps of the spikes are represented by thin vertical lines; black bars indicate the close action potentials that merged into each other at this resolution.
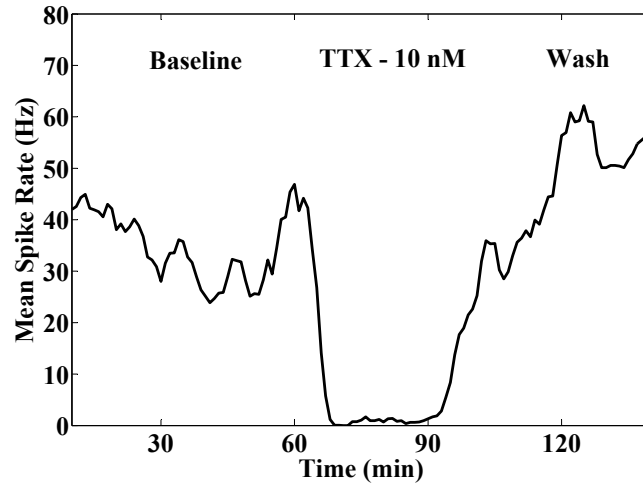
Figure 2.8: Reversible inhibition of mean spike rate in a representative frontal cortex neuronal culture with administration of TTX.

2.3.5 Advantages of PEN arrays over conventional arrays

Although MEAs have been well established in neuronal research [20, 22, 23], the novel PEN array advances this technology. Our design is consistent with modeling of the spike activity and our data demonstrate that the arrays support long-term neuronal culture of electrophysiologically active networks. Many of the currently available MEA architectures are both fragile and expensive. This expense is not only in the initial capital investment, but also in the cost associated with cleaning and re-use. The flexibility of the PEN array permits easy handling and the low cost allows it to become effectively disposable. Since PEN MEA is manufactured using flexible display fabrication technology, the process can be readily scaled and is cost efficient. We estimate that the production cost can be as low as \$0.13 per cm^2 such that a PEN array using our current form factor could be fabricated for as little as \$3.50. It should be noted that the cost can be further reduced by scaling the size of the array to the dimensions of a single well in a 96-well plates, i.e. 0.32 cm^2 surface area, achieving an array cost of \$ 0.05.

18

2.4 Conclusion

We have demonstrated a new design for a plastic, flexible MEA which is readily manufactured and disposable. This novel MEA platform tolerates steam autoclave sterilization and is conducive to neuronal culture. Consistent with previous studies indicating biocompatibility of parylene-C [45, 46], our neuronal networks were still viable after 30 days in culture. Findings from finite-element simulations incorporating material properties and physiologically relevant membrane currents support the design layout of the MEA. Suppression in spike activity after applying TTX confirmed the acquired signal was biological. Although this novel design has several advantages over the conventional glass-based MEAs, the PEN array is optically translucent, which makes it more difficult to visualize neuronal growth on the array surface with an inverted microscope. We are currently exploring alternative substrate materials which can be readily substituted in the manufacturing process to address this limitation.

Citation & Contributions:

This work has been published as:

- **H.Charkhkar**, G.L.Knaack, B.E.Gnade, E.W.Keefer, J.J.Pancrazio. Development and demonstration of a disposable low-cost microelectrode array for cultured neuronal network recording. J. Sens. Actuat. B vol. 161, 2012.

HC and JJP wrote the paper. HC performed the experiments and did the data analysis. GLK performed the primary cell culture and editted the manuscript. BEG, EWK, and JJP designed the experiment.

19

Chapter 3: Amyloid beta modulation of neuronal network activity *In Vitro*

3.1 Introduction

Alzheimers disease (AD) is a neurodegenerative disorder in which the loss of synapses and neuronal apoptosis in cortex and hippocampus lead to behavioral deficits such as memory deficits and cognitive impairment [47]. Amyloid plaques which consist of aggregated fibrillar amyloid beta (Aβ) peptides are considered a pathological marker for AD [48]. Aβ peptides are produced by cleavage of amyloid precursor protein (APP) generating peptides of lengths ranging from 36 to 43 amino acids [49]. The major protein constituents of AD plaques are peptides of 40 and 42 amino acids in length or Aβ_{40} and Aβ_{42}, respectively [50]. The longer peptide, Aβ_{42}, has a high tendency to aggregate and it readily oligomerizes to form soluble dimers, trimers, and higher order oligomers [51, 52]. The oligomers then aggregate further and form Aβ fibrils which constitute the amyloid plaques. However, prior work suggests that the most neurotoxic forms of Aβ are not the senile plaques or fibrillar Aβ but soluble Aβ oligomers [53, 54]. In patients with AD, declines in cognition and memory appear correlated with increases in the fraction of soluble Aβ oligomer suggesting a dynamic equilibrium between multiple forms of the biomolecule [55].

The exact mechanisms of neurotoxic effects of Aβ are not yet clearly understood. Formation of toxic pores in the cell membrane [56], increase in the intracellular oxidative stress [57], cell cycle re-entry [58], disrupting intracellular calcium release [59], and interruption of synaptic transmission [60] are all among the proposed mechanisms. In addition, there have been numerous studies concerning the target receptor for Aβ oligomers. Aβ appears to interact with a wide range of cellular receptors including but not limited to nicotinic

20

cholinergic receptors, glutamatergic receptors, ephrin-type B2 receptors, etc. (for review see [61,62]). With respect to synaptic transmission changes that are correlated with altered cognitive function, prior studies point to a role for N-methyl-D-aspartate (NMDA) receptors as either receptors for $A\beta_{42}$ or as an intermediary of its neuroactive effects [63–66].

To date, various transgenic animal models and mammalian cell assays have been utilized to identify potential therapeutics for AD [67–69]. In particular, *in vitro* assays are advantageous for drug screening applications because they reduce animal usage, provide initial risk assessment, and thus have the potential to accelerate the drug discovery process [70]. To this end, assays ranging from mammalian cells which accumulate $A\beta$ [71] to human induced pluripotent stem (iPS) cells expressing APP [72] have been proposed. However, most of the available *in vitro* preparations do not provide functional endpoints that capture physiologically relevant neuronal activity. In addition, the associated experiments are not designed to assess immediate effects of the oligomer [73]. As such, a network-level functional assay which can provide reliable, fast, and high-content measures is desirable. An approach which has gained attention and interest as a platform for neuropharmacology and neurotoxicity testing involves the use of neuronal networks on MEAs. Murine primary cultures derived from neural tissue form spontaneously active networks on substrate-integrated MEAs. Previous work has demonstrated successful applications of this platform as a biosensor in neuropharmacology [13, 74–76], assessing biocompatibility of novel materials [77] and basic neuroscience [78–80]. This method is well established [22] and has been validated across different laboratories [81]. Compared to single-cell techniques such as patch clamp, the MEA method is non-invasive and allows the concurrent examination of populations of neurons.

In this paper, we demonstrate that $A\beta_{42}$ oligomer, but not monomer, produces significant reductions in neuronal spike activity of cultured neuronal networks without demonstrable cytotoxicity. These network inhibitory effects appear to depend, either directly or indirectly, on modulation of both AMPA and NMDA mediated glutamate receptors. Moreover, two model compounds that have shown clinical promise in treating AD, methylene

21

www.manaraa.com

blue (MB) and memantine, appear to reverse or suppress the inhibitory effects of $A\beta_{42}$ oligomer. These observations suggest that cultured neuronal networks may be a potentially useful platform for screening therapeutic candidates for AD.

3.2   Methods

3.2.1 $A\beta_{42}$ synthesis

$A\beta_{42}$ monomer was acquired commercially from Anaspec (Fremont, CA). Stable oligomer was produced by a process described in [82] that has been optimized for maximal stability [83]. In brief, $A\beta_{42}$ monomer was first dissolved in DMSO (1.0 mg/44 μL), and then sonicated for 5 min. Phosphate buffered saline (PBS) and anionic surfactant sodium dodecyl sulfate (SDS) were added to the solution to achieve $A\beta_{42}$ concentration of 100 μM. After incubation at 37°C for 24 hours, samples were centrifuged to remove any fibrils that had formed. Following dialysis into a stabilizing buffer (10 mM sodium phosphate, pH 7.4, 300 mM sucrose, 1.9% glycine), samples were centrifuged for 10 min and subsequently diluted in the buffer to 100 μM (based on $A\beta_{42}$ monomer molecular weight), and lyophilized. Lyophilized oligomer samples have been shown to be stable for at least one year when stored at 4°C. Before use, lyophilized oligomer samples were reconstituted in deionized water. For monomeric experiments, the monomer powder was reconstituted in PBS with 1.0% NH_4OH as solvent [84].

3.2.2   Microelectrode array preparation

Planar MEAs were purchased from ALA Scientific Instruments (Farmingdale, NY). Each MEA had 60 electrodes with an electrode diameter of 10 - 30 μm and inter-electrode spacing of 200 μm. As described in [77], MEAs were first disinfected by 70% ethanol for 20 minutes under laminar flow in a biohood and then rinsed with sterile de-ionized water. Similar to that described in section 2.2.2, to obtain better cell adhesion, the center regions of the MEAs were coated with 50 μg/mL of PDL in deionized water overnight. After the incubation with

22

PDL, the arrays were then washed with sterile deionized water three times to remove any excess PDL. The arrays were then coated at the center with 20 μg/mL of laminin for at least an hour. Prior to cell seeding, laminin was removed from the MEAs.

3.2.3 Primary neuronal culture

The primary neuronal culture method was similar to that described in [85] and section 2.2.2. The procedure was approved by the Institutional Animal Care and Use Committee of George Mason University (Fairfax, VA). Briefly, timed pregnant, embryonic day 17, CD-1 mice (Charles River, Wilmington, MA) were euthanized with carbon dioxide followed by decapitation. Embryos were extracted in ice cold Leibovitz's L15 (Life Technologies, Grand Island, NY). Upon isolation of the frontal cortex, the tissue was stored up to 24 hours in hibernate media (BrainBits, Springfield, IL) supplemented with 2% B27 (Life Technologies) and 0.5 mM Glutamax (Life Technologies). Later, the hibernate media was removed, the tissue was minced with scalpels and then dissociated through incubation with DNAase and papain (Worthington Biochemical Corp., Lakewood, NJ) for 15 minutes followed by mechanical trituration using disposable graduated pipettes (Fisher Scientific, Pittsburg, PA). After centrifuging at 2500 rpm for 5 minutes, the supernatant was removed and cells were re-suspended in culture medium. The cells were counted using a hemocytometer (Life Technologies) and immediately seeded on MEAs at a density of 100,000 in a 50 μL culture media droplet. The cell culture media and the maintenance of the cultured neurons are already described in 2.2.2.

3.2.4 Extracellular recordings and analysis

All recordings were performed after at least 3 weeks *in vitro* to ensure that the neural networks had reached maturity and consistency in activity. The multichannel extracellular recordings were similar to that described in 2.2.3. The recording time for baseline as well as all the following phases of the experiments was limited to 20 minutes for each phase. During the recording session, the culture temperature was controlled at 37°C.

During extracellular recordings from the neuronal networks, the mean noise level was calculated for each individual channel and a threshold was set at 5 standard deviations from this mean. A spike was then detected if the signal surpassed this threshold. Channels were considered to be active if the spike rate was at least 0.1 Hz. The recorded spikes from each channel were sorted off-line into well-resolved units using Offline Sorter V.3 (Plexon Inc.). The spike sorting method was based on the 2D principle component analysis of spike waveforms followed by scanning K-Means to find and separate clusters. Each unit presumably corresponds to the signal from an individual neuron. Consistent with [86], a burst was defined as an occurrence of a minimum of 4 spikes seperated by no more than 75 ms. The minimum inter-burst interval was set to 100 ms.

3.2.5 Pharmacological exposure

Monomeric and oligomeric forms of $A\beta_{42}$ were administered to the cultures on MEAs to assess the changes in the spontaneous activity of the neuronal networks in response to different species of $A\beta_{42}$. The oligomer was tested in concentration of 200 nM, 1 μM, and 5 μM; whereas the monomer was tested only in high concentrations of 5 and 10 μM. All of the $A\beta_{42}$ solutions were prepared immediately before the experiments. Prior work with $A\beta_{42}$ on neuronal cultures suggested a time-dependent effect [87]. Although our pilot studies did not confirm such an observation, to determine possible alterations in the spiking activity due to $A\beta_{42}$ over time, we recorded the activity immediately, 4 and 24 hours after the $A\beta_{42}$ administration. The NMDA-dependent activity was blocked by administering 10 μM D-2-Amino-5-phosphonopentanoic acid (APV), a general blocker of NMDA receptors [76]. Similarly, the AMPA-dependent activity was blocked by 10 μM of 6-Cyano-7-nitroquinoxaline-2,3-dione (CNQX), an antagonist of AMPA/kainate receptors [13, 76]. To study the effects of model therapeutics, either MB at the concentration of 200 nM or memantine at the concentration of 20 μM were administered to the cultures. Two hours following the therapeutic treatment, the cultures received 5 μM $A\beta_{42}$ oligomer. In all scenarios, the activity of the networks was monitored and recorded prior to and after administration of any reagents.

24

Additional recording was performed 4 and 24 hours post $A\beta_{42}$ exposure. Between recording sessions, cultures were maintained in the cell incubator.

3.2.6 Live/dead assay

To measure the cytotoxicity of $A\beta_{42}$ on cultured cortical neurons, Live/Dead Viability/ Cytotoxicity Assay Kit for mammalian cells (Life Technologies) was utilized. The procedure was similar to that described in [77]. A mixture of 5 μL calcein AM, 20 μL ethidium homodimer, and 10 mL DPBS was prepared for the assay. Neurons were treated either with cell culture medium (negative control), or 70% methanol for 3 hours at 37°C (positive control), or with $A\beta_{42}$ oligomer at concentrations of 200 nM or 5 μM for 24 hours at 37°C. After treatment, media was removed, 150 μL of the assay was added, and incubated at 37°C for 30 min. After incubation, the neurons were imaged at 10x magnification with a fluorescence microscope (Nikon eclipse Ti; Nikon Instruments, Melville, NY). The percentage of live cells was quantified using the ratio of the area occupied by live cells to the area occupied by all cells (live and dead).

3.2.7 Data analysis

The spiking data were normalized to their baseline level activity. In the cases where more than one drug was applied to a culture, the activity was normalized to the pre-$A\beta$ level. All statistical analysis was performed in either MATLAB (Mathworks Inc.) or IBM SPSS Statistics (SPSS Inc.). The comparison of each group to the baseline level was done using one-sample t-test. To compare between group effects, mixed-mode analysis of variance (ANOVA) was utilized. In all case, $P < 0.05$ was considered significant. Data are expressed as mean $\pm$ standard error of the mean (SEM).
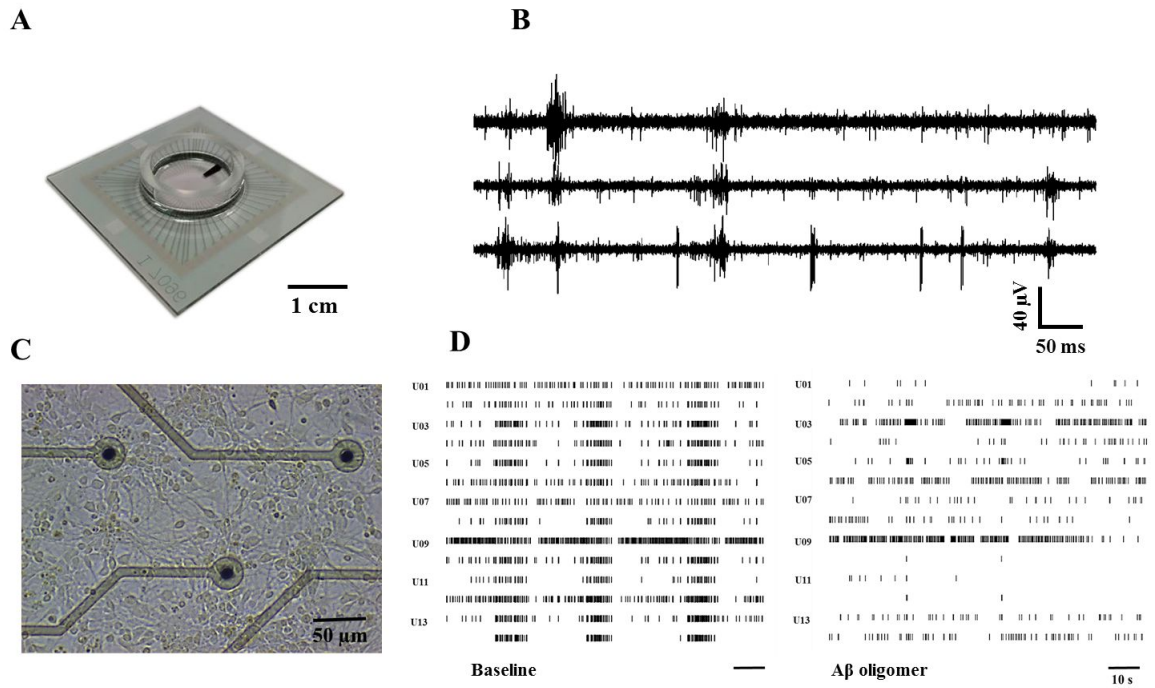
Figure 3.1: Neuronal cultures on microelectrode arrays form spontaneously active networks. (A) 60-electrode planar MEA with inter-electrode distance of 200 μm and electrode diameter of 10-30 μm. (B) Extracellular recordings registered from three electrodes of a MEA with cultured cortical neurons. The recordings consist of different patterns of activity such as tonic firing and synchronous bursting across the channels. (C) Optical image of the population of neurons and glia on a MEA at day 14 *in vitro*. The controlled growth of glia supports the longevity of the cultured neurons. The networks become fully mature and maximally active 3 weeks after seeding. (D) Raster plots of a representative neuronal network from 15 units prior (left) and after (right) the administration of 5 μM Aβ_{42} oligomer. Each row represents the activity of one unit over time. The presence of a spike is shown by a vertical black line.

26

3.3 Results

3.3.1 Extracellular recordings from *in vitro* cortical networks

In total, 67 cultured neuronal networks *in vitro* derived from 10-11 mice were utilized in this study. As shown in Fig. 3.1A-C, cultured neurons on MEAs formed dense networks and became spontaneously active. The extracellular recordings were performed between days 21 32 *in vitro*. The overall percentage of the active electrodes or yield was $61 \pm 5\%$ (mean $\pm$ SEM). Based on [81], any neuronal network with the yield below 25% was not considered sufficiently active for subsequent experiments. In the baseline recordings, the overall spike rate was 3.7 ± 0.3 Hz and the number of bursts per minute was 7.3 ± 0.3, while each burst had on average 11 spikes. All the reported measures were above the acceptance criteria for an active neuronal network [81]. The average spike amplitude in each unit was approximately 69 ± 9 μV peak-to-peak. Consistent with prior work, the cortical networks showed synchronous bursting across a majority of the active channels. The signal-to-noise ratio (SNR) for a unit was defined as the mean peak-to-peak spike amplitude over the root mean square (RMS) value of the noise for the corresponding unit. The overall SNR for the baseline recordings was 11.2 ± 0.2, suggesting the detection of well-resolved units from the neuronal networks on MEAs in this study.

3.3.2 Functional responses to different forms of Aβ_{42}

To compare the effects of Aβ_{42} monomer and oligomer, the neuronal cultures were exposed at the concentration of 5 μM each. A raster plot of extracellular activity from a representative culture before and immediately after administration of 5 μM Aβ_{42} oligomer is shown in Fig. 3.1D. Along with the decrease in the spike rate, it can be seen that other activity features such as synchronous bursting were affected by the oligomer. In most of the experiments, the changes in the burst parameters and spike rate were consistent, so for the rest of this report, we only focus on the spike rate.

As shown in Fig. 3.2, Aβ_{42} monomer failed to inhibit the spiking activity in the cultures

27
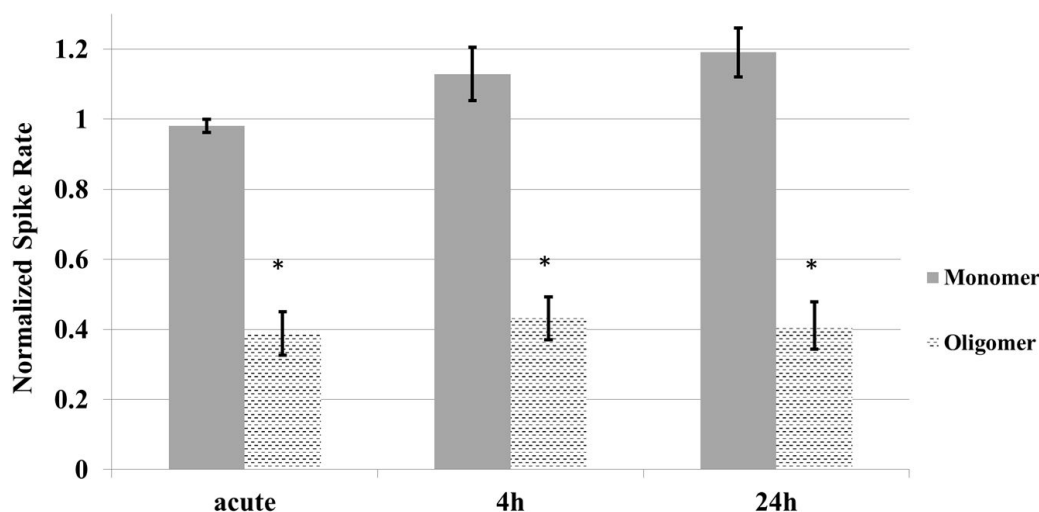
Figure 3.2: Changes in the spike rate for two different forms of Aβ_{42} at 5 μM over 24h. A significant reduction in activity only occurred for Aβ_{42} oligomer. All the network spike rates are normalized to their baseline level activity. N = 7 networks for monomer and N = 6 networks for Aβ_{42} oligomer.

over 24 hours (N = 7 networks). However, in comparison, 5 μM Aβ_{42} oligomer significantly reduced the normalized spike rate by approximately 60% from the baseline and the spike rate remained consistently low after the 24 hours following initial exposure (P < 0.01, N = 6 networks). A pilot experiment was performed with Aβ_{42} monomer at the concentration of 10 μM (N = 2 networks). Similar to 5 μM monomer, no reduction in the spiking activity was observed with the higher concentration of the monomer (data not shown). Exposure to oligomer concentrations at 200 nM (N = 4 networks) and 1 μM (N = 4 networks) failed to alter the spike rate in a statistically significantly manner.

3.3.3 Testing Aβ_{42} oligomer cytotoxicity with live/dead assay

We examined the *in vitro* cytotoxicity induced by exposure to Aβ_{42} oligomer for 24 hours. Fig. 3.3A-C show representative images of the Live/Dead assays performed on a negative control (cell culture media), a culture treated with Aβ_{42} oligomer for 24 hours, and a positive control (methanol). Negative controls showed 89.2 $\pm$ 8.7 % live cells (N = 4). Exposure

28
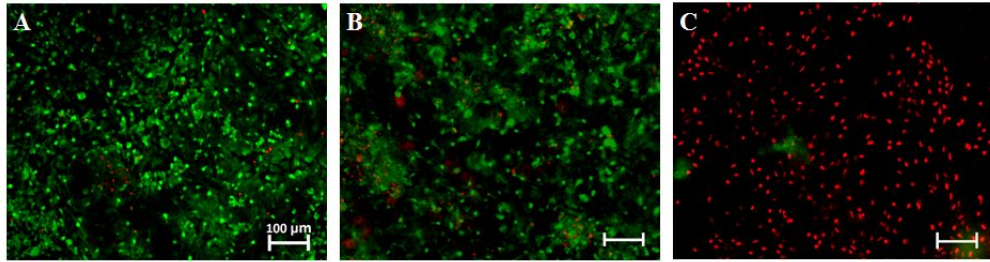
Figure 3.3: Representative fluorescently labeled images of cultured neuronal networks exposed for 24 hours to the negative control (A), 5 μM Aβ_{42} (B), and the positive control (C). The green and red fluorescent labels are indicators of live and dead cells, respectively. The quantified results do not suggest significant differences in the percentage of viable cells for Aβ_{42} treated cultures compared to the negative control.

to 200 nM Aβ_{42} oligomer for 24 hours showed $75.2 \pm 8.1\%$ live cells (N = 4), a level not significantly different from the negative control. Increasing the concentration to 5 μM Aβ_{42} oligomer did not induce any further cytotoxicity. After 24 hours of incubation, cultures exposed to 5 μM Aβ_{42} oligomer showed $73.1 \pm 3.8\%$ (N = 4) live cells. The treatment with the positive control showed substantial apoptosis and resulted in only $8.1 \pm 4.3\%$ live cells (N = 5). Therefore, it is unlikely that the alterations in spike rate are associated with cytotoxic effects of the oligomer.

3.3.4   The effects of Aβ_{42} oligomer on ionotropic glutamate receptors

To study the role of NMDA-mediated neuronal network activity in the effects of Aβ_{42} oligomer, cultures were first treated with 10 μM APV which is a NMDA receptor antagonist that competitively blocks the glutamate binding site of NMDA receptors. As such, the normalized spike and burst rates were reduced 32.3 ± 8.1 % and $28.4 \pm 10.1\%$, respectively (N = 3 networks). Considering the role of NMDA receptors in regulating the spontaneous activity of neuronal cultures, such a reduction was consistent with the previously reported findings [76, 88]. Administration of Aβ_{42} oligomer to the APV-treated cultures resulted in significant reduction in the activity immediately after and 4 hours later, however the spike rate was almost fully recovered to the pre-Aβ_{42} level after 24 hours. As shown in Fig. 3.4,

when compared to pre-Aβ_{42} activity levels, the normalized spike rate in the cultures treated with APV + Aβ_{42} was reduced to 31.2 $\pm$ 8.3 % immediately after Aβ_{42} administration. The normalized spike rate was then increased to 35.1 $\pm$ 5.2 % and 88.4 $\pm$ 14.1% of the baseline after 4 and 24 hours of Aβ_{42} exposure, respectively (N = 3 networks). These data suggest blocking the NMDA receptors does not change the immediate and 4 hour effects of Aβ_{42} oligomer on the activity of the neuronal cultures, however after 24 hours the effects of the oligomer are in part NMDA mediated.

To study the role of AMPA/kainate receptors for the effects of Aβ_{42} oligomer, networks were first exposed to 10 μM CNQX, a competitive antagonist of AMPA/kainate receptors. Compared to the baseline, the normalized spike and burst rates after CNQX treatment were reduced by 25.4 $\pm$ 7.1% and 18.1 $\pm$ 10.3%, respectively (N = 3 networks). The subsequent treatment with 5 μM Aβ_{42} oligomer resulted in significant inhibition of the activity immediately after the oligomer administration. As shown in Fig. 3.4, the normalized spike rate reduced to 65.7 $\pm$ 6.5% immediately after the oligomer treatment and then increased to 118.1 $\pm$ 10.5% and 101.3 $\pm$ 8.2% after 4 and 24 hours, respectively (N = 3 networks). These data suggest that AMPA/kainate receptor mediated transmission has an integral role, either directly or indirectly, in the Aβ_{42} mediated inhibition of neuronal network activity.

Control experiments were performed where either 10 μM APV or 10 μM CNQX (without administration of Aβ) were applied to the cultures and the changes in the activity were monitored over 24 hours. In both cases, no change in the activity was observed over time (data not shown).

3.3.5 Responses to Aβ_{42} in the cultures pre-treated with model therapeutics

The normalized activity in the cultures remained almost unchanged after exposure to 200 nM MB, reaching 94.1 $\pm$ 12.5 % immediately after MB treatment. The administration of Aβ_{42} oligomer in the MB-treated cultures resulted in a significant acute reduction in
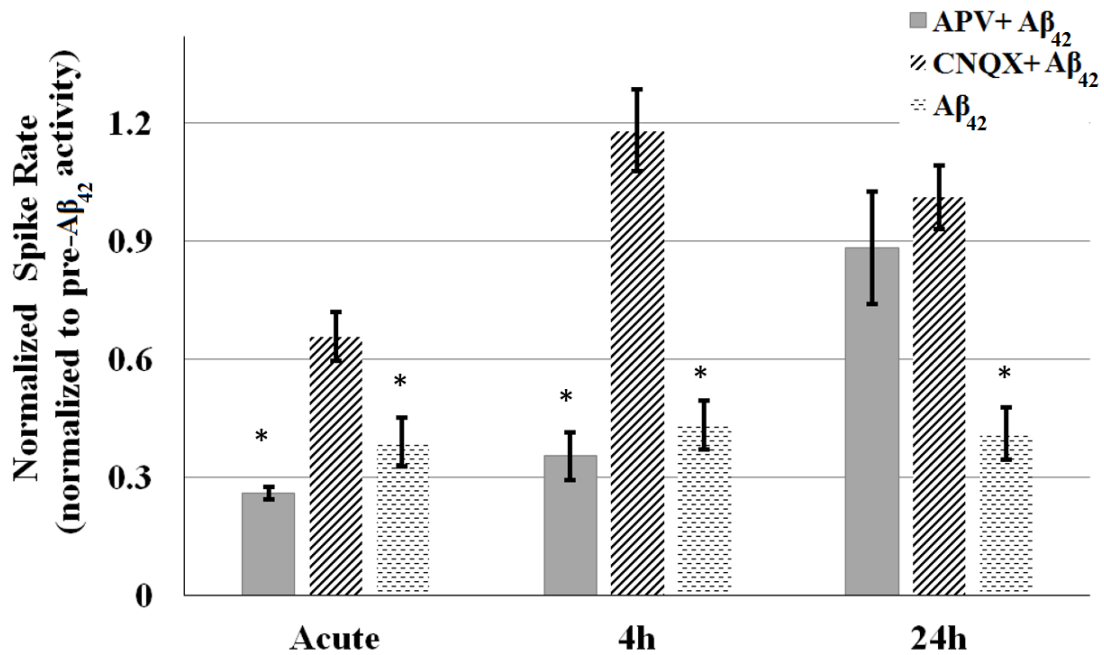
Figure 3.4: The effects of 5 μM Aβ_{42} oligomer on the spike rate of cultures which received APV, antagonist of NMDA receptors; CNQX, antagonist of AMPA/Kainate receptors; or Aβ_{42} only. Administration of Aβ_{42} oligomer to the APV-treated cultures resulted in significant reduction in the activity immediately after and 4 hours later, however the spike rate was almost fully recovered to the pre-Aβ_{42} level after 24 hours. The Aβ_{42} oligomer caused a significant inhibition in the activity in the CNQX-treated cultures only immediately after treatment followed by an almost full recovery in the activity after 4h and 24h. For APV + Aβ_{42} and CNQX + Aβ_{42}, N = 3 networks each. N = 6 for Aβ_{42} oligomer only. $*$ denotes statistically significant differences when compared to the pre- Aβ_{42} level.

31

activity (Fig. 3.5). The normalized spike rate fell to 31.8 ± 4.1 %, well below the pre-Aβ baseline level (P < 0.05, N = 4 networks) and consistent with effects of Aβ_{42} in the absence of MB. However, within 4 hours, the activity level rose to 78.3 ± 16.5 % followed by a full recovery 24 hours later with normalized spike rate at 114.2 ± 16.6 %. This did not appear to be due to a slow excitatory effect of MB. Control experiments were conducted to monitor the activity changes only due to MB over 24 hours. The normalized spike rate remained at 86.3 ± 11.4 % and 85.3 ± 24.1 % after 4 and 24 hours of MB treatment, suggesting MB did not independently cause elevation in the activity levels. Therefore, the recovery in the spike rate with MB suggests the suppression of Aβ effects in the presence of MB.

Application of 20 μM memantine to the cultures caused reduction in the activity by 48.1 ± 2.2 %, an effect consistent with its role as an open-channel antagonist of the NMDA receptor [89, 90]. However, Aβ_{42} oligomer failed to induce any significant inhibition in the memantine-treated cultures over 24 hours. Shown in Fig. 3.5, immediately after Aβ_{42} oligomer administration, the normalized activity was reduced to 57.3 ± 14.2 % and it reached 108.2 ± 15.4% and 106.3 ± 8.3 % after 4 and 24 hours, respectively (N = 4). Similar to MB, control experiments with 20 μM memantine showed a consistent spike rate that persisted at 35% reduction for over 24 hours.

3.4   Discussion

In this work, we show that oligomeric rather than monomeric forms of Aβ_{42} induce electrophysiologic changes to network level activity, without cytotoxicity, and that these effects are reversed by model AD therapeutic agents. Our findings are consistent with prior work demonstrating that the oligomeric form, compared to Aβ_{42} monomer, is the more neuroactive form. Our results suggest that inotropic glutamate receptors, AMPA/kainate and NMDA, are both involved in the effects of Aβ_{42} oligomer. However, it is more likely that the immediate effects of the oligomer on the activity of the networks are mainly AMPA/kainite receptor mediated. Our findings demonstrating a neuronal network modulatory effect of

32

Aβ_{42} oligomer are consistent with prior studies. Kuperstein et al. in [91] showed that 1 μM Aβ_{42} oligomer can rapidly and persistently depress spike activity in cultured hippocampal neuronal networks. Varghese and colleagues [87] reported that hippocampal neuronal networks on MEAs exhibit sensitivity to a multimeric formulation of Aβ_{42} at 20 μM.

Although several studies point to the neuroactive effects of Aβ_{42} oligomer, inconsistent reports exist on the effective concentration of the oligomer ranging from nanomolar to micromolar [92, 93]. Beside the differences in the cell types or experimental design, the structure and order of the oligomer seems to be strongly but not linearly related to its potency [94]. Despite the reports on high toxicity of low-order Aβ such as dimers and tetramers, it is not fully clear how the peptide toxicity would change with the increase in the oligomer order [49, 94, 95]. The synthesized peptides in our work were $\sim$20-mers and reported to have a stable structure [83]. In contrast to the results reported in [87], the highest dose of Aβ_{42} oligomer, 5 μM, in our experiments showed a constant effect over 24 hours which may be indicative of the stability of the oligomer formulation used in our study.

Our observations with monomeric Aβ_{42} do not suggest any inhibitory effects of monomer at 5 μM. This finding is consistent with the prior work pointing to the neurotoxicity of oligomer rather than monomer [96, 97]. In [98], LTP was not disrupted in presence of the Aβ_{42} monomer whereas the oligomer caused inhibition of LTP. In cortical pR5 brain cells, Aβ_{42} oligomer but not monomer reduced the mitochondrial function [60]. However, Görtz et al. in [99] reported that networks, derived from cryopreserved rat cortical neurons, exhibited transient reductions in spike activity with exposure to 1 μM of monomeric Aβ_{42}. Similar results were reported for monomeric Aβ_{42} at concentrations between 1 to 20 μM [100]. Such inconsistency in the potency of the monomer might be due to the fact that the monomer peptide in aqueous solutions contains a mixture of conformations which would aggregate dissimilarly and thus result in different toxicity profiles [48].

The suppression in the effects of Aβ_{42} oligomer occurred with a delay in the cultures pretreated with the NMDA receptor antagonist, APV. This observation is consistent with previous reports that Aβ_{42} oligomer interferes with signaling pathways downstream of NMDA

33
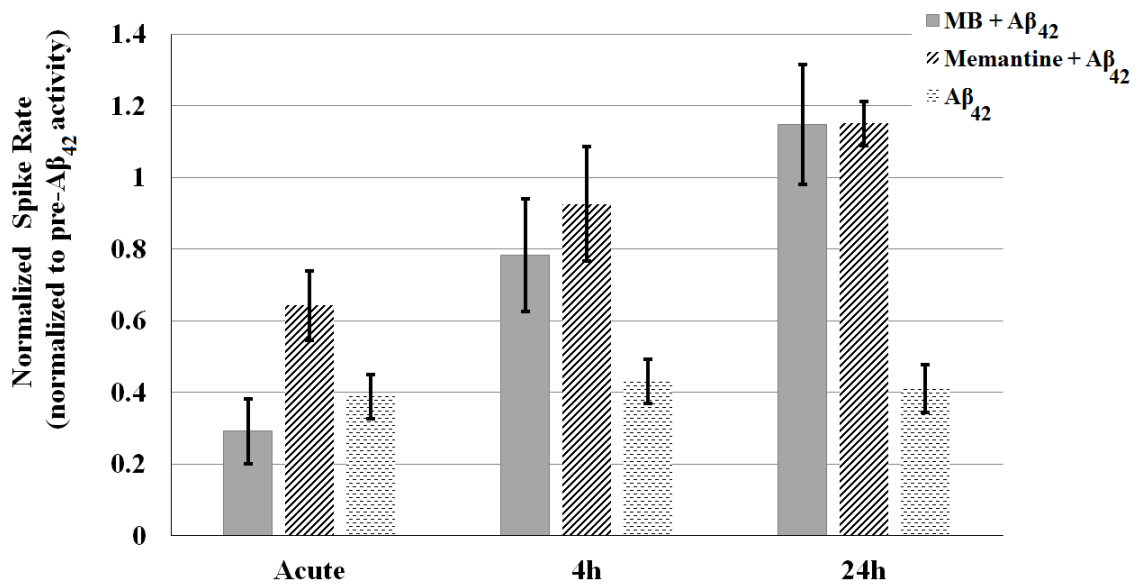
Figure 3.5: The effects of Aβ_{42} oligomer on neuronal activity in cultures treated with either MB or memantine. For both MB and memantine, the activity level shows full recovery to the pre-Aβ_{42} baseline within 4 hours of administration of the Aβ_{42} oligomer. (N = 4 networks for memantine + Aβ_{42} and MB + Aβ_{42}, N = 6 for Aβ_{42}). $*$ denotes statistically significant differences when compared to the pre-Aβ_{42} level.

receptors rather than direct calcium ion flux through the receptors [66, 73]. Additionally, our results are consistent with the previous single-cell studies that Aβ_{42} oligomer has an important role in disrupting AMPA receptor function. Parameshwaran et al. in [101] demonstrated that 1.4 μM Aβ_{42} peptide significantly reduced the AMPA-specific currents in area CA1 of hippocampus. It has also been suggested that the AMPA receptor subunit GluR2 might be a binding site for Aβ_{42} oligomer [47].

We observed a recovery in activity after Aβ_{42} administration for cultures pre-treated with either MB or memantine. MB has been shown to be effective for different medical applications such as treating malaria, urinary tract infections, bipolar disorder, and most recently in improving the cognitive functions of patient with AD [102–104]. Memantine has also been reported to be effective in delaying the progress of AD [67]. An uncompetitive NMDA antagonist, memantine is among the few FDA approved therapeutics for AD [105]. Although, different hypotheses have been suggested as to how memantine might reduce the detrimental effects of Aβ oligomer, the exact mechanism of action for memantine in relation with AD is still unclear [106–108]. Based on our results, the gradual recovery in the activity over time for MB + Aβ cultures suggest MB plays a protective role against Aβ oligomer. Prior work with MB in AD models demonstrate that MB reduces excess reactive oxygen species [109, 110], enhances mitochondrial function [111, 112], and prevents the aggregation of tau protein [113].

The application of memantine prior to Aβ_{42} oligomer resulted in almost full recovery of the activity 4 hours after oligomer administration. This observation is consistent with the notion that memantine sensitive classes of NMDA receptors are a possible target for Aβ_{42} oligomer. Comparing the results of memantine + Aβ_{42} with APV + Aβ_{42}, it can be seen that Aβ_{42} oligomer effects on the activity were further suppressed when cultures were pre-treated with memantine. Such a difference in response to Aβ_{42} oligomer for memantine and APV pre-treated cultures points to a more complicated interaction between the oligomer and NMDA receptors.

35

3.5   Conclusions

In summary, our findings show the suitability of neuronal cultures on MEAs as functional assays for neurotoxicity assessment and drug screening in AD research. In this work, we focused on the effects of $A\beta_{42}$ oligomer on neuronal cultures and showed how two potential therapeutics could reverse the functional effects of the oligomer. The MEA approach could be adapted to achieve more specific *in vitro* models of AD. Recent studies suggest a strong interplay between $A\beta_{42}$ effects and another protein marker associated with AD, tau protein [58,114,115]. The modulatory effect of $A\beta_{42}$ and its dependence on tau could be validated by MEAs using harvested tissue from tau-knockout mice. As such, the MEA-based functional assay provides the potential to advance the development of new therapeutic tools for AD by offering a high-content and adaptable platform.

Citation & Contributions:

This work is under review in the Brain Research as a full-length article:

- **H.Charkhkar**, S.Meyyappan, E.Matveeva, D.G. McHail, N.Peixoto, R.O.Cliff, J.J.Pancrazio. Amyloid beta modulation of neuronal network activity *in vitro*. Brain Res. *Under review*

HC wrote the paper. HC, SM, and DGM performed the experiments. HC analyzed the data and generated the figures. EM and ROC synthesized and provided the oligomer. JJP, HC, and NP designed the study. NP edited the manuscript. JJP revised the manuscript and provided feedback on data visualization and analysis.

Chapter 4: Effects of Aβ_{42} on functional connectivity of *in vitro* neuronal networks

4.1 Introduction

As mentioned in previous chapters, the MEA approach is considered a high-content assay. Recording extracellular spikes from MEAs provides us not only with information on single units, but also allows us to investigate how certain activity patterns emerge in the network and how different neurons within the network interact with each other. In chapter 3, we utilized spike rate as a simple measure to evaluate the effects of Aβ_{42} on cultured neurons. Although measures such as spike and burst rate are informative about the overall effects of Aβ_{42}, they offer little or no insight into the changes in functional connectivity among the neurons that may result from administration of a compound. Such changes in the connectivity are especially important because it has been suggested that Aβ_{42} disrupts the synaptic transmission between neurons and alters the connectivity in different brain regions [116, 117]. As such, assessing the changes in the network connections in the *in vitro* model would help examine the effects of Aβ_{42} on the cultured neurons in more depth.

A common method to investigate the functional connectivity among neurons in a cultured neuronal network is cross correlation (CC) [88, 118, 119]. In CC, the spike train from one neuron is shifted in time and compared against the another neuron's spike train to find the similarities between their spiking activities. However, CC does not identify causal connectivity between two neurons and assumes linear dependency between their firing patterns [120]. In addition, CC shows marginal performance on the data collected from inter-connected neuronal cultures [120]. For example, CC results in a large false positive rate in the networks with high synchronous discharges across many neurons, a typical pattern in *in vitro* cortical networks. Recently, Transfer Entropy (TE), an information-theory

based method, has been shown to be more advantageous over CC to detect functional connectivity of modeled neuronal networks [120,121]. In TE, the firing history of the neurons is utilized to infer the probability of future firing. TE takes into account linear and nonlinear interactions and provides information on causal dependencies between neurons [122].

In this chapter, we first demonstrate the higher performance of TE over CC in detecting the connectivity in a modeled network where the "ground truth" connectivity is known. We, then, investigate the changes in the functional connectivity in neuronal networks *in vitro* in response to $A\beta_{42}$. Two representative networks that were either treated with $A\beta_{42}$ or memantine $+ A\beta_{42}$ were utilized in the analysis. Our findings indicate that for the network exposed to 5 μM $A\beta_{42}$ oligomer the connectivity among the units was drastically reduced. On the other hand, the memantine treated cultures showed minimal connectivity loss after $A\beta_{42}$ oligomer treatment.

4.2   Methods

4.2.1   Cross Correlation

All the spike train recordings were binned into binary strings. The CC between two neurons was defined as:

$$CC_{xy}(\tau) = \begin{cases} \sum\limits_{n=0}^{N-\tau-1} (x_{n+m})(y_n) & \tau \geq 0 \\ CC_{xy}(-\tau) & \tau < 0 \end{cases} \tag{4.1}$$

Where x and y are the spike train recordings from neurons A and B, respectively. τ is the time lag and N is the total number of time bins. Ideally, if neuron A and B, corresponding to spike trains x and y, show exact spiking activity without any delays, their CC will be maximum at $\tau = 0$. To evaluate the connectivity within a network of neurons using this method, the CC function is evaluated for the spike trains of every possible pairs of distinguished units in the neuronal networks recording. As suggested in [120], the maximum

value of the CC function for every two units was considered as their connectivity strength.

4.2.2 Transfer entropy

The TE is defined as follows:

$$TE_{x \to y} = \sum_{y_{t+1}, y_t^n, x_t^m} p(y_{t+1}, y_t^n, x_t^m) \ log \left(\frac{p(y_{t+1} \mid y_t^n, x_t^m)}{p(y_{t+1} \mid y_t^n)} \right) \tag{4.2}$$

Where, similar to 4.2.1, x and y are the spike train recordings from neurons A and B, respectively. $x_t^m = (x_t, x_{t-1}, ..., x_{t-m+1})$ and $y_t^n = (y_t, y_{t-1}, ..., y_{t-m+1})$, while m and n are the order of the past time bins in the x and y spike trains, respectively. $p(y_{t+1} \mid y_t^n, x_t^m)$ denotes the probability of a future spike event conditioned to the past n and m observations of the spike trains y and x, respectively. If neuron A and B are independent from each other, x_t^m has not influence on y_{t+1}, resulting in $p(y_{t+1} \mid y_t^n, x_t^m) = p(y_{t+1} \mid y_t^n)$ which yields to small $TE_{x \to y}$. On the contrary, large $TE_{x \to y}$ values indicates the influence of x on y. Consistent with [120, 123], we select $m = n = 1$ to reduce the complexity of the analysis and increase the computational efficiency.

4.2.3 Modeled neuronal network

The modeled neuronal network was based on Izhikevichs network model [124], and consisted of 10 neurons with random synaptic weights. The Izhikevich neuron model, an extension of integrator-and-fire neuron model, is computationally efficient and capable of producing rich firing patterns [125, 126]. The membrane voltage of every simulated neurons in this model is described by the following equations:

$$\dot{\mathbf{v}} = 0.04\mathbf{v}^2 + 5\mathbf{v} + 140 - \mathbf{u} + I$$
$$\dot{\mathbf{u}} = a(b\mathbf{v} - \mathbf{u}) \tag{4.3}$$

39

Where $\mathbf{v}$ represents neuron's membrane voltage and $\mathbf{u}$ is the membrane recovery variable which provides a negative feedback to the membrane voltage. $\dot{\mathbf{v}}$ and $\dot{\mathbf{u}}$ are the time derivatives of $\mathbf{v}$ and $\mathbf{u}$, respectively, where I is the synaptic input to the neuron. The membrane voltage and the membrane recovery variables are reset after occurrence of an action potential as follows:

$$\text{if } \mathbf{v} \geq 30 \ mV, \ \text{then} \ \begin{cases} \mathbf{v} \leftarrow \ c \\ \mathbf{u} \leftarrow \ \mathbf{u} + d \end{cases} \tag{4.4}$$

In equations 4.3 & 4.4, the coefficients a, b, c, and d determine the firing rate and pattern [126]. To achieve a regular spiking, the parameters were initialized to $a = 0.02$, $b = 0.2$, $c = -65$, and $d = 8$. The modeled network consisted of both excitatory and inhibitory neurons and was generated using these initial values. However, the parameters were randomly varied around the initial values to achieve non-identical firings for each neuron in the network (see [124] for details).

4.2.4 Connectivity of $A\beta_{42}$ oligomer treated cultures

To assess the changes in the functional connectivity due to $A\beta_{42}$ oligomer, neuronal networks that were either treated with $A\beta_{42}$ oligomer or Memantine + $A\beta_{42}$ oligomer were utilized (n = 4 networks for each scenario). The TE connectivity map was calculated for the recordings from pre-$A\beta_{42}$ (baseline), immediately and 24 hours after $A\beta_{42}$ oligomer administration. To quantify the overall changes in the connectivity, we defined a measure called Connectivity Index (CI). In every recordings that connectivity matrix was calculated, the elements of the matrix were summed up. The CI was then defined by normalizing the summation values to their corresponding baselines. The time window for the connectivity analysis was set to 600 s for all the analyzed recordings.
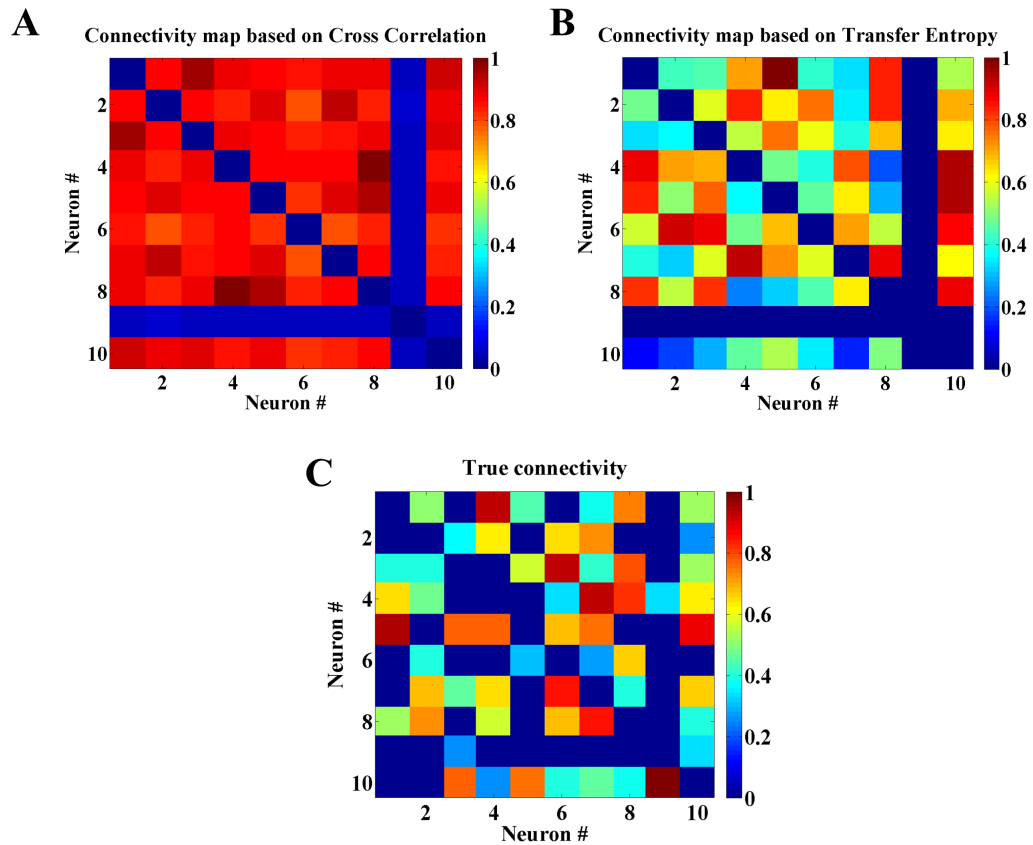
Figure 4.1: CC and TE methods were utilized to examine the connectivity among neurons in a modeled neuronal network. The connectivity maps obtained by CC (A) and TE (B) versus the ground truth (C). The modeled network consisted of 10 neurons with random synaptic weights to every neuron.

4.3 Results and Discussion

4.3.1 The performance of CC and TE on modeled neuronal network

Figs. 4.1A&B show the normalized connectivity maps obtained by CC and TE methods for the simulated network of 10 neurons. The true connectivity map, the normalized synaptic weights to every neuron in the model, is also depicted in Fig. 4.1C. As predicted, CC showed a relatively poor performance in detecting the connectivity in the network (Fig. 4.1A). Based on the CC results, the majority of the neurons in the network are highly connected to each other indicating a large false positive rate for this method. On the other hand, despite some misclassifications, TE provides a more realistic connectivity map of the network. To compare the performance of the two methods, similar to [120,127], we first plotted Receiver Operating Characteristic (ROC) curves (Fig. 4.2) and then calculated Area Under the Curves (AUCs) for each method. An ROC curve shows the true positive rate (TPR) versus the false positive rate (FPR). When an algorithm correctly identifies all the connections, the true positive rate is 100% and the false positive rate is 0% resulting in a high ($\sim$ 1) AUC. In contrast, as the number of the false positives grows, the AUC becomes smaller ($\sim$ 0) suggesting a poor performance for the method. Based on Fig. 4.2, the AUCs for CC and TE were 0.63 and 0.75, respectively. Consistent with previous reports, our results confirm a better performance for the TE method compared to CC. In addition, we show the correlations between the synaptic strengths calculated by CC and TE versus the "true connectivity" strengths (Fig. 4.3). In the ideal scenario, the estimated connectivity strengths plotted versus true connectivity values should fall on a diagonal line between (0,0) and (1,1) indicating the estimates are equal to true values. In Fig. 4.3, compared to CC, the fitted line for the TE method is more diagonal suggesting a higher correlation between the TE estimated values and ground truth.
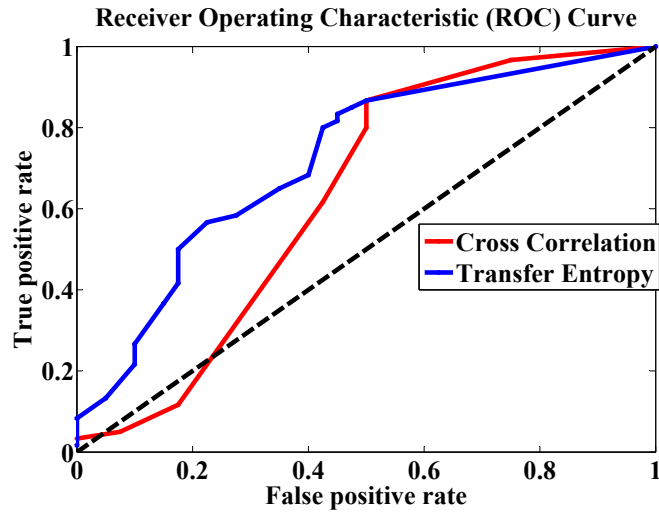
Figure 4.2: The ROC curves to compare the performances of CC and TE methods on the simulated neuronal network.The dashed diagonal line corresponds to random guess. The dashed diagonal line corresponds to a complete random guess suggesting the performance of a method which can not discriminate between true and false positives.
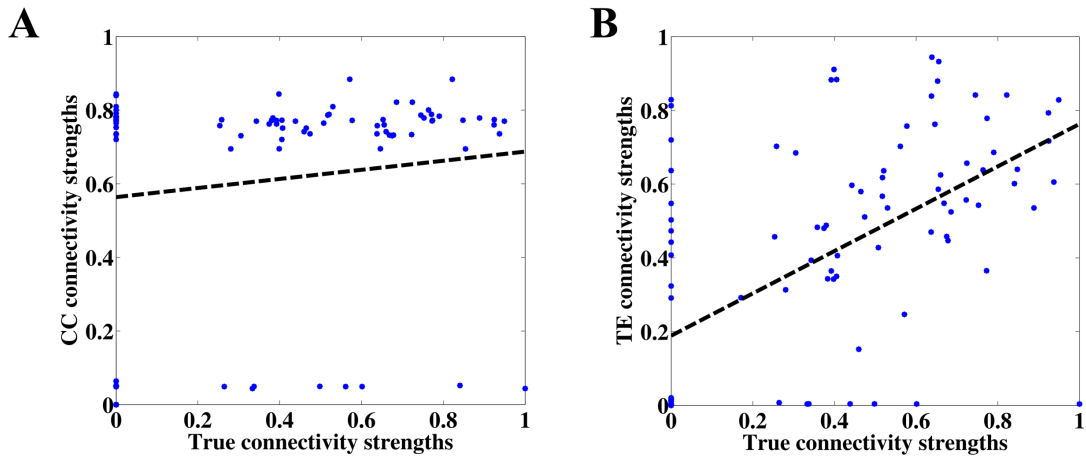
Figure 4.3: Correlations between the synaptic strengths calculated by CC (A) and TE (B) versus the "true connectivity" strengths. The dashed lines show the fitted lines to the data using least-squares method. Compared to the CC, the estimates obtained by TE method shows higher correlation to the true synaptic strengths.

43
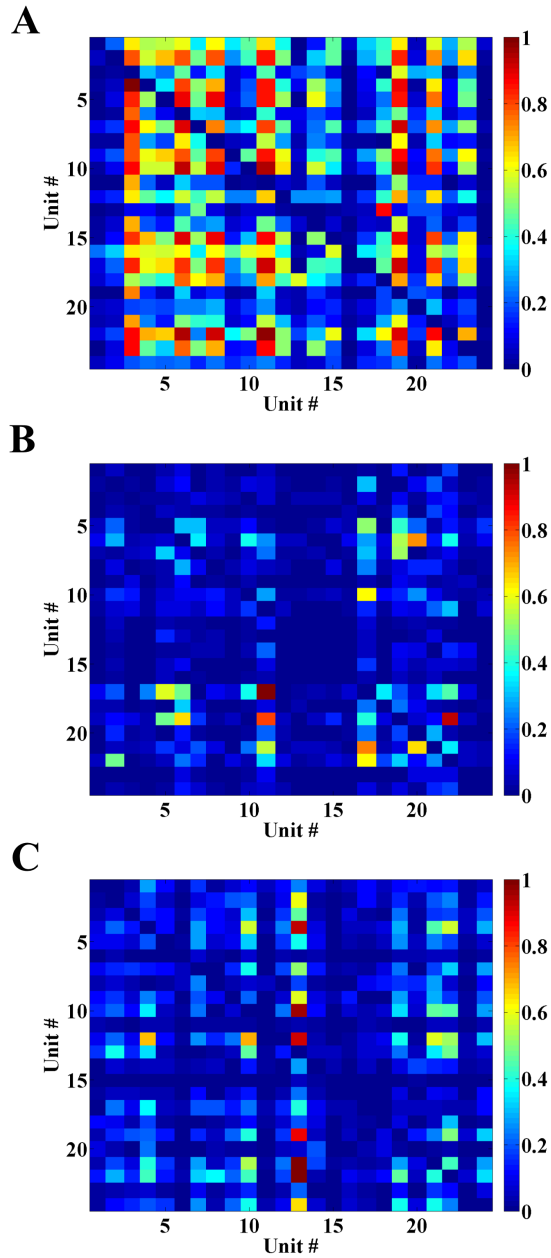
Figure 4.4: The changes in the functional connectivities of a representative network in response to 5μM Aβ_{42} over 24 hours. The connectivity maps of the baseline (A), immediately (B) and 24 hours after (C) the Aβ_{42} administration.

44

Figure 4.5: The connectivity index(CI) for cultures treated with either 5μM Aβ_{42} or memantine + Aβ_{42}. Compared to spike rate, CI seems to be a more sensitive measure to examine the effects of Aβ_{42} oligomer and memantine. n = 4 networks in each scenario, error bars indicate SEM.

4.3.2   Changes in connectivity due to Aβ_{42}

Considering the better performance of TE compared to CC, we chose the former to investigate the changes in a representative network due to the administration of 5μM Aβ_{42} oligomer over 24 hours. Fig. 4.4 shows the connectivity maps before, immediately and 24 hours after Aβ_{42} oligomer administration. It can be seen that Aβ_{42} oligomer greatly affected the functional connectivity among the units in the network. As shown in Fig. 4.5, the CI values were 0.31 ± 0.04 and 0.30 ± 0.07 for immediately and 24 hours after Aβ_{42} oligomer, respectively (mean $\pm$ SEM, n = 4 networks). However, the normalized spike rates for the same cultures were 0.47 ± 0.06 and 0.59 ± 0.07 at the same time points. The difference between the CI values and the normalized spike rate changes suggest that CI is a more sensitive measure to examine the effects of Aβ_{42} oligomer.
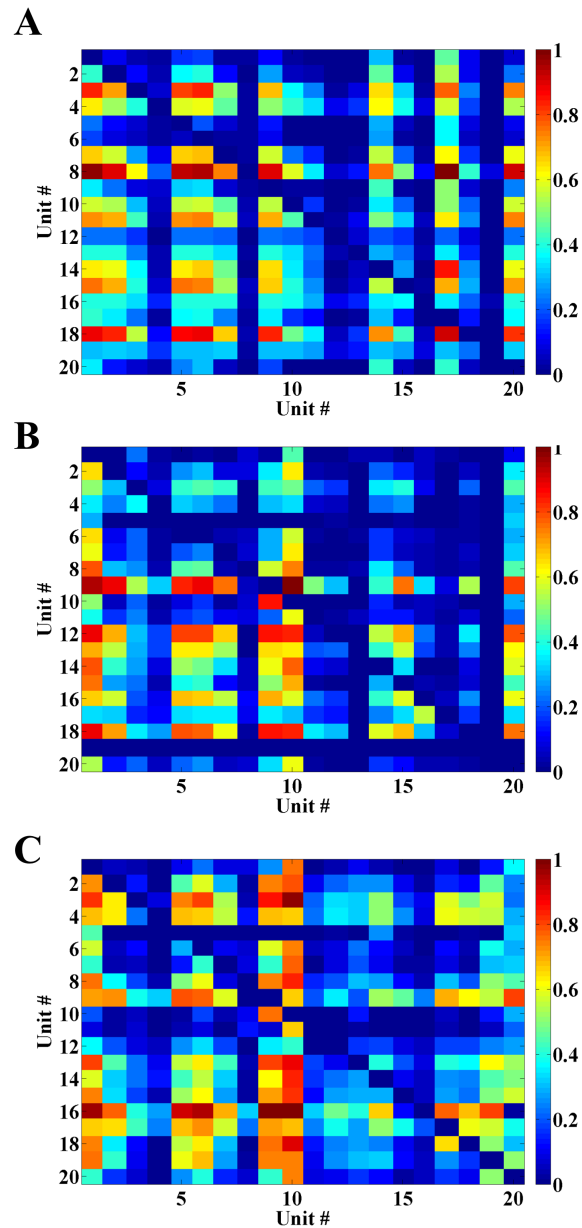
Figure 4.6: The protective role of memantine against the effects of $A\beta_{42}$ on connectivity. The connectivity maps for a representative network pre-treated with memantine before (A), immediately (B) and 24 hours after (C) the $A\beta_{42}$ administration.

4.3.3 Protective role of memantine against the effects of Aβ_{42} on connectivity

As we showed in section 3.3.5 the reduction in the spike rate after memantine $+$ Aβ_{42} was not significant from the baseline and the activity level showed full recovery after 24 hours. Our analysis of the functional connectivity of the network pre-treated with memantine confirms minimal changes after Aβ_{42} over 24 hours (Fig.4.6). The CI values, shown in Fig. 4.5, were 0.73 ± 0.05 and 1.15 ± 0.18 immediately and 24 hours after Aβ_{42}, respectively (mean $\pm$ SEM, n = 4 networks). Although, the connectivity map for 24 hours suggest formation of some new connections, a control study should be performed to examine the spontaneous changes in the connectivity of neuronal cultures over period of 24 hours.

4.4 Conclusions

The information-theory based method, TE, showed better performance over CC in detecting the connectivity in a modeled neuronal network. We also showed that the functional connectivity would be largely affected in a neuronal culture after administration of Aβ_{42} oligomer. On the other hand, the memantine treated cultures showed minimal connectivity loss after Aβ_{42} oligomer administration.

Although TE showed better performance over CC for the modeled neuronal network, both methods suffer from limitations. In both methods, it is assumed that spike trains are stationary i.e. their statistical properties do not change with time. This assumption is hard to justify considering the stochastic nature of neuronal firings and their possible time-varying responses to external stimuli. In addition, the discussed methods are limited to the evaluation of interactions between pairs of neurons whereas a multivariate analysis seems more appropriate in studying the interactions among group of neurons [128]. In the TE method, the choice of bin width and the number of past bins could affect the overall results and as such it is hard to find an optimal value for these parameters.

Novel methods such as pattern searching algorithms that can evaluate the neuronal

47

interactions among ensemble spiking activities are desired to extract the embedded information in the MEA recordings. Such multivariate methods that could incorporate multiple spike train analysis might expand our ability to reliably detect and quantify connectivity within a neuronal network.

48

Chapter 5: Use of cortical neuronal networks for *in vitro* material biocompatibility testing

5.1   Introduction

The international standard ISO 10993 provides regulatory guidance aiming to ensure that new biomedical devices consist of materials that are biocompatible. As described in ISO 10993-5, consideration of new medical device materials typically begins with *in vitro* testing where cytotoxicity serves as the main endpoint. In general, cytotoxicity testing is considered to be a standardized and sensitive approach to assess whether or not a novel material, or residual reagent used in the fabrication process, can induce deleterious biological effects. While a negative cytotoxicity test result does not necessarily imply suitability of the material for *in vivo* use, these tests can be useful to identify reactive materials. The standard describes systematic methods of exposing materials or material extractions to cells for multiple cell viability assays.

In clinical settings, implantable devices are being increasingly used to provide therapeutic neuromodulation to individuals suffering from neurological disease and injury. In addition, emergent devices such as implantable MEAs for brain machine interface applications leverage advances in fabrication and material science to achieve microscale systems [129–131]. Clearly, materials which are enabling for these novel implantable devices should neither induce cytotoxicity nor negatively influence the function of neuronal tissue.

In the present study, we examine the utility of living neuronal networks as functional assays for *in vitro* material biocompatibility. Neural tissue derived from primary murine dissection can be cultured on substrate-integrated MEAs to form functional networks. Such networks are spontaneously active and action potentials or neuronal firings can be monitored via the MEA. Previous work has demonstrated that neuronal networks cultured on MEAs

49

provide a valuable platform for neurotoxicology [7, 74, 132–134] and neuropharmacology [76, 135, 136]. Spike firing rate, amplitude, bursting, and synchronization of firing among neurons, or units, can be readily observed and quantified [5,80,137]. Systematic analysis of a large set of chemical compounds across several laboratories demonstrated the reproducibility and reliability of the MEA method [81].

Given the well documented use of frontal cortex derived neuronal networks for neuropharmacological applications [76, 81, 135], we examined the utility of frontal cortex networks for functional testing of biomaterials. We describe a method for exposing networks which provides 1) stable neuronal activity under control conditions, and 2) consistency with ISO 10993-5 guidance. Using materials considered either conductive or insulating, exposure to established negative controls failed to significantly alter neuronal network activity while positive controls elicited marked reductions in spike firing rate. We validated our method against an established cytotoxicity measure using L929 fibroblast cells and show that neuronal networks exhibit enhanced sensitivity to positive control materials. Lastly, we report the functional neurotoxicity of tungsten, a common microelectrode material, and two conducting polymer formulations that have been used to modify microelectrode properties for *in vivo* recording and stimulation.

5.2   Material and Methods

5.2.1   Materials and sample preparation

The testing materials were divided into two categories: conductor and insulator. For each category a positive and negative control material was selected. For conductors, gold (Au) and copper (Cu) and for insulators, polyethylene (PE) and polyvinyl chloride (PVC) were chosen as negative and positive controls, respectively. The choice of control materials was in line with the ISO 10993-12 standard as well as prior work on the cytotoxicity of implantable devices [138]. According to the same standard, a positive material is one that, when tested by a specific procedure, will cause a reactive response while a negative control will induce

50

a non-reactive or minimal response under the same test procedure. In addition to positive and negative controls, the functional assay was used to test three other materials including tungsten (W), PEDOT-PSS, and PEDOT-PSS-CNTs.

For Au, W, and Cu, thin films were deposited onto 8 mm x 10 mm rectangular silicon (Si) coupons using the following process. 100 mm diameter wafers of (100) Si (Wafer World, West Palm Beach, FL) were cleaned using a standard RCA clean process [139] and then placed in a 4-pocket E-beam evaporator and loaded with ceramic crucibles containing titanium (Ti) and either Au, W, or Cu, respectively. 500 Å of Ti was evaporated onto the surface of the Si as it allows the target metals to attach to the surface of the Si. 5000 Å of the target metal was then evaporated onto the Ti film surface. The wafers were removed from the evaporator and diced into 8 mm $\times$ 10 mm rectangular coupons using a dicing saw equipped with a diamond blade. The samples were then solvent cleaned ultrasonically in acetone and isopropanol followed by a de-ionized water rinse.

A bulk high density polyethylene (PE) sheet was purchased from Ridout Plastics Co. Inc. (San Diego, CA) and cut into the 8 mm $\times$ 10 mm rectangular coupons using a dicing saw. Tygon F-4040-A tubing designed for use with fuels and industrial lubricants, which consists of polyvinyl chloride (PVC) with a plasticizer, was used as a positive control material [138].

PEDOT-PSS and PEDOT-PSS-CNTs were electrochemically deposited on gold coated 8 mm $\times$ 10 mm Si coupons using both galavnostatic and potentiostatic techniques [140,141]. Prior to electrochemical deposition, Au coated coupons were first rinsed in de-ionized water and then cleaned by voltammetric cycling in 0.1 M H_2SO_4 from 0 to 1.2 V. All the samples were sterilized by ethylene oxide exposure for 12 hours.

5.2.2 Microelectrode array preparation

The MEA preparation is already described in section 3.2.2.

5.2.3 Cell culture

Fibroblast culture

Mice fibroblast cells, NCTC clone 929 (strain L) which are commonly known as L929 mouse fibroblasts were obtained from ATCC (Manassa, VA) and then cultured in Dulbeccos Minimum essential medium (DMEM) (Life Technologies, Grand Island, NY) supplemented with 10% fetal bovine serum (FBS) (Life Technologies), 2 mM GlutaMAX-I CTS (Life Technologies), and 1% antibiotic/ antimycotic solution (Sigma-Aldrich, St. Louis, MO). The L929 cells were cultured in 75 cm^2 tissue culture flasks (CytoOne T75 filter cap; USA Scientific, Ocala, FL) in a water jacketed incubator at 37°C, 95% relative humidity, and 5% CO_2. The L929 cultures were maintained within the flask, receiving a 50% media change every two days until they were required for a cytotoxicity assay or the culture confluence level exceeded 90%.

Primary neuronal culture

The primary neuronal culture procedure is already described in section 3.2.3. However, to avoid overgrowth of glial cells, both FBS and HS were removed at day 3 and the cultures were thereafter maintained by a 50% media exchange twice a week for at least 21 days. The resulting cultured neuronal networks consist of multiple cell types which are native to the tissue of origin. Specifically, these networks consist of GABAergic and glutamatergic neurons as well as supporting glial cells.

Fibroblast cytotoxicity assay and analysis

The rectangular samples with effective surface area of 0.8 cm^2 were placed in a polystyrene 12 well plate (USA Scientific) with 267 μL of complete DMEM media to maintain the $3cm^2$/mL ISO 10993-5 extract concentration. The 3.56 mm OD, 2.03 mm ID Tygon F-4040-A PVC tube was cut to a length of 14 mm (surface area of approximately 3 cm^2), and placed inside 1 mL of the complete DMEM media. The 12-well plate was sealed

52

with Parafilm M© (Fisher Scientific) and placed on a 55S single platform shaker (Reliable Scientific, Inc., Nesbit, MS) inside a hot room maintained at $37 \pm 1°$C for 24 hours $\pm$ 1 hour. The extract media was then diluted with complete DMEM media to develop the various testing concentrations utilized for this study.

Fibroblasts were harvested from the flasks by first removing the media and rinsing three times with sterile phosphate buffered saline (PBS), then 2 mL of a 0.25% trypsin/ 0.02% EDTA solution (Sigma-Aldrich,) was added to the flask and then incubated at $37°$C for 5 to 10 minutes. Once the cells released from the surface of the flask, 6 mL of cell culture media was added to the trypsin solution and then relocated into a 15 mL capped conical tube (USA Scientific). The tube was centrifuged at 400 x g for 5 minutes to form a pellet. The supernatant was removed, and the cells were re-suspended in 10 mL of fresh cell culture media. Cell counts were obtained with a hemocytometer and 1.8×104 fibroblasts were seeded into each well of a CytoOne TC 96 well plate (USA Scientific). 100 μL of complete media was added into each well and incubated using the same parameters as discussed in section 5.2.3. After 24 hours, all media was removed from each of the wells and replaced with extract media. To determine dose response profiles, extract media was diluted with extract free media and exposed to the cells. The baseline for cytotoxicity tests was set based on the reactions of the cells to extract free media.

To measure the cytotoxicity for fibroblasts, Live/Dead Viability/Cytotoxicity Assay Kit for mammalian cells (Life Technologies) was utilized. Live cells metabolize non-fluorescent calcein AM into green-fluorescent calcein which appears throughout their cytoplasm. Red fluorescence indicates the presence of ethidium homodimer which penetrates compromised membranes and binds to the DNA in the nucleus, indicating dead cells. The presence of granulated green calcein and red ethidium homodimer in the same cell is an indicator of apoptosis. To perform the assay, a mixture of 2.50 μL calcein AM, 3.75 μL ethidium homodimer, and 5 mL PBS was first prepared. Extraction media was removed from each well, 50 μL of the assay was added, and incubated at $37°$C for 15 minutes. After incubation, the wells were observed under an Axio Imager M2 fluorescent microscope (Carl Zeiss,

53

Oberkochen, Germany). Digital photographs of each well were captured by an Axiocam Imaging system (Carl Zeiss) at 10X magnification for cell counting and measuring the area covered by the cells (i.e. level of confluence). The cells were additionally imaged at 50X magnification for cell morphology and lamellipodia/ filopodia extensions. The cell count and confluence was calculated using the Zen Software (Carl Zeiss, Oberkochen, Germany). Cell count data were normalized to the mean of the counts obtained from extract free wells.

5.2.4 Functional assays and analysis

All recordings were performed after at least 3 weeks *in vitro* to ensure that the neural networks had reached maturity and consistency in activity. The multichannel extracellular recordings were similar to that described in 2.2.3. In order to increase the number of simultaneous experiments, another MEA data acquisition system, MEA2100-32 (Multi Channel Systems, Reutlingen, Germany), was also utilized. The MEA2100-32 had only 32 channels with sampling rate per channel of up to 50 KHz. In both recording systems, the culture temperature was controlled and set at 37°C.

Extracts of materials were prepared by incubating 1 ml serum-free cell culture media for every 3 cm^2 of material sample (according to ISO 10993-12 and ISO 10993-5) in 35 mm diameter polystyrene petri dishes (Fisher Scientific) at 37°C for 24 hours under constant agitation using a laboratory shaker (Genemate; BioExpress, Kaysville, UT). Control extracts also underwent the same procedures except they were incubated with material-free cell culture media.

Complete media change was performed 24 hours before baseline recording to rule out any effects due to media replacement itself. The exposure paradigm, as depicted in Figure 5.1, consisted of baseline recordings followed by exposing the culture to the extracts with 100% media change and measuring the activity again 24 hours later. The 24 hour period between the recordings was adapted from standard ISO 10993-5. The cultures were inspected under an optical microscope before every recording session to identify any obvious morphological changes or signs of media contamination.

54
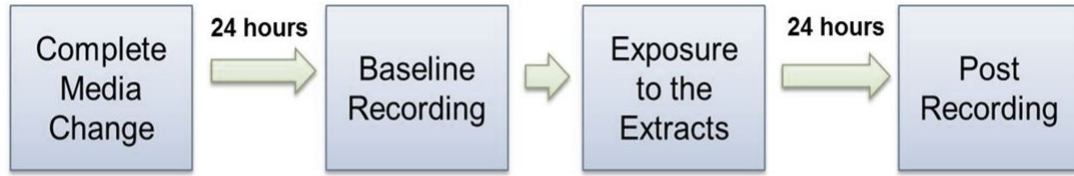
Figure 5.1: Exposure paradigm for functional toxicity testing using cultured neuronal networks.

During extracellular recordings from the neuronal networks, the mean noise level was calculated for each individual channel and a threshold was set at 4.5 - 5 standard deviations from this mean. A spike was then detected if the signal passed this threshold. Recording sessions were 30 minutes long and channels with spike rates above 0.1 Hz were considered active. The recorded spikes from each channel were sorted off-line into well-resolved units using Offline Sorter V.3 (Plexon Inc.) based on the method described in section 3.2.4. Consistent with [142], our quantification for functional neurotoxicity focused on the determination of mean spike rate across each network. Exposure data were normalized to the corresponding baseline levels measured before exposure to the material sample.

5.2.5 Dose-response curve fitting

Dose-response curves for the positive controls (i.e., PVC and Cu extracts) were calculated for both assays. For each assay, the responses corresponding to different concentrations were tted to the following sigmoid function:

$$R = \frac{R_{max}}{1 + (\frac{D}{EC_{50}})^{nH}} \tag{5.1}$$

where R_{max} was the maximum mean spike rate (maximum response), EC_{50} was the half maximal effective concentration, D the extract concentration and nH is the slope factor

55

or Hill coefficient [143]. For Cu extracts, in order to relate the EC_{50} value to actual concentration of Cu ions in the extract, the molarity was determined by using a copper ion-selective electrode (Cole Parmer, Vernon Hills, IL) and a pH/ion meter (Fisher Scientific).

5.2.6 Statistical analysis

All statistical analysis was performed using MATLAB Statistics Toolbox Version 7.10 (Mathworks, Natick, MA). Data are expressed as mean $\pm$ SEM. Students t-test was used to compare any two sets and P $<$ 0.05 was considered statistically significant.

5.3 Results

5.3.1 *In vitro* cytotoxicity of positive and negative controls using L929 fibroblasts

Using established negative (Au, PE) and positive (Cu, PVC) controls; we examined the *in vitro* cytotoxicity of material extracts using fibroblasts in an exposure protocol consistent with regulatory guidance. Fig. 5.2 shows representative images obtained from the Live/Dead assays performed on 100% extracts derived from the conductor and insulator materials. 24 hours after exposure to the 100% extract, there is little morphological difference between the cells cultured with extracts of Au (Fig. 5.2A), PE (Fig. 5.2B), and regular media (data not shown). Overall, there appeared to be very few lysed or apoptotic cells after exposure to the negative control material extracts. In contrast, the majority of L929 cells exposed to Cu (Fig. 5.2C) and PVC (Fig. 5.2D) appeared lysed or in the process of apoptosis which is consistent with the expected results for positive control material extracts.

Results from the Live/Dead assay support the cell culture images where extracts from neither Au nor PE displayed cytotoxic effects, but both Cu and PVC did. Figure 5.3 shows the normalized results (mean $\pm$ SEM) of cell counts for viable cells exposed to the four materials. According to ISO 10993-5, exposure to materials that result in a 30% reduction in viability indicates that material is potentially cytotoxic. At 100% extraction, Au and

56
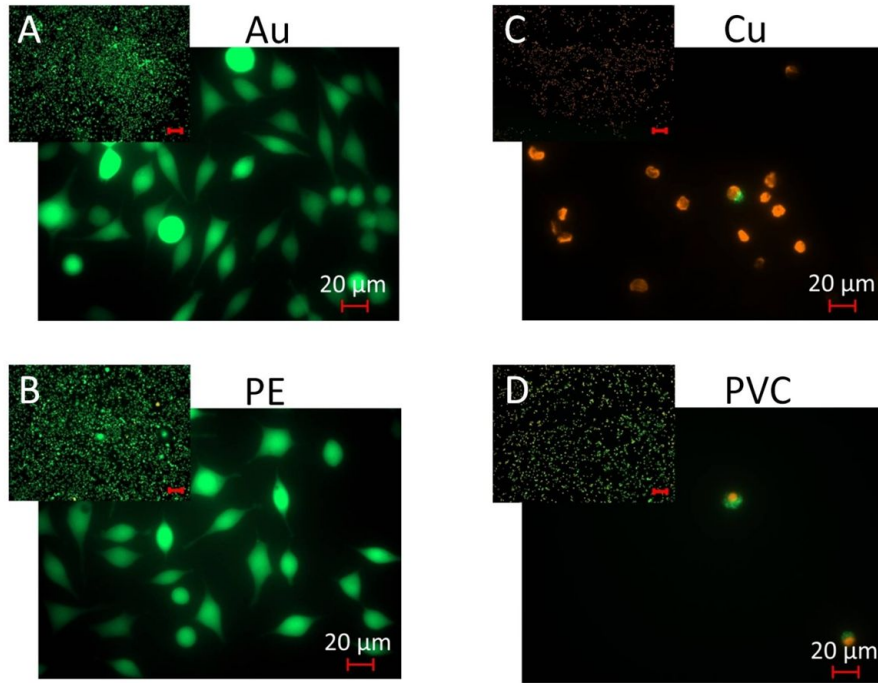
Figure 5.2: Images of representative Live/Dead assay results using L929 mouse fibroblasts 24 hours after being exposed to 100% extracts of conductor and insulator materials. The reaction of L929 cells to 100% media extractions to A) gold (Au) B) polyethylene (PE), C) copper (Cu), and D) polyvinyl chloride (PVC). Live cells are green, dead cells are read, and cells that are both red and green are in the process of apoptosis. Each image shows an inset which was used to count the cells and confluence level (the scale bar is 200 μm), while the higher magnification image allows examination of cellular morphology and relative surface attachment.

57
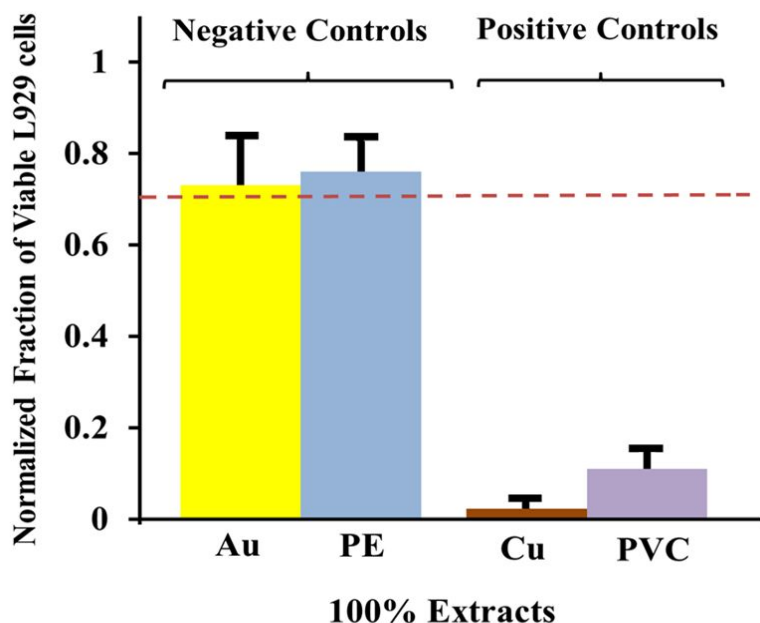
Figure 5.3: Bar graphs showing the minimum level of material extract exposure that L929 cells need to pass the viability requirements of ISO 10993-5 cytotoxicity testing. Cell viability data are shown as the mean and SEM of the test normalized to the baseline, cell-treated polystyrene. Exposure to 100% extracts from negative control materials gold (Au) and polyethylene (PE) show high fibroblast viability whereas exposure to extracts from positive control materials copper (Cu) and PVC resulted in very low cell viablity The red dashed line at 70% indicates the maximum deviation of viability from baseline as directed by ISO 10993-5.

PE exhibited 73.3 ± 7.6% (N = 11) and 76.4 ± 10.8% (N = 13) viability, respectively, compared to cell treated polystyrene (CTPSt) controls. In contrast, only low percentage extracts from positive control materials Cu and PVC satisfied the standard. Cu passed the cytotoxicity test (73.1± 13.1% relative viability, N = 9) at an extract concentration of 13%, and PVC was considered not cytotoxic (77.6 ± 2.8% relative viability, N = 9) at an extract concentration of 7%. As expected, 100% extracts from the positive control materials Cu and PVC produced considerably lower cell viability of 2.2 ± 1.5% (N = 15) and 11.2 ± 3.1% (N = 9), respectively (Fig. 5.3).

By systematic dilution of the material extracts, we more completely examined the dose dependent effects of the positive controls Cu and PVC. The dose response curves for different

58
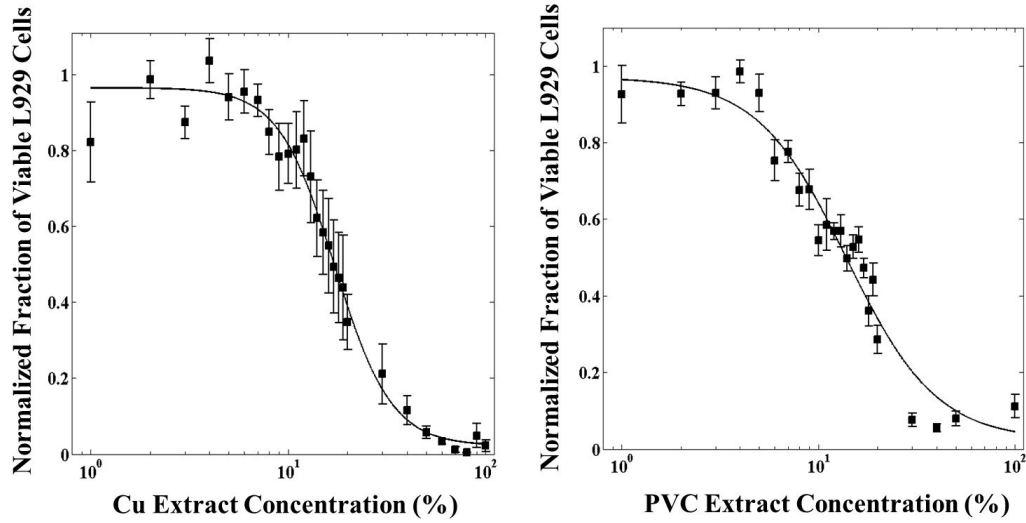
Figure 5.4: Normalized fibroblast viability as a function of media extraction concentrations for positive control materials Cu (left) and PVC (right). In both materials, $N \geq 6$ for each concentration.

media extraction concentrations of Cu and PVC are shown in Fig. 5.4. The EC_{50} values derived from curve fitting for Cu and PVC were 17.2% and 15.7%, respectively. The Hill coefficients were also 3.0 and 1.9 for Cu and PVC, respectively.

5.3.2 Frontal cortex neuronal networks

The frontal cortex data consist of measurements from 1202 total units over 41 networks cultured from 14 different mice. On these MEA substrates, neuronal networks typically show a carpet of cells (Fig. 5.5A) and exhibit consistent, well resolved single units after three weeks *in vitro* (Fig. 5.5B). In total, MEAs had the yield, defined as the percentage of active electrodes, of $56 \pm 4\%$ (mean $\pm$ SEM). The average single unit amplitude was approximately 70 ± 2 μV peak to peak, and the mean spike firing rate was 3.0 ± 0.4 Hz. Consistent with prior work, unit activity occurred in both single spikes and bursts [5,80,137] where coordinated activity was readily apparent (see Fig. 5.5C). The SNR ratio was defined as the ratio of peak-to-peak spike amplitude to the standard deviation of baseline noise. The mean SNR value for the detected spikes was 9.5 ± 0.21, indicating that single units

59
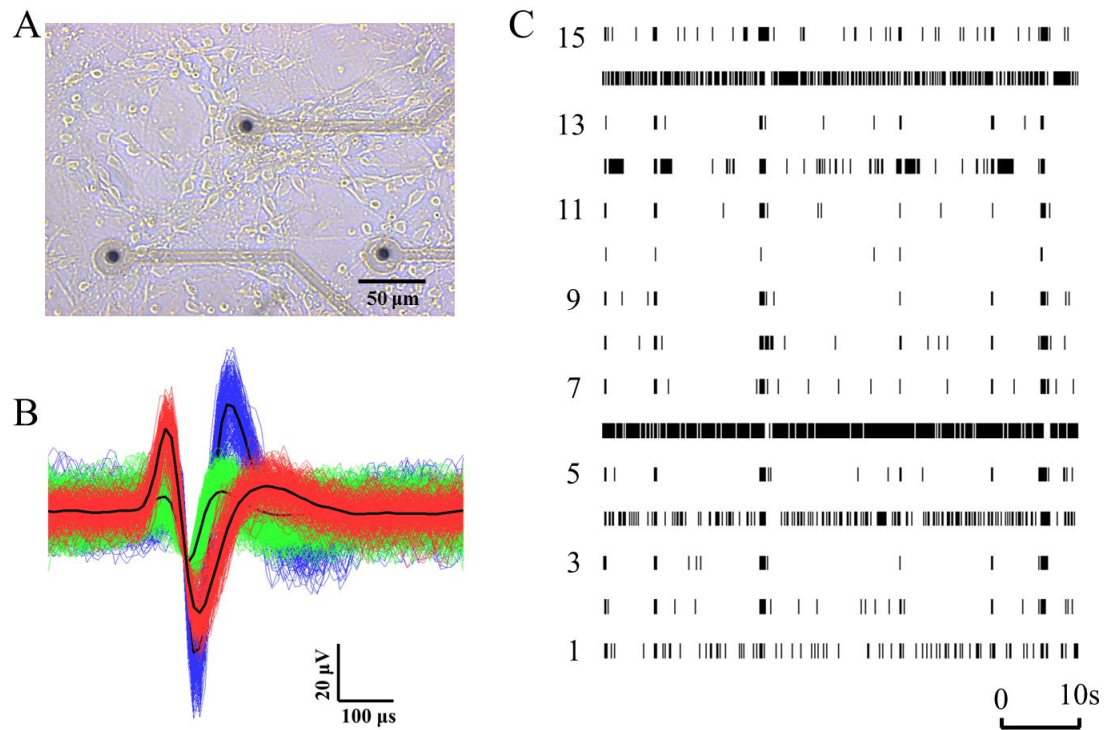
Figure 5.5: Frontal cortex neuronal network cultured on an MEA producing spontaneous single unit or spike activity. A) Neurons extend processes and form a mature network within 3 week, B) sorted action potentials from a representative microelectrode channel of a MEA with 3 well-resolved units, C) raster plot from 15 representative units from the same MEA which shows typical extracellular activity of a frontal cortex culture.

could be well resolved in our experiments.

5.3.3 Functional neurotoxicity of positive and negative controls

Sample-free extracts, which had no material samples at the time of preparation, were exposed to neuronal cultures to determine the effect of feeding and test procedure on possible changes in their activity. The normalized spike rate after exposure to such extracts was 1.11 ± 0.07 (N = 5 networks, mean $\pm$ SEM), indicating that the process of media exchange under the exposure protocol did not induce significant changes in spike activity. Note that the stability of this metric is dependent on network maturity. Initial tests performed with networks younger than three weeks *in vitro* showed larger fluctuations in mean spike rate

60
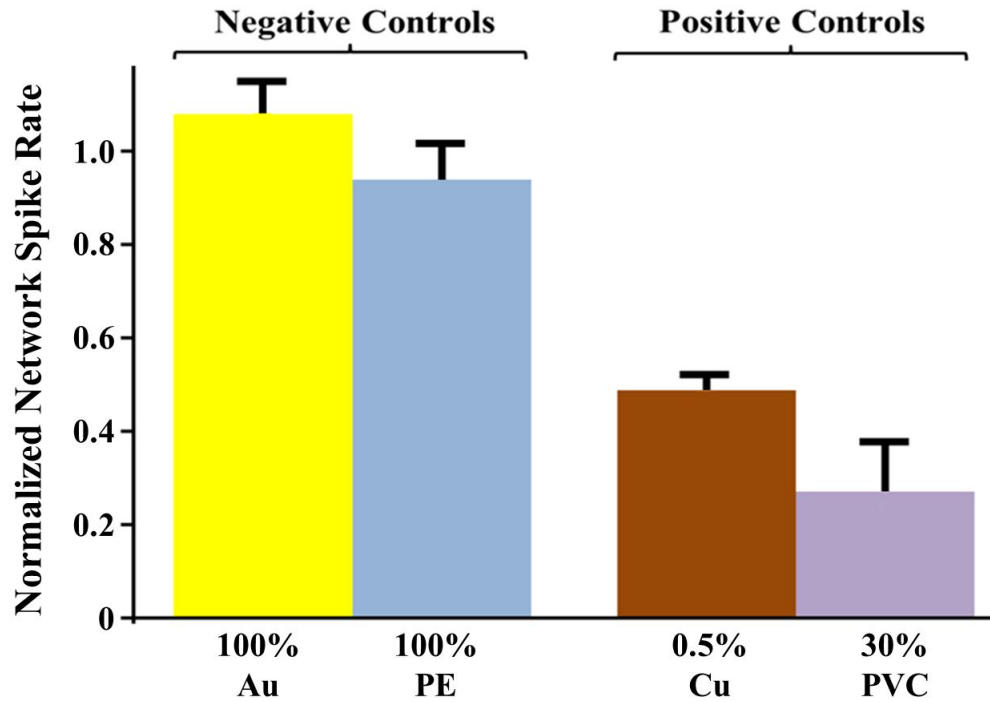
Figure 5.6: Effects on neuronal network activity 24 hours after exposure to the negative and positive control material extracts. For positive controls, the responses to lower extract concentrations are shown because exposure to 100% extracts wiped out the activity for all the networks. The spike rates were normalized to the baseline activity measured prior to adding the extracts. Data are shown as mean normalized spike rate and SEM for N = 5 networks for negative controls and N = 3 networks for the positive controls.

with media replacement.

Exposure to extracts derived from negative control materials failed to alter the neuronal network spike firing rate. Application of extracts from Au and PE at 100% media extraction did not significantly affect neuronal network firing and cortical cultures maintained their typical synchronous bursting (Fig. 5.6 and 5.7). For all of the experiments, network activity recorded 24 hours after extract exposure was normalized to the baseline (pre-exposure) activity. The normalized spike rate for Au and PE was 1.08 ± 0.06 and 0.93 ± 0.07, respectively (N = 5 networks for each material).

In contrast, exposure to extracts derived from positive control materials resulted in a

significant reduction in the mean network spike rate. Cu and PVC extracts at 100% concentration completely blocked the activity (data not shown). Therefore, lower concentrations of positive extracts were tested on functional assays to determine if neuronal spiking could persist. For Cu, extract concentrations above 5% eliminated all spike activity whereas 0.1% or below had no observable effect on the activity. As shown in Fig. 5.6, 0.5% Cu extracts resulted in a $52 \pm 3\%$ reduction of spike rate (N = 3 networks). For exposures to PVC extracts, the activity dropped by $63 \pm 1\%$ after applying the 30% extracts (N = 3 networks, Fig. 5.6), but no reduction was observed for 1% extracts. The raster plots shown in Fig. 5.7 suggest that the overall reduction in spike rate with exposure to positive control material extracts was accompanied with changes in burst and synchronization dynamics. The dose response curves based on functional assay responses are shown in Fig. 5.8. The EC_{50} values derived from curve fitting for extracts from Cu and PVC were at 0.4% and 18%, respectively. The Hill coefficient for the Cu curve was 1.3 and it was 1.1 for PVC curve. For Cu extracts, the molarity of Cu^{2+} ions at EC_{50} concentration was found around 145 μM which was consistent with previously reported levels of Cu toxicity in primary cortical cultures [144] and cerebellar cultures [145].

To quantify the suitability of the functional assay, Z'-factor as a measure of assay performance was calculated [146]. For the Z'-factor, a value between 0.5 to 1 is an indicator of an excellent assay whereas values between 0-0.5 reflect a marginal assay [147]. The estimated Z'-factor for the functional assay was 0.65 which suggests the high quality of such an assay for screening purposes.

5.3.4 Functional neurotoxicity of conducting materials

In addition to control materials, three conducting materials including tungsten, PEDOT-PSS, and PEDOT-PSS-CNT were examined by the functional neuronal network assay. Tungsten has been commonly used in neuronal implants for brain-computer interface applications [148–150]. Materials with nanostructures such as PEDOT-PSS and PEDOT-PSS-CNTs have recently attracted a lot of interest in neuronal interfaces as they have shown

62
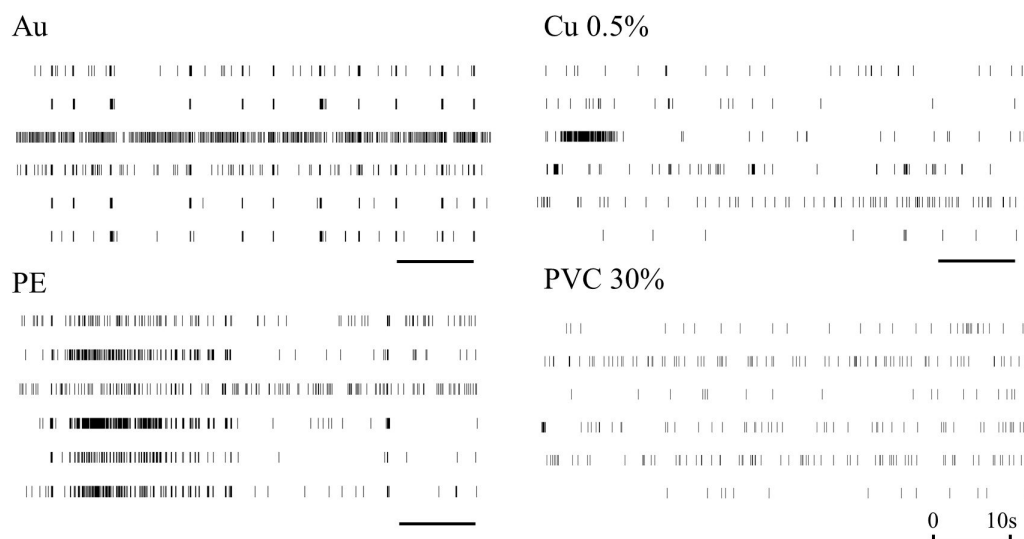
Figure 5.7: Raster plots of 60s activity for 6 representative units after exposure to extracts derived from control materials. 100% extracts from negative controls (Au or PE) did not alter typical pattern of activity for frontal cortex network. However, spike rate was decreased after application of Cu and PVC extracts.

improvement in neuronal recordings and provided more effective electrical stimulations to the brain tissue [140, 151–153]. As shown in Fig. 5.9, neither 100% PEDOT-PSS-CNT extract nor 100% PEDOT-PSS extract produced a statistically significant reduction compared to baseline. In contrast, the normalized spike rate after exposure to tungsten extracts fell to 0.66 ± 0.11 ($P < 0.05$).

5.4 Discussion

The use of living neuronal networks cultured on MEAs for pharmacological and toxicological studies has been well established [74, 75, 81, 135]. For the first time, the present study extends the utility of this approach to biomaterial testing applications, in particular for materials intended for implantable neural interfaces. Emerging applications of neural interfaces include MEA technology where the ability to record spike activity is a key feature. By relying on the analysis of spike activity as an end-point, this approach to material testing provides a highly relevant and sensitive measure to the functionality of such devices.

63
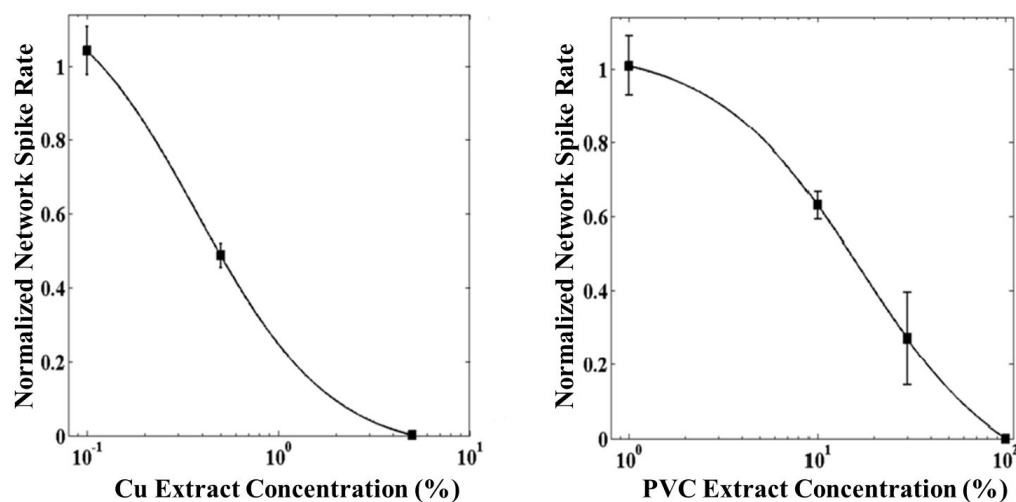
Figure 5.8: Neuronal network functional assay dose response curves for PVC and Cu extracts. Data are mean ± SEM (N = 3 networks at each concentration of each material extract).

The exposure paradigm utilizing extracts from culture media we have described is consistent in time and dilutions with the established ISO 10993-5 methodology. While the positive and negative controls elicited effects in cultured neuronal networks that were in line with the L929 fibroblast cytotoxicity findings, the neuronal networks appeared to be more sensitive to Cu as a positive control. It has been shown that Cu ions lead to formation of reactive oxygen species in cellular microenvironment that cause oxidative stress and apoptosis [154]. Comparing to other cell lines, neurons are highly sensitive to oxidative stress [144]. Such higher sensitivity could be a reason for the large difference in response to Cu between the conventional L929 and functional neuronal assays.

Consistent with prior work, neither PEDOT-PSS [155, 156] nor PEDOT-CNT [157] materials demonstrated functional toxicity using the neuronal cells *in vitro*. Interestingly, tungsten, which is commonly used as a conductor for implantable microelectrodes, produced a significant reduction in spike activity. Our observations are consistent with recent work demonstrating the relative toxicity of tungsten in neuronal cells [158]. In addition, concern has been recently expressed regarding the stability of tungsten microelectrodes for long-term

64
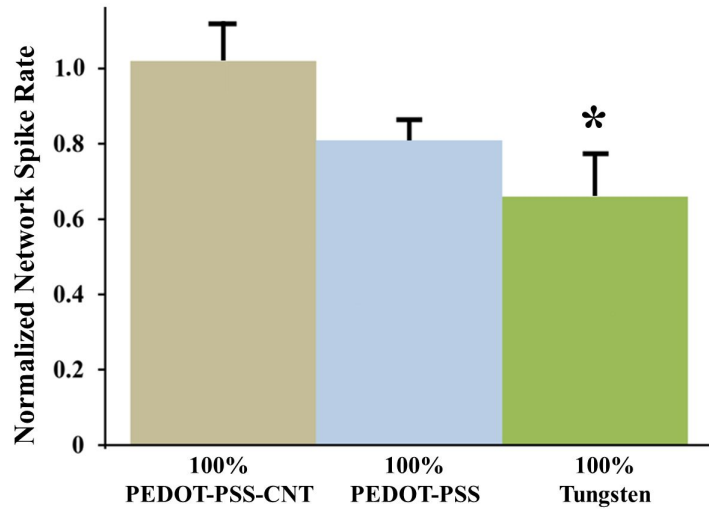
Figure 5.9: Changes in the network activity after 24 hours exposure to extracts derived from three different conducting materials. The mean spike rates were normalized to the baseline activity. Data shown as mean $\pm$ SEM, N = 3 networks for each material.* indicates statistically significant difference at P < 0.05

in vivo recordings where localized toxicity due to tungsten corrosion may impede long-term recordings [159].

A wide range of neural cell types has been previously used to assess the biocompatibility of materials *in vitro*. A common choice has been tumor derived neural cells such as neuroblastoma or primary neuronal cultures [160–162] with endpoints that include neurite extension and the expression of neural specific proteins such as MAP2 and neurofilament 200. Relevant to our work, primary neuronal culture has been shown to exhibit a markedly, albeit qualitatively, higher level of complexity and relevance over immortalized cell lines [70]. In addition, primary derived neurons offer the opportunity to include functional physiological measures of neural activity which are directly relevant to brain-machine interface applications.

While *in vitro* cytotoxicity testing is a valuable and standard initial step, it is not sufficiently predictive for *in vivo* biocompatibility. Clearly, any material, or residual reagent used in fabrication, that induces toxicity *in vitro* is likely to induce deleterious effects *in*

65

vivo, however the converse is not necessarily true. According to ISO 10993, to evaluate the biological effects of an implantable device, a series of at least 6 additional tests must be performed to more completely assess biocompatibility. We suggest that use of *in vitro* tests will reduce the number of animal tests necessary to develop and refine novel materials for biomedical applications.

A limitation to the approach we have presented is the expense and low throughput of MEA-based studies. Our assays were conducted in single well MEA dishes that, while reusable, are somewhat costly. Recent work by our group suggests that MEAs can be readily fabricated at low cost and of materials that are suitable for disposal [163]. Furthermore, multi-well MEA systems have become commercially available and offer the promise of increased throughput [142].

5.5   Conclusions

Our findings suggest cultured neuronal networks on MEAs could be utilized to assess functional toxicity of materials for neural implants. In the functional assay, change in the spike rate is a measure of functional toxicity which is a relevant metric to brain-machine interface applications. Furthermore, compared to the conventional live/dead L929 assay, the functional assay showed more sensitivity in response to copper as a positive control. The estimated Z factor for the assay also reflects the high quality in the performance for screening purposes. Considering the developed assay is consistent with the ISO standard in extract preparation and exposure time, the functional assay can be regarded as complementary method to the conventional cytotoxicity assays.

Citation & Contributions:

This work has been published as:

- **H.Charkhkar**, C.Frewin, M.Nezafati, G.L.Knaack, N.Peixoto, S.E.Saddow, J.J.Pancrazio. Use of cortical networks for *in vitro* material biocompatibility testing.

66

Biosens. Bioelectron. vol. 53, 2013.

HC, CF, and JJP wrote the paper. HC ran the functional assay recordings. CF and MN ran the fibroblast cytotoxicity experiments. HC and GLK performed the primary cell cultures. HC and CF analyzed the data. JJP, SES, and NP designed the study and edited the manuscript.

Chapter 6: Effects of carbon Nanotube and conducting polymer coated microelectrodes on single-unit recordings *in vitro*

6.1 Introduction

Planar MEAs are commonly used to record extracellular action potentials from excitable cells such as neurons and cardiomyocytes *in vitro* [21, 164, 165]. A typical MEA consists of a glass substrate patterned with a conductor such as gold or indium tin oxide [20, 166]. The recording sites, commonly 10-30 μm in diameter, are exposed while the remaining surface is passivated by an insulator such as polydimethylsiloxane or parylene C [21, 163]. In contrast to single-cell techniques e.g. patch clamp, MEAs are non-invasive and can record activity from multiple neurons simultaneously. Therefore, MEAs are suitable platforms for a variety of applications including pharmacological assessments [13], detecting neuroactive compounds [167], or studying neuronal network dynamics [6].

Although MEAs are intended to quantify network-level activity, the number of well-resolved action potentials from distinct neurons or so-called 'units' is limited compared to the total number of neurons on the substrate [6, 85]. The problem is exacerbated by the fact that: 1) the magnitude of extracellular potentials decays rapidly over distance [168]; and 2) metal microelectrodes can exhibit high impedance resulting in thermal noise which can mask single units by reducing the SNR [169]. Therefore, approaches which reduce the impedance of microelectrodes offer the promise of improving the SNR and enhancing the detection of units for neuronal recordings [170].

In recent years, it has been reported that coating the microelectrodes with nanomaterials such as CNT and conductive polymers(CPs) might improve the quality of neuronal

68

recordings, e.g. larger spike amplitudes or higher spike rates both *in vivo* and *in vitro* [151, 171, 172]. Such nanomaterials produce microelectrodes with a large surface area, high electrical conductivity and robust mechanical properties. Having a large surface area and significant porosity, the coatings enable microelectrodes to behave as super-capacitors which may improve the coupling with electrically active cells [172]. Additionally, the rough surface of the CNTs may provide scaffold-like structure to promote cell adhesion and growth [173].

In this work, we have examined the basis by which electrochemically-deposited PEDOT-PSS-CNT and PEDOT-PSS microelectrodes affect neuronal recordings *in vitro*. We observed that the yield, defined as percentage of microelectrodes with neuronal activity, was significantly higher for modified microelectrodes. However, activity measures, such as spike rate, were similar for modified and unmodified microelectrodes. The density of neurons and astrocytes surrounding modified and unmodified electrodes was compared using immunocytochemical labeling. There was significantly more neuronal labeling proximal to the modified electrode sites suggesting that an increased density of neurons surrounding coated sites may contribute to increased yield in single unit recording.

6.2 Methods

6.2.1 Electrochemical deposition of PEDOT-PSS-CNT and PEDOT-PSS

An aqueous CNT solution was prepared by ultrasonically dispersing 200 μg/ml carboxylic-functionalized CNTs (Cheap Tubes Inc., Brattleboro, VT) in deionized (DI) water with 0.5% poly(sodium 4-styrenesultanate) (PSS; Sigma-Aldrich, St. Louis, MO) as surfactant. To obtain EDOT-CNT solution for PEDOT-PSS-CNT coatings, 10 mM ethylenedioxythiophene (EDOT) monomer was added to the dispersed CNTs prior to the electrodeposition at the ratio of 4:1. In a similar way, EDOT solution for PEDOT-PSS-only coatings was prepared by making an aqueous solution containing 10 mM EDOT and 100 mM PSS.

Substrate-integrated MEAs each consisting of an 8×8 grid of 60 μm^2 microelectrodes,

were purchased from the University of North Texas (MMEP3; Center for Network Neuroscience, University of North Texas, Denton, TX). A potentiostat/galvanostat Reference 300 (Gamry instruments, Warminster, PA) was used to electrochemically polymerize and deposit either PEDOT-PSS-CNT or PEDOT-PSS on every other microelectrode of the MEA. Such patterning allowed for comparison between modified and unmodified microelectrodes within the same culture. The deposition was performed under potentiostatic condition by applying 0.9 V for 40-45 seconds using a large platinum wire (Ward Hill, MA) as the reference/counter electrode.

6.2.2 Electrochemical and morphological characterization

EIS was performed on representative subsets of modified and unmodified microelectrodes before and after the deposition. The measurements were done in the presence of 1x PBS under a two-electrode configuration. A sinusoidal waveform with 10 mV amplitude was applied over frequencies of 1 Hz to 100 KHz.

The surface morphology of modified and unmodified microelectrodes was examined with a field emission scanning electron microscope (SUPRA-55 VP; Carl Zeiss Microscopy, Thronwood, NY). The SEM was operated at 3 KV.

6.2.3 MEA preparation and primary cell culture

The MEA preparation and primary cortical cell culture methods were similar to that described in sections 3.2.2 and 5.2.3. All animal procedures were approved by the Institutional Animal Care and Use Committee of George Mason University (Fairfax, VA).

6.2.4 Extracellular recording

The cultures were allowed to mature for at least three weeks *in vitro*. The multichannel extracellular recordings were similar to that described in 2.2.3. The recording sessions were 30-40 minute in duration and the temperature was controlled at 37 ± 1^oC during the session. Spikes were detected if they passed a threshold that was set to be at least 5 times higher

70

than the standard deviation of the background noise. The recorded spikes from each channel were sorted off-line into well-resolved units using Offline Sorter V.3 (Plexon Inc.) based on the method described in section 3.2.4.

6.2.5 Immunocytochemistry

The cells were fixed using 4% paraformaldehyde (PFA) followed by permeabilization with 0.1% Triton X-100 (Sigma-Aldrich). The samples were then incubated in the blocking buffer which contained 4% normal goat serum (Sigma-Aldrich) in PBS. Rabbit anti-mouse glial fibrillary acidic protein (GFAP; 1:725, Dako North America Inc., Carpinteria, CA) and mouse anti-rat neuronal nuclei (NeuN; 1:1000, Millipore, Billerica, MA) were used as primary antibodies to detect reactive astrocytes and neurons, respectively. For GFAP and NeuN, goat anti-rabbit IgG Alexa fluor 488 (1:200, Life Technologies) and goat anti-mouse IgG Alexa fluor 546 (1:200, Life Technologies) were used as secondary antibodies, respectively. The samples were then imaged with a fluorescence microscope (Nikon eclipse Ti; Nikon Instruments, Melville, NY).

6.2.6 Data analysis

For extracellular recordings, sorted units with spike rate greater than 0.1 Hz were considered active and networks with more than 10 active units were included in data analysis. A burst was defined as an occurrence of at least three spikes with maximum inter-spike interval (ISI) of 100 ms [174]. For each active unit, SNR was defined as average of peak-to-peak spike amplitudes over the standard deviation of the noise for the corresponding channel. All the calculations for spike rate, spike amplitude, SNR, burst rate and inter-burst interval (IBI) were done in MATLAB (Mathworks, Natick, MA). All the activity measures were normalized to the mean of the same measure for unmodified electrodes.

The fluorescence microscopy images were processed with a custom routine in MATLAB designed to quantify the intensity of fluorescent labeling as a function of distance around modified and unmodified microelectrodes.

71
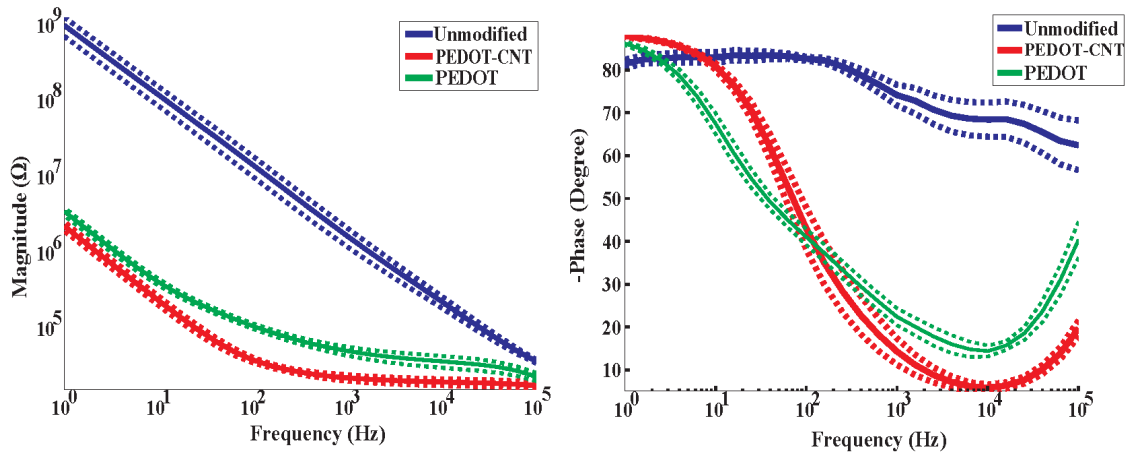
Figure 6.1: EIS measurements of typical coated versus uncoated microelectrodes. Reduction in the magnitude (left) and shift in the phase of the EIS (right) suggests an increase in the surface area after deposition of PEDOT-PSS and PEDOT-PSS-CNT. $N = 9$ microelectrodes for each group. Solid lines are mean and dashed lines show the $\pm$ SEM.

Data are reported as mean $\pm$ standard error of the mean. To statistically compare the yield between modified and unmodified electrodes, the test of proportion was utilized. For all the other measures, a non-parametric, two-sample Kolmogrov-Smirnov test (KS test) was utilized to determine whether any given two datasets i.e. modified vs. unmodified had different distributions [175]. For all the statistical tests, $P < 0.05$ was considered significant.

6.3 Results

6.3.1 Electrochemical characterization and morphology

Both PEDOT-PSS-CNT and PEDOT-PSS were successfully electrodeposited on gold microelectrodes. Magnitude and phase of the impedance for representative modified and unmodified microelectrodes are shown in Fig. 6.1. A significant reduction in the magnitude between frequencies of 1 to 10 KHz occurred after deposition of PEDOT-PSS-CNT and PEDOT-PSS. Specifically, the magnitude of the impedance at 1 KHz, the typical frequency associated with extracellular recordings, significantly dropped from 1.7 ± 0.3 $M\Omega$ ($n = 9$)

72

to 22.9 ± 2.2 $K\Omega$ ($n = 9$) and to 51.8 ± 6.9 $K\Omega$ ($n = 9$) for PEDOT-PSS-CNT and PEDOT-PSS modified microelectrodes, respectively. The shift in the phase of the impedance for modified microelectrodes suggests an increase in effective surface area. Such changes in impedance for both PEDOT-PSS-CNT and PEDOT-PSS were consistent with previous findings [140, 176].

SEM images of the unmodified and modified microelectrodes are shown in Fig. 6.2. The microstructures on the surface of the gold microelectrode (Fig. 6.2A) became smaller and formed nanostructures after the deposition of PEDOT-PSS-CNT and PEDOT-PSS (Fig. 6.2B and 6.2C). The CNTs were embedded inside the polymer (Fig. 6.2B), which provided a rougher and more porous surface. Such observations are consistent with the features previously reported for PEDOT-PSS-CNT and PEDOT-PSS modified surfaces [157, 177].

6.3.2 Extracellular recordings

The frontal cortex recording data consist of measurements from 431 total units over 10 networks cultured from 7 different mice. Out of the total 10 MEAs, 5 were modified with PEDOT-PSS-CNT and the other 5 had only PEDOT-PSS on every other microelectrode.

Spike waveforms recorded from the coated microelectrodes were similar to those from uncoated sites. (Fig. 6.3). The peak-to-peak (p-p) spike amplitude for the units from unmodified microelectrodes had the range of 40 - 207 μV whereas those from PEDOT-PSS-CNT and PEDOT-PSS microelectrodes had the range of 25 - 338 μV and 30 - 278 μV, respectively. Although the modified microelectrodes had lower impedance, which should result in lower thermal noise, the RMS noise values in extracellular recordings were similar between modified and unmodified microelectrodes. The RMS noise was 6.7 ± 0.2 μV_{rms} for PEDOT-PSS, 6.6 ± 0.1 μV_{rms} for PEDOT-PSS-CNT and 7.0 ± 0.3 μV_{rms} for unmodified electrodes.
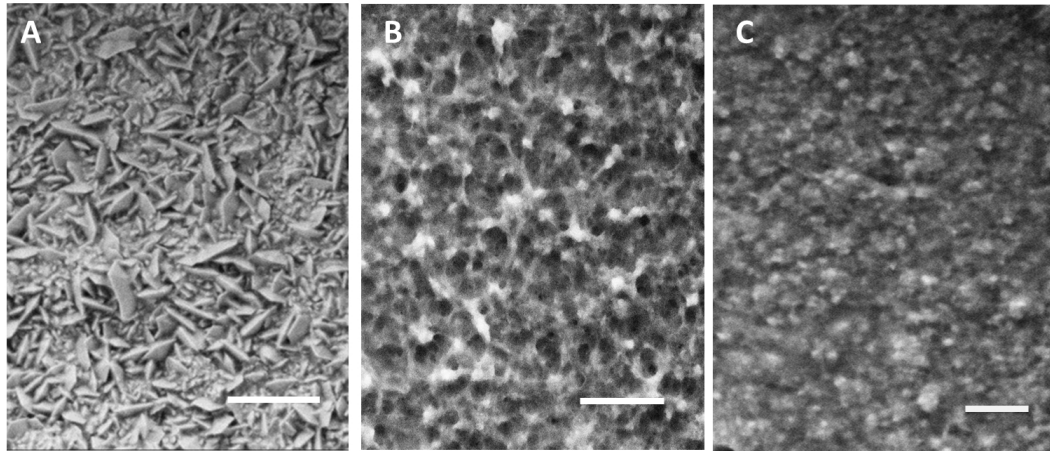
Figure 6.2: SEM images of unmodified and modified microelectrodes. The surface contained more nano features and porosity after modification with PEDOT-PSS-CNT and PEDOT-PSS. A) bare (gold) microelectrode with poly crystalline structure. B) PEDOT-PSS-CNT modified surface in which CNTs are embedded inside the polymer C) PEDOT-PSS modified microelectrode. The scale is 1 μm.
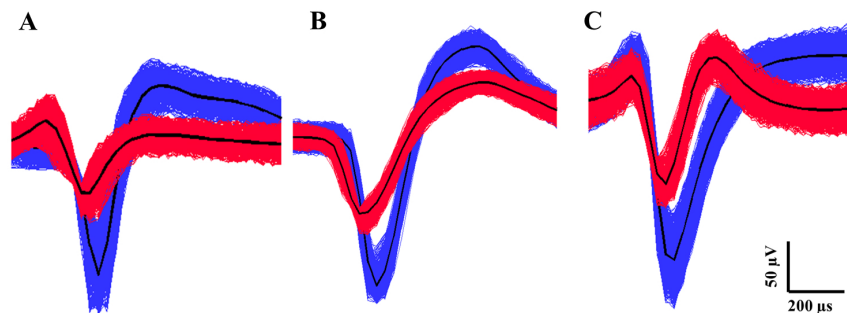
Figure 6.3: Represantative well-resolved units detected from an unmodified (A), PEDOT-PSS (B), and PEDOT-PSS-CNT (C) microelectrode. The spike waveforms from modified electrodes resmebles those from unmodified ones. All the detected spikes were sperated into different clusters using scanning K-means algorithm.

74

Table 6.1: Normalized extracellular recording measures for modified microelectrodes. All the values are normalized to the mean of the corresponding measure from unmodified microelectrodes. IBI is inter-burst interval.

	Spike Rate	P-P amplitude	RMS noise	SNR	IBI	Burst duration	Burst rate
PEDOT-PSS-CNT	1.7 ± 0.5	1.2 ± 0.1	1.0 ± 0.1	1.4 ± 0.2	1.2 ± 0.3	1.6 ± 0.5	1.6 ± 0.4
PEDOT-PSS	1.3 ± 0.4	0.9 ± 0.1	0.9 ± 0.1	1.0 ± 0.2	1.2 ± 0.6	1.1 ± 0.2	1.2 ± 0.4

The PEDOT-PSS-CNT and PEDOT-PSS modified microelectrodes had yields, i.e. percentage of microelectrode sites showing observable single units, of 53% and 56%, respectively. However, the yield was only 34% for the unmodified microelectrodes which is consistent with prior work [6,85]. The yield for modified microelectrodes was significantly higher than for unmodified microelectrodes ($P < 0.01$). For those microelectrodes that showed activity, the number of units per microelectrode was 1.53 ± 0.09 for PEDOT-PSS-CNT and 1.65 ± 0.12 for PEDOT-PSS modified microelectrodes. The unmodified microelectrodes had 1.35 ± 0.1 units per microelectrode. The cumulative distribution of microelectrodes with active units (Fig. 6.4) shows that comparing to unmodified microelectrodes, it was more likely to have a modified microelectrode with at least one active unit ($P < 0.05$).

The differences between the extracellular recordings from both modified and unmodified microelectrodes were further investigated by examining SNR and burst parameters (Table 1). No significant differences were found for spike rate, SNR and burst parameters, which suggests the electrophysiological properties of neurons around the modified microelectrodes were not affected by the nanomaterials.

6.3.3 Immunocytochemistry

Immunostaining for neurons and astrocytes was performed on PEDOT-PSS-CNT (N = 2 networks) and PEDOT-PSS (N = 1 network) modified MEAs to assess the proximity of the cells to the microelectrodes. As illustrated in Fig. 6.5, the mean intensity of the NeuN marker was higher by 36% and 43% between 10 μm to 40 μm away from the center of
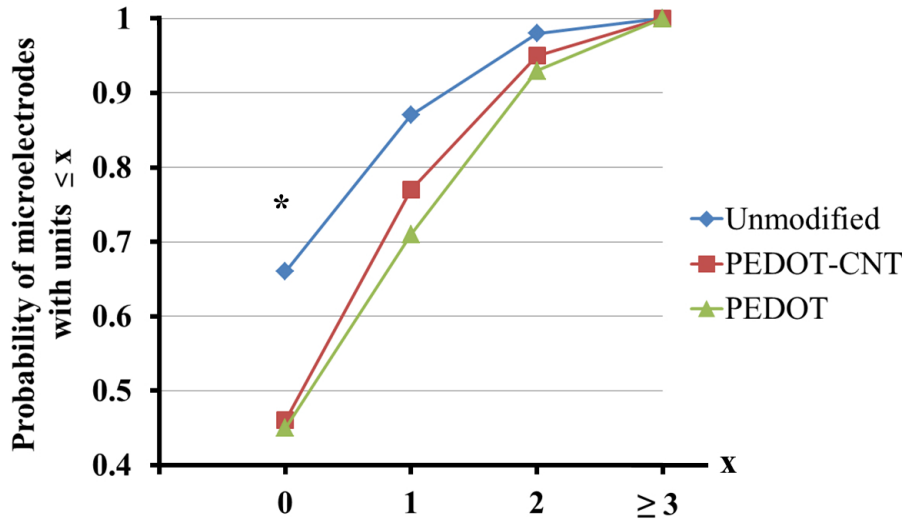
Figure 6.4: The cumulative distribution of electrodes with x active units ranging from 0, 1, 2 or ≥ 3. The unmodified microelectrodes had a higher percentage of being non-active ($x = 0$). The modified electrodes were compared against non-modified electrodes. * denotes the significance ($P < 0.05$).

the microelectrodes for PEDOT-PSS-CNT and PEDOT-PSS compared to the unmodified group ($P < 0.05$). These findings suggest that more neuronal cell bodies were localized proximal to the modified microelectrodes than unmodified ones, an observation consistent with the higher yield for modified microelectrodes. In contrast, the immunostaining for GFAP yielded no statistical difference, suggesting that the density of astrocytes was similar for modified and unmodified microelectrodes (data not shown).

6.4 Discussion

Our findings suggest that modifying microelectrodes with thin layers of PEDOT-PSS-CNT and PEDOT-PSS increases the yield in the extracellular activity for *in vitro* neuronal cultures whereas the electrophysiological behavior of the networks might not necessarily be affected. By depositing these nanomaterials on every other microelectrode of a MEA, we were able to study and compare the effect of such coatings on neuronal recordings while the variables such as inter-culture differences were minimized. Furthermore, we observed

76
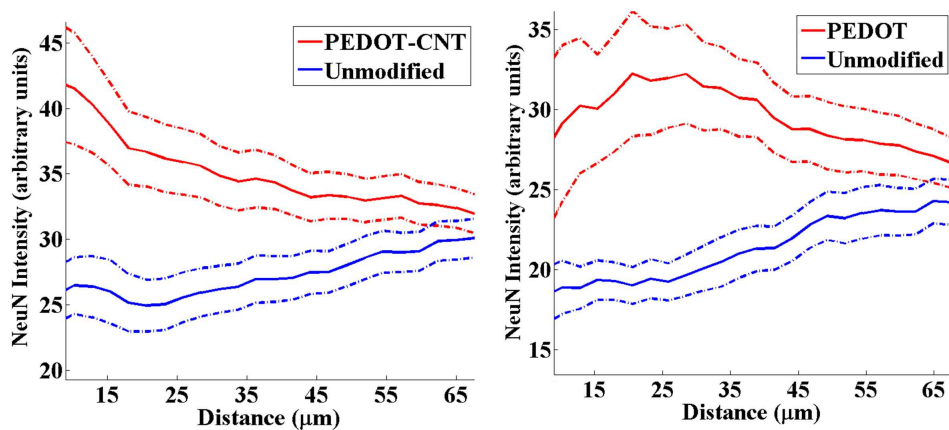
Figure 6.5: Quantitative immunohistochemical analysis of neuronal nuclei using NeuN for PEDOT-PSS-CNT (left) and PEDOT-PSS (right) modified microelectrodes. NeuN intensity suggests there was a higher density of neuronal cell bodies around the coated microelectrodes (between the 10 μm to 40 μm away of the center). The solid line in every figure is the mean and the dashed lines are standard error of the mean. ($P < 0.05$)

that the improvement in neuronal recording yield was concurrent with an increased density of neuronal cell bodies around the coated microelectrodes. Considering that the action potentials rapidly decay over distance in extracellular environment [168, 178], a larger yield from modified microelectrodes could be potentially explained by presence of more neurons in proximity of such electrodes, a finding consistent with our immunocytochemistry results.

Although, no significant differences were detected in spike rate and burst parameters between modified and unmodified microelectrodes, some previous studies reported higher spike rate specifically for neurons on CNT-coated substrates [179, 180]. However, those results were in the presence of pristine CNTs, which either had vertically-aligned 3D structures or were deposited on large surface areas e.g. glass coverslips. Our SEM observations indicate that the coatings in the present study had thin mesh-like morphology and were confined to the microelectrode area. The differences in the surface density of the nanomaterials between previous work and the present study may explain the lack of network modulation observed in our experiments.

77

Considering the large decrease in the impedance after modification of the microelectrodes with PEDOT-PSS and PEDOT-PSS-CNT, lower RMS noise values on the modified microelectrodes was expected [181]. Surprisingly, the RMS noise was similar for modified and unmodified microelectrodes, which could possibly be due to an increase in the impedance of the coated films over time for modified microelectrodes. As reported in [153], aggregation of proteins in the polymer layer could result in such an increase in the modified microelectrodes. Furthermore, delamination of the coatings, which has been reported to be a limitation for many CPs coatings, might also be a reason that the modified microelectrodes did not sustain their low impedance [152, 182].

Compared to PEDOT-PSS coatings, the embedded CNTs inside the PEDOT-PSS-CNT coatings provided higher electrical conductivity, which was confirmed by the EIS measurements. The more porous surface observed under SEM for PEDOT-PSS-CNT microelectrodes also suggests a larger surface area compared to the PEDOT-PSS coating. These findings are in accordance with prior work suggesting excellent conductivity and huge surface area for PEDOT-PSS-CNT surfaces [157]. However, in our study, such distinction in the impedance and the surface morphology for PEDOT-PSS-CNT coatings did not result in substantial differences in neuronal recordings between these microelectrodes and those that were modified with PEDOT-PSS only.

Interestingly, our observations from immunocytochemistry suggest a higher density of neuronal cell bodies around modified microelectrodes. It has been reported that nanoscale surface topography of CNT or PEDOT-PSS films could provide a scaffold structure which might influence the neuronal adhesion [182]. In addition, it is also possible that adhesion promoters e.g. laminin as well as growth factors in cell culture medium could accumulate in the deposited films and provide a suitable microenvironment for neuronal attachment and growth [183].

6.5   Conclusion

We have investigated the possible effects of PEDOT-PSS-CNT and PEDOT-PSS modified microelectrodes on neuronal activity *in vitro*. Our findings suggest that the yield in neuronal recordings was higher for the modified electrodes while the electrophysiological behavior of the network remained similar for both modified and unmodified electrodes. Such improvement *in vitro* may be due to the closer proximity of the neurons to the modified electrodes rather than a reduction in noise. Although the role of CNTs must be further investigated in improving the stability of the coating, we did not find any significant differences in neuronal recordings *in vitro* between PEDOT-PSS-CNT and PEDOT-PSS modified microelectrodes.

Citation & Contributions:

This work has been published as:

- **H.Charkhkar**, G.L.Knaack, H.S.Mandal, E.W.Keefer, J.J.Pancrazio. Effects of carbon nanotube and conducting polymer coated microelectrodes on single-unit recordings *in vitro*. Proceedings of 36th Annual International Conference of the IEEE, Engineering in Medicine and Biology Society (EMBC'14), Chicago, IL, Aug. 2014, pp. 469-473.

    HC wrote the paper. HC analyzed the data and generated the plots. GLK performed the primary cell cultures and edited the manuscript. EWK provided the recipe for PEDOT-PSS-CNT solutions. HSM helped with the scanning electron microscopy. JJP and HC designed the experiments. JJP revised the manuscript and provided feedback on data visualization and data analysis.

Chapter 7: Chronic intracortical neural recordings using microelectrode arrays coated with a new variant of PEDOT

7.1 Introduction

Implantable MEAs are miniature devices that allow recording of the electrical activity of single or multiple neurons in the brain. Compared to other modalities such as functional magnetic resonance imaging (fMRI) or electroencephalogram (EEG), implantable MEA recordings have higher temporal and spatial resolution which make them suitable candidates for applications such as brain-machine interfaces [184–186]. Although MEAs are fabricated in different shapes and designs, small electrodes facilitate spatial selectivity and high electrode density on a probe. However, reduced electrode size is associated with an increase in impedance, which elevates thermal noise level [40, 187] and contributes to poor electrical coupling between the electrode and tissue [42]. Simply, high impedance electrodes could result in low SNR or loss of neuronal signals at the interface. Therefore, it is desirable to increase the effective surface area of the electrodes while keeping their geometrical area unchanged.

CPs such as PEDOT and polypyrrole (PPy) have frequently been utilized over the last decade as coatings for neural probes [151, 171, 188, 189]. The CPs reduce the electrode impedance by providing a porous and fuzzy surface. In addition, they benefit from excellent intrinsic electrical conductivity and flexibility in use [188,190,191]. Among the CPs, PEDOT in particular has gained more interest because of its electrochemical characteristics including a low oxidation voltage for the monomer [192] and high electrical conductivity due to the conjugate double bonds in the polymer backbone [193]. However, the long-term stability of the PEDOT film, especially for chronic neural applications, is still unclear. In a study

80

by [194], the PEDOT coated microelectrodes on silicon shank probes were able to register activity only up to 8 days. In another report [195], the PEDOT coated microwires showed mechanical delamination after 5-6 weeks.

Electrochemical polymerization of the EDOT monomer requires a supporting counter ion which is embedded in the polymer film and plays an important role in the stability, electrical characteristics, and macroscopic features of the deposited polymer [196, 197]. The most common counter ion for PEDOT electrochemical polymerization is PSS [40, 43, 188, 198]. However, there have been new reports that replacing PSS with a smaller molecule could enhance the electrical properties of the PEDOT as well as its long term stability [197, 199]. Prior work has shown that, neural probes coated with PEDOT polymers which were doped with perchlorate ions, smaller than PSS, showed unit activity up to six weeks post implant [171]. Recently, our group demonstrated improving the in vitro long-term stability of PEDOT by using an alternative smaller counter ion, TFB [200]. PEDOT-TFB microelectrodes exhibited smaller impedance and longer lifetime in age acceleration studies when compared with PEDOT-PSS or PEDOT-PSS blended with carbon nanotubes [200].

Here, we report for the first time the use of highly stable PEDOT-TFB coated microelectrodes for long-term neural recordings. We show that PEDOT-TFB microelectrodes on average register more units compared to control gold (Au) microelectrodes. In addition, we demonstrate that the impedance of PEDOT-TFB microelectrodes remains lower than Au microelectrodes over at least 12 weeks. Moreover, our equivalent circuit model of the in vivo EIS data suggests stability of the polymer-related components of the circuit model for the duration of the study.

7.2   Material and Methods

7.2.1   Electrochemical modification of neural probes

Single-shank silicon-based chronic probes were purchased from Neuronexus (Neuronexus Inc., Ann Arbor, MI). Each probe consisted of 16 iridium microelectrodes with surface area

81

of 177 μm^2 and 100 μm inter-microelectrode distance. All the electrochemical modifications and characterizations were done using a CHI 660D electrochemical workstation (CH Instruments Inc., Austin, TX). Similar to the process described in (Mandal et al., 2015), initial impedance profiles of the microelectrodes were measured by running EIS in PBS over 0.1 Hz to 100 KHz using a 20 mV sine wave. A thin layer of Au was electrochemically deposited on the microelectrodes using an aqueous solution of 5 mM chloroauric acid (HAuCl$_4$) in 0.1 M NaClO$_4$ as the supporting electrolyte. To avoid cyanide incorporation in the deposited Au, chloroauic acid was preferred over potassium dicyanoaurate which is commonly utilized in Au electrodeposition. The deposition was performed by running fast voltage sweeps between -1.5 to 0 V at a rate of 1 V/s for $\sim$ 6 cycles. Subsequently, PEDOT-TFB was deposited on alternate blocks of 4 consecutive microelectrodes in each probe. To counterbalance the bias due to the position of the PEDOT-TFB modified microelectrodes in the cortical layers in the brain, the location of the PEDOT-TFB blocks was also shifted by 4 sites between the microelectrodes. The scheme for the probe modification and an optical image of a modified probe are shown in Figs. 7.1A & 7.1B. The solution for the conductive polymer deposition contained 10 mM EDOT, the PEDOT monomer, in 0.1 M tetrabutylammonium tetrafluoroborate in acetonitrile. The deposition process was performed by cyclic voltammetry between 0 to 1.2 V with a scan rate of 1 V/s. The microelectrodes were then cycled between 0 and 0.5 V in PBS, which exchanges the loosely attached TFB anions, to reduce possible cytotoxic effects. The successful deposition after Au and PEDOT-TFB deposition was confirmed with EIS measurements on the deposited microelectrodes. A pilot study revealed that the polymer coated microelectrodes showed less variation in impedance if they were kept moist. As such, the probes were prepared within 3 days before the implantation and stored in deionized water until they were packaged for sterilization. The probes were then air dried and sterilized by exposure to ethylene oxide gas for 24 hours.
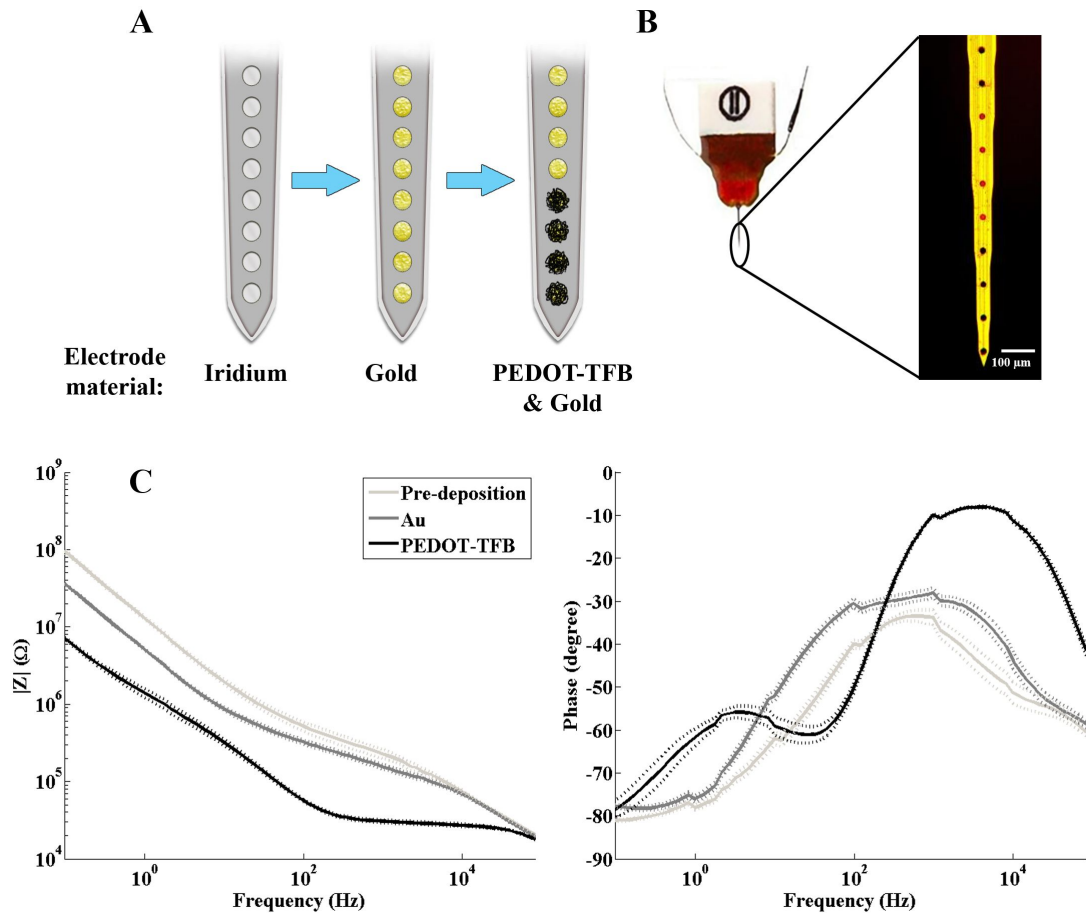
Figure 7.1: The probe modification process and changes in impedance due to gold (Au) and PEDOT-TFB deposition. (A) The single shank 16-microelectrode probes were first electrodeposited with Au. The probe microeelectrode sites were grouped in blocks of 4 and microelectrodes in every other block were modified with PEDOT-TFB. (B) An optical image of the modified probe showing 10 microelectrodes. (C) EIS Magnitude (left) and phase (right) versus frequency for a single probe after modifications with Au and PEDOT-TFB. The solid lines are the mean and dotted lines are SEM (N = 16 microelectrodes for pre-deposition and Au, N = 8 for PEDOT-TFB).

83

7.2.2 Surgical procedure

Five Long Evans rats were implanted in motor cortex with the modified probes using a similar procedure described in [200]. Briefly, anesthesia was induced by applying 5% isoflurane oxygen mixture at a rate of 1 L/min. The animal was secured and positioned in a stereotaxic apparatus (David Kopf Instruments, Tujunga, CA). Puralube eye ointment (PharmaDerm, Florham Park, NJ) was applied. Four skull screws were placed in burr holes drilled with a micro drill. After locating bregma, the craniotomy window was prepared at -1.5 to +1.5 mm anterior/posterior and 0.5 to 2.5 mm medial/lateral. The probe was placed in a holder attached to the stereotaxic arm and positioned over the craniotomy, avoiding any surface vasculature. The ground and reference wires of the probe were secured to separate skull screws and coated with conductive silver paint (West Chester, PA). A hole was made in dura just below the tip of the probe and then the probe was lowered to the surface of the cortex. The probe was inserted using a micropositioner and advanced every 40 seconds at the following increments: 100 m steps for the first 400 μm, then 50 μm steps to a depth of 1500 μm, and finally 25 μm steps to the final depth of 1800-2000 μm. This was done to monitor neuronal spiking throughout insertion and locate a position where activity could be recorded on at least half of the microelectrodes. The craniotomy was filled with silicone elastomer (kwik cast, World Precision Instruments, Sarasota, FL) and allowed to dry. To secure the probe to the skull and screws, a layer of Loctite prism 454 adhesive (Electron Microscopy Science, Hatfield, PA) was applied and dried instantly with Loctite accelerant 7452 (Newark Element 14, Chicago, IL). Dental cement (Lang Dental Manufactures, Wheeling, IL) was used to cover the screws and adhesive to create a robust head cap. To close the surgery site, skin was attached to the dental cement using gluture (World Precision Instruments, Sarasota, FL), and a non-prescription tri-antibiotic cream (Target Corporation, Minneapolis, MN) was applied. Ketoprofen was administered subcutaneously at 5 mg/kg and continued twice daily for three days. Gentamicin was also injected subcutaneously at 8 mg/kg and continued once a day for one week. All animal procedures comply with the

National Institute of Health guidelines and were approved by the Institutional Animal Care and Use Committee at George Mason University, Fairfax, VA.

7.2.3 Data collection

At day 2 and 7 post implant, neural recordings and impedance measurements were performed for each animal. Data were collected weekly thereafter for the remainder of the study. The duration of the study was intended for 12 weeks, but data collection continued for two of the animals until weeks 19 and 23. Animals were freely moving during the neural recording sessions. However, to reduce the noise, animals were anesthetized for the EIS data collections.

7.2.4 Neural recordings and data analysis

Neural signals were acquired using a Cerebus system (Blackrock Microsystems, Salt Lake City, UT) in 10-minute recording sessions. The data were sampled at 30 KHz and high-passed filtered at 250 Hz. To remove any movement artifacts, a common average reference was subtracted from each channel [201] using a custom routine in Matlab (Mathworks, Natick, MA). For spike detection, a threshold was set at six standard deviations from the mean noise level for each individual channel. The captured spikes were then sorted for each channel into well resolved units using the Scanning K-means in Offline Sorter V.3 (Plexon, Inc, Dallas, TX) and confirmed by visual inspections. Similar to [171, 202], the SNR ratio for a unit was defined as:

$$SNR = \frac{Peak-to-peak\ amplitude\ of\ the\ mean\ waveform}{2 \times RMS\ noise\ of\ the\ recording\ site} \tag{7.1}$$

A unit was considered valid if it had SNR greater than 2 [171, 194] and showed at least 30 spikes in the 10 minute recording period.

7.2.5 *In vivo* impedance measurements and circuit modeling

In vivo EIS measurements were made using a CHI 604E potentiostat by applying a 20 mV sine wave between 0.1 Hz to 100 KHz with frequencies logarithmically spaced in every decade. The measurements were in two-electrode configuration using a stainless steel skull screw as the reference electrode. The sedated animals were placed in a small faraday cage to provide electrical shield and lower the ambient noise.

The collected EIS data were fit to equivalent circuit models discussed in 7.3.4 using ZSimpWin (Princeton Applied Research, Oak Ridge, TN). A good fit was determined based on Chi-square (χ^2) value and percent error for every component of the model [189]. The acceptable χ^2 value for the models was chosen to be 10^{-2} or below with the percent error values for every circuit component at less than 10%.

7.2.6 Data analysis

Data are reported as the mean $\pm$ SEM. The statistical significance between group means was determined by analysis of variance (ANOVA). To compare the proportions from two independent samples, Z-test for proportions was utilized. In all statistical tests, P < 0.05 was considered significant. All statistical analysis was performed in either Matlab (Mathworks Inc.) or IBM SPSS Statistics (SPSS Inc.).

7.3 Results

7.3.1 Probe modification

As shown in Fig. 7.1C, the deposition of a thin Au layer on the iridium microelectrodes resulted in reduction in the impedance for frequencies between 0.1 1 KHz. The electroplated Au provides a rough surface which contributes to the lower impedance values compared to bare Ir [203]. In addition, the rough Au surface improves adhesion between the metallic microelectrode and the conductive polymer [200]. The deposition of PEDOT-TFB resulted in much greater reduction in impedance throughout the entire spectrum due to formation

86

of the porous and fuzzy polymer film. The magnitude of the impedance at 1 KHz frequency, the most relevant frequency in multiunit neuronal activity, was reduced from 2.32 ± 0.3 MΩ to 1.58 ± 0.11 MΩ (N = 16 microelectrodes) after the Au deposition and subsequently to 30.92 ± 1.18 KΩ (N = 8 microelectrodes) after the PEDOT-TFB. The phase of the impedance became more positive around 1 KHz, suggesting that increased effective surface area after the PEDOT-TFB deposition induced high conductivity of the film [204]. As shown in [200], under similar deposition profiles, PEDOT-TFB causes more reduction in impedance compared to the common variant of PEDOT specifically PEDOT-PSS. Such a difference could be explained by the role of the counter ion, TFB, which creates a more porous surface and perhaps improved crystalline structure of the polymer.

7.3.2 Neural recordings

Both Au and PEDOT-TFB microelectrodes registered well-resolved units over time (Fig. 7.2A), demonstrating that PEDOT-TFB microelectrodes can record neuronal activity in chronic studies. Overall, 78% of the PEDOT microelectrodes (N = 36 microelectrodes) and 52% of the Au microelectrodes showed (N = 38 microelectrodes) unit activity 2 days after the implantation. After 11 weeks post implantation, the percentage of microelectrodes with unit activity reduced to 39% and 33% for PEDOT and Au microelectrodes, respectively. On average, the number of units per microelectrode was significantly higher for the PEDOT-TFB compared to Au microelectrodes over 12 weeks of recordings (Fig. 7.2B, P < 0.01). As shown in Fig. 7.3A, the number of PEDOT-TFB microelectrodes with two or more units was significantly greater for the first four weeks. For the PEDOT-TFB microelectrodes with unit activity, 36% had two or more active units during weeks 1-2 and weeks 3-4. In contrast, for the Au microelectrodes with unit activity, these ratios were only 16% and 19% over the same time periods. The SNR values spanned a wide range between 3-25 for both PEDOT-TFB and Au. However, PEDOT-TFB microelectrodes had significantly more units with SNR greater than 6 for the first two weeks (Fig. 7.3B). The higher number of units per microelectrode and better SNR values for the first few weeks suggest the improved

87
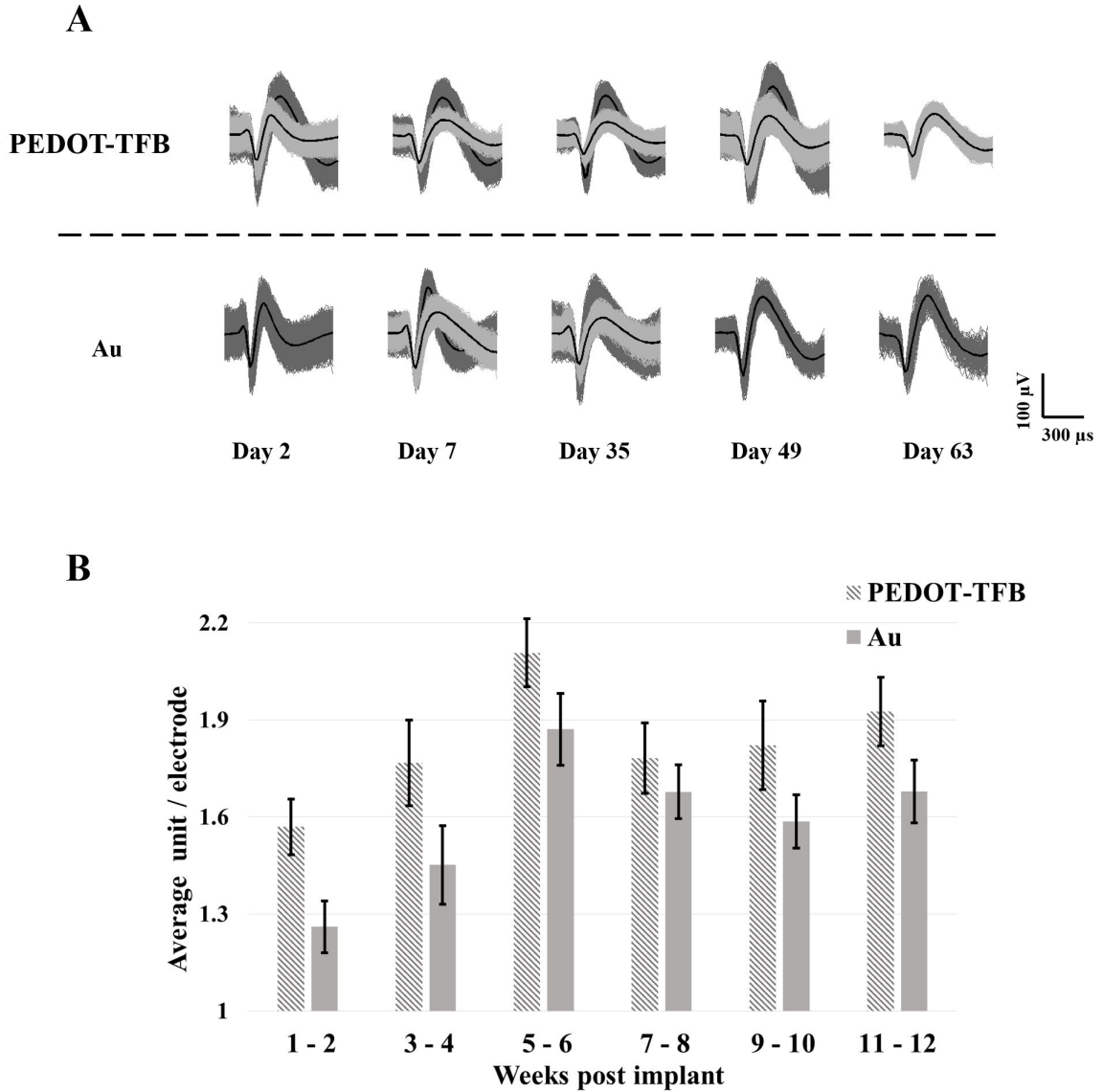
Figure 7.2: Unit recordings from PEDOT-TFB and Au microelectrodes. (A) Representative well-resolved units registered by a PEDOT-TFB (top) and Au (bottom) microelectrodes over time. (B) The average number of units per microelectrode. The PEDOT-TFB microelectrodes had significantly higher number of units per microelectrode ($P < 0.01$).
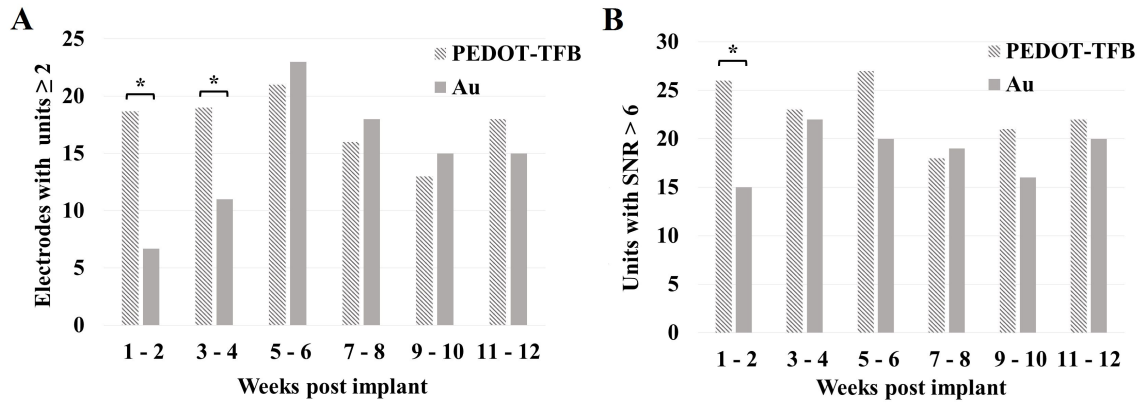
Figure 7.3: Comparing multiple unit detection and high SNR recordings between PEDOT-TFB and Au. (A) Compared to Au, the number of PEDOT-TFB microelectrodes with two or more units was significantly greater for the first four weeks ($P < 0.05$). PEDOT-TFB microelectrodes showed more units with SNR greater than 6 only for the first two weeks.

recording capability with PEDOT-TFB microelectrodes, at least for a limited time. It has been suggested that brain-tissue response and the glial scar formation around an implanted probe would impact the chronic recordings [205]. Although PEDOT-TFB microelectrodes had lower impedance compared to Au microelectrodes, the root mean square (RMS) noise was similar in both Au and PEDOT-TFB microelectrodes. This observation is consistent with other reports that the dominant noise in unit recordings is not necessarily due to the thermal noise of the microelectrodes [206].

7.3.3   Impedance profiles *in vivo*

As demonstrated in Fig. 7.4, over the first week of the implantation, the magnitude of the impedance at 1 KHz increased in both Au and PEDOT-TFB microelectrodes. Such a trend is consistent with prior work reporting an increase in impedance values for intracortical microelectrode arrays after implantation [183, 194, 207]. However, compared to Au microelectrodes, PEDOT-TFB microelectrodes had consistently lower impedance values at 1 KHz over time (P < 0.05). Figure 7.5 shows the Bode plots for the EIS measurements for both PEDOT-TFB and Au microelectrodes prior to implantation, as well as 2, 14, and 70 days
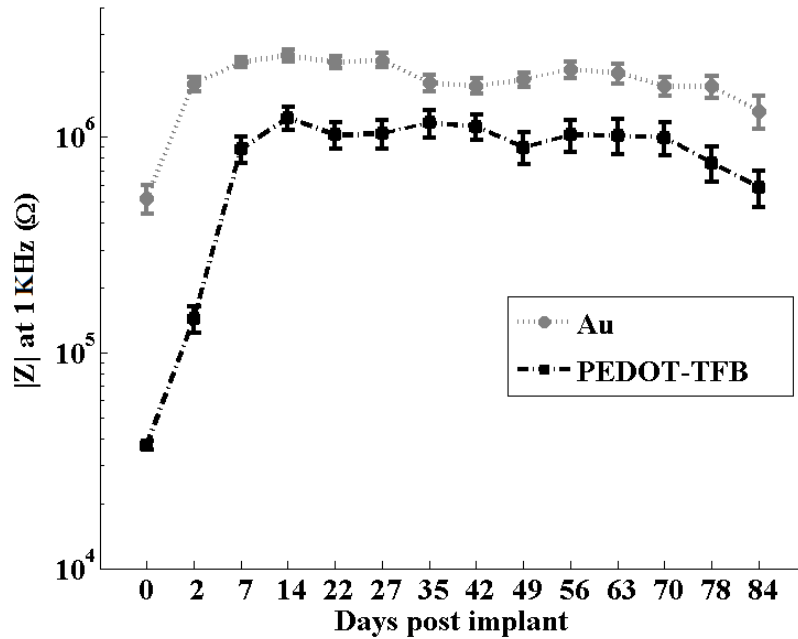
Figure 7.4: The impedance at 1 KHz for Au and PEDOT-TFB microelectrodes over time. The PEDOT-TFB microelectrodes maintained lower impedance for 12 weeks (P < 0.05). The error bars denote the SEM (N = 36 for PEDOT-TFB microelectrodes and N = 38 for Au microelectrodes).

post implantation. The impedance values at 1 KHz for PEDOT microelectrodes initially increased to 143.5 ± 20.4 KΩ and then to 1.22 ± 0.15 MΩ after the first 2 and 14 days of implantation, respectively (N = 36 microelectrodes). However, as shown in Fig. 7.5A, between days 14 to 70, the EIS did not show any marked differences throughout the spectrum suggesting the stability of the PEDOT-TFB film over time. For the Au microelectrodes, the 1 KHz impedance increased from 520.4 ± 80.3 KΩ prior to implantation to 1.76 ± 0.13 MΩ and 2.16 ± 0.15 MΩ at days 2 and 14 post implantation, respectively (N = 38 microelectrodes). Although the 1 KHz impedance remained almost unchanged following implantation, it can be seen in Fig. 7.5B that impedance values at low frequencies, e.g. below 10 Hz, show consistent reduction over time. Such a reduction in impedance at low frequencies might be due to delamination of the insulator around the edges of the metal microelectrodes [208].

90

Interestingly, the 1 KHz impedance for the PEDOT-TFB microelectrodes which registered unit activity was significantly lower compared to those without activity ($P < 0.05$). As shown in Fig. 7.6, after day 14 of implantation, the difference in the impedance could be seen between the PEDOT-TFB microelectrodes with and without activity. However, we did not find a similar trend for the Au microelectrodes. This observation suggests that the chance of identifying units on PEDOT microelectrodes is increased if they have lower impedance.

7.3.4   Equivalent circuit modeling

To interpret the EIS results and gain insight about the changes at the microelectrode-tissue interface, we fit the data according to previously well-established models for both the microelectrodes and the tissue [197, 209, 210]. The equivalent circuit models, which include separate compartments for the microelectrode and the tissue, for the microelectrode-tissue interface for both PEDOT and Au microelectrodes are shown in Fig. 7.7. The model for the tissue compartment included a tissue resistor (R_t), a tissue capacitor (C_t), and a resistor for the encapsulation layer around the device (R_{en}). The C_t represents the membrane capacitance of the cells in the surrounding tissue and Rt represents the resistive extracellular pathways between the cells [211, 212]. For the PEDOT-TFB microelectrodes, the polymer film was characterized by a resistor (R_{poly}), describing the charge transfer resistance of the polymer, in series with a constant phase element (Q_{poly}) [213] representing the diffusion-related effects mainly due to the porous surface of the polymer [197, 203]. In parallel with R_{poly} and Q_{poly}, there is a capacitor (C_{dl}) which represents the double layer capacitance for the entire polymer surface [176, 197]. The model for the Au microelectrodes consists of a constant phase element (Q_{gold}), representing the rough surface of the Au, in parallel with a resistor (R_{gold}), representing the impurities trapped in the deposited Au [203].

The results for both PEDOT-TFB and Au microelectrode-tissue interfaces for selected time points are summarized in tables 1 and 2, respectively. The R_t and R_{en} for both microelectrode types increased from day 2 to 7 suggesting changes in the brain tissue due to the

91
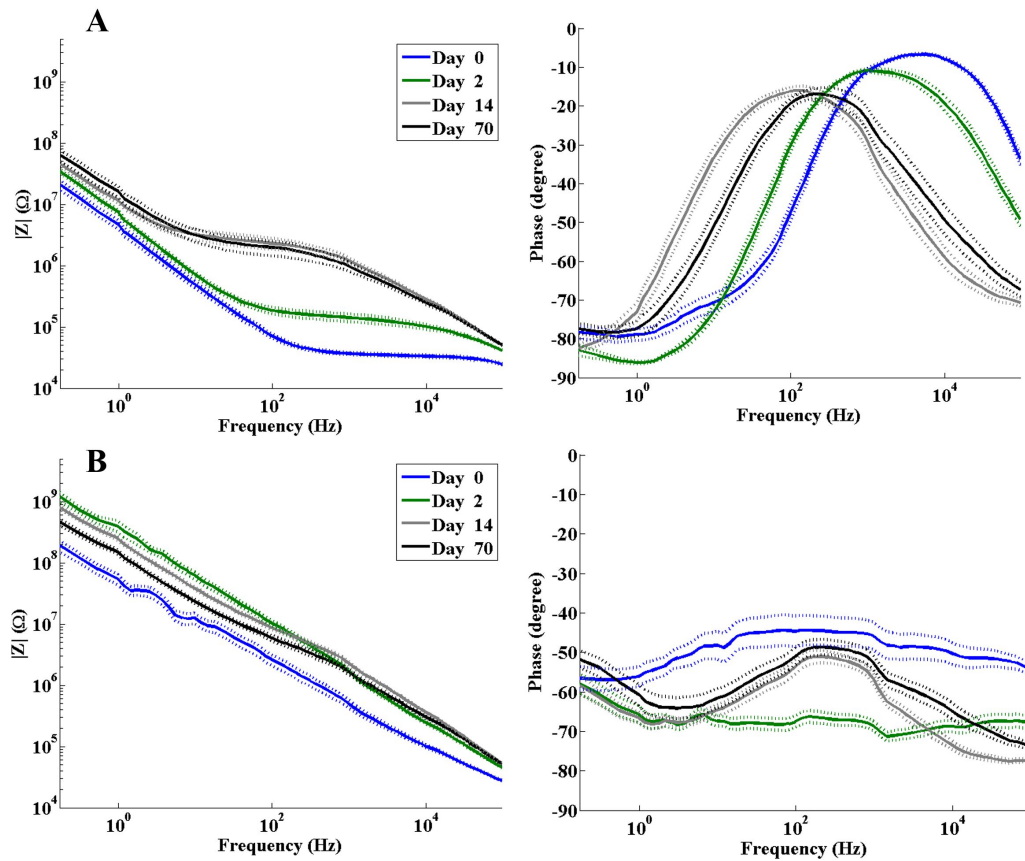
Figure 7.5: Bode plots for the EIS measurements from both PEDOT-TFB and Au micro-electrodes prior to implantation, as well as 2, 14, and 70 days post implantation. A large increase in the impedance magnitude and a shift in the phase occurs for both PEDOT-TFB and Au microelectrodes between pre-implant and day 2 post implant. Between days 14 70, the impedance remains stable throughout the whole frequency spectrum for PEDOT-TFB microelectrodes whereas the Au microelectrodes show reduction in the magnitude of the EIS for low frequencies.
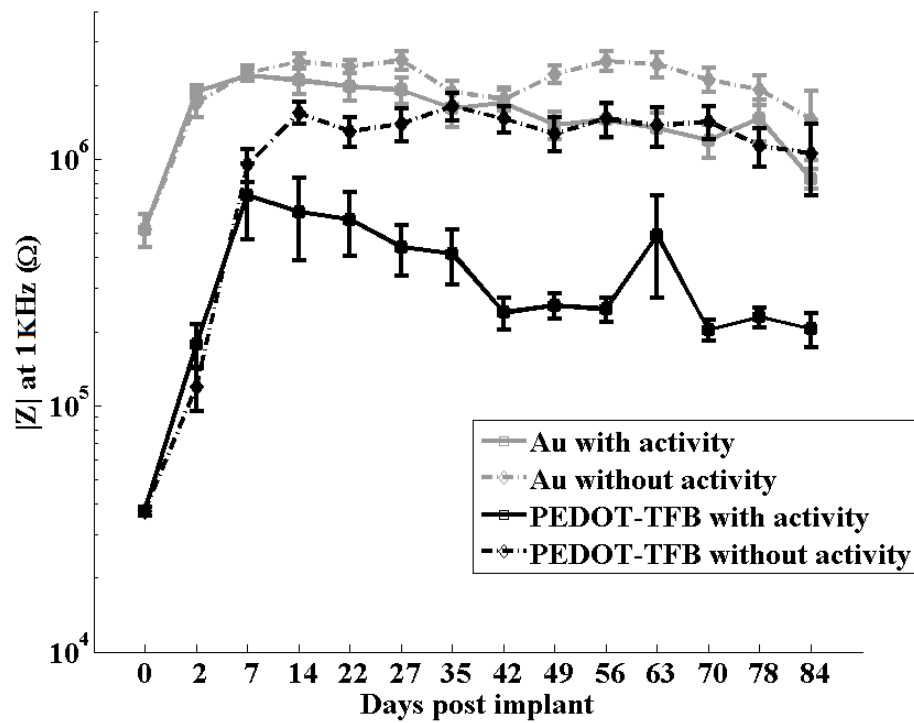
Figure 7.6: The 1 KHz impedance for the PEDOT-TFB microelectrodes which registered unit activity was lower compared to those without activity ($P < 0.05$). Date are shown as mean $\pm$ SEM.
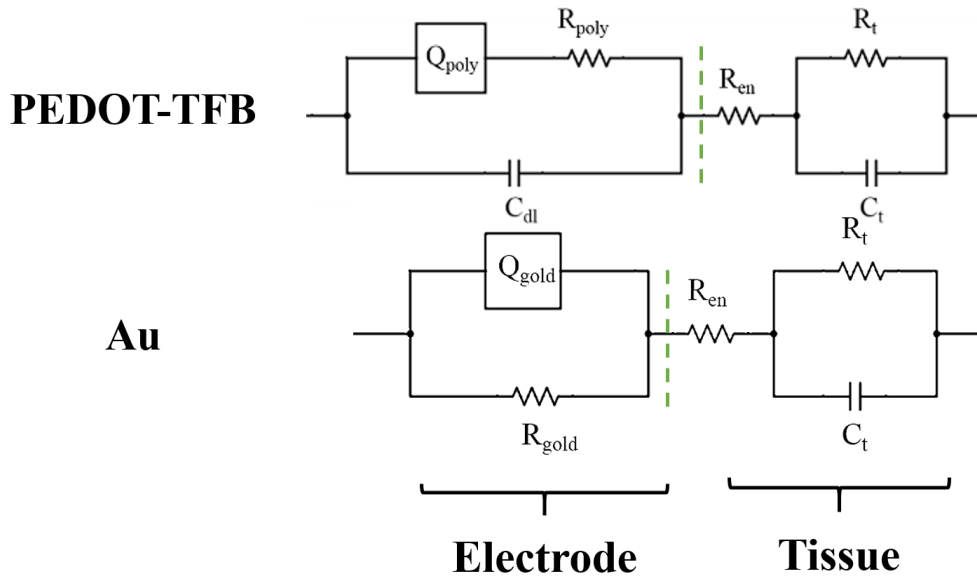
Figure 7.7: Equivalent circuit models to fit the EIS data for PEDOT-TFB and Au microelectrodes-tissue interfaces.

device. However, the R_t values for PEDOT-TFB microelectrodes were much smaller than Au microelectrodes, implying a possible differential response for the two interfaces. The C_t in the Au microelectrode-tissue drops $\sim$ 3.5-fold from day 2 to 7 which could be due, at least in part, by cell migration from the Au microelectrodes. The polymer related parameters exhibit large changes in the first week post implantation mainly due to the interaction between the tissue and the polymer film. Possible protein absorption or cell attachment to the surface of the PEDOT microelectrode has been shown to affect the microstructure of the polymer surface [190, 214]. However, as shown in Fig. 7.8B after the first week, both R_{poly} and Q_{poly} show stable trends suggesting the stability of the polymer and lack of degradation of the PEDOT or delamination from the underlying Au-coated substrate. As shown in Fig. 7.8A, the tissue resistance (R_t) for the PEDOT microelectrodes was highest between weeks 1-3 and afterward decreased gradually for 4 consecutive weeks. This observation was consistent with prior histology findings on acute tissue response after the cortical implants [215, 216]. We did not observe a similar effect for the Au microelectrodes indicating that the R_t was already so high for the Au-tissue interface that any subtle changes could not be

www.manaraa.com
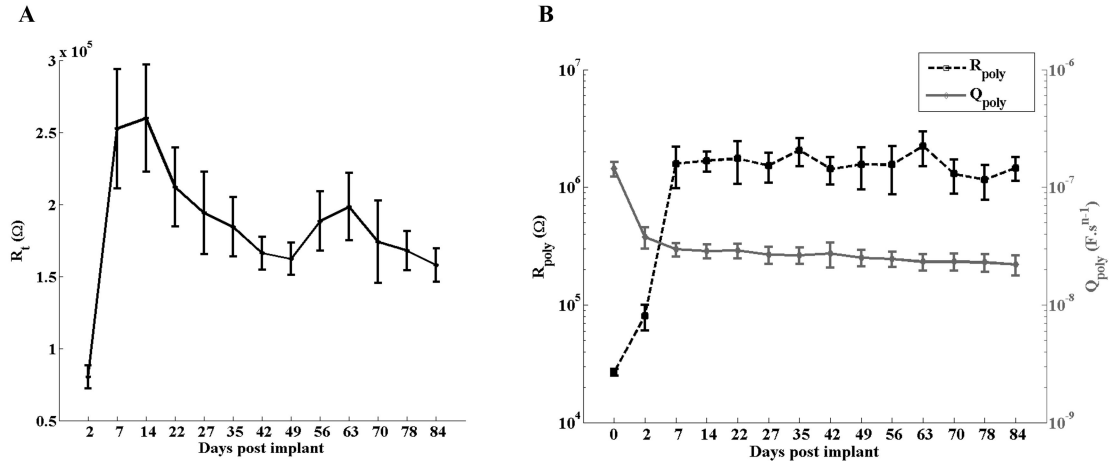
Figure 7.8: The tissue resistance for the PEDOT-TFB microelectrodes (A) and the polymer-related components, Rpoly and Qpoly (B) over time. R_{poly} and Q_{poly} in the circuit model reflect the characteristics of the microscopic structures in the polymer film. R_t for PEDOT-TFB microelectrodes reaches its maximum value between weeks 1 and 2. Afterward, the tissue resistance decreases to a level approximately 75% of the maximum.

detected.

We also used the circuit model to investigate the basis for differences in the impedance between the PEDOT-TFB microelectrodes with and without activity reported in section 7.3.2 and shown in figure 7.6. It was found out that both C_{dl} and R_{poly} are significantly different between the two groups. As shown in Fig. 7.9, the C_{dl} was much higher for PEDOT-TFB microelectrodes that registered activity, suggesting the larger functional interface for these recording sites. In addition, the PEDOT-TFB microelectrodes with activity had lower R_{poly} which suggests that the morphology of the polymer film had much larger changes for those PEDOT microelectrodes that did not register any neuronal activity.

7.4 Discussion

In this work, we demonstrated stable long-term unit recordings with PEDOT polymer doped with a small counter ion, TFB. The PEDOT-TFB coating showed marked lower impedance and higher number of units per microelectrode over time. While most of the prior work with

95
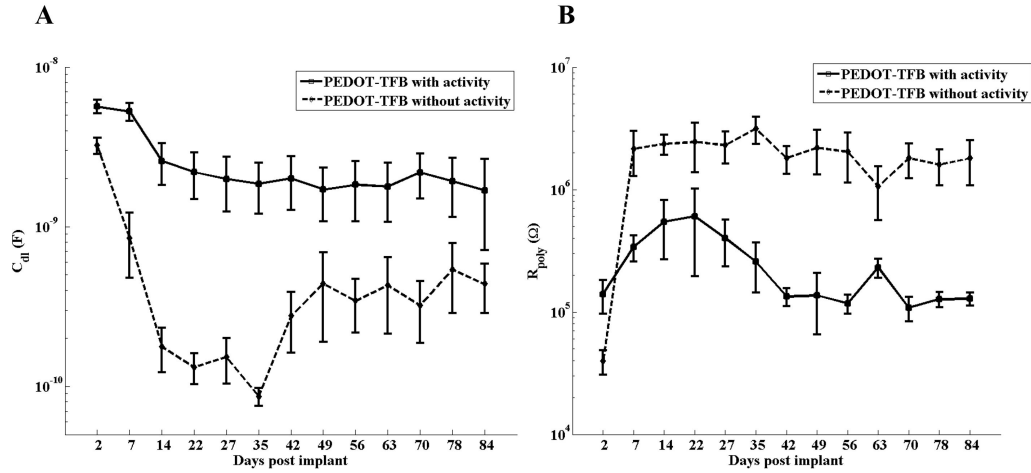
Figure 7.9: The double layer capacitance (A) and polymer charge transfer resistance (B) showed the largest differences for PEDOT-TFB microelectrodes with and without unit recordings.

PEDOT coated neural probes reported recordings for up to 6-7 weeks [43,171,183,194,195], our recordings lasted at least for 12 weeks and for two studies we were able to discern well-resolved units beyond 18 weeks. Such long-term recordings suggest that this new variant of PEDOT may be advantageous for chronic neural applications.

A major concern with any new materials for invasive applications is the possible toxic effects that could impede its utility especially for brain implants. Consistent with the lack of in vitro functional toxicity of the material reported by our group previously [200], our long lasting neuronal recordings with PEDOT-TFB microelectrodes suggest the suitability of this material in vivo for, at least, the duration of the study.

We observed a large increase in the impedance after implantation throughout the whole frequency spectrum in both Au and PEDOT-TFB microelectrodes. Similarly, an increase in impedance was also reported previously [207] where the findings suggested that this affect was due to the change in the microelectrode-electrolyte interface and not degradation the microelectrode material. We also observed steady increase in impedance for the first week which reached a plateau afterward. As suggested by Ludwig and co-workers [171], the early brain-tissue response to the implant starts after the implantation and lasts for 1-2 weeks.

96

Table 7.1: The fitted parameters for the equivalent circuit model for PEDOT-TFB microelectrode-tissue interface. For the pre-implant, the R_{en} is the resistance of the electrolyte.

	Pre-implant	Day 2	Day 7	Day 28	Day 56	Day 77
Q_{poly} (nF.cm^{-2}.s^{n-1})	142.5 ± 20.4	37.6 ± 7.7	29.6 ± 3.8	26.6 ± 4.3	24.5 ± 3.6	23.0 ± 3.9
n (0<n<1)	0.87 ± 0.02	0.97 ± 0.02	0.91 ± 0.01	0.90 ± 0.01	0.93 ± 0.01	0.93 ± 0.01
R_{poly} (MΩ)	0.02	0.08 ± 0.01	1.6 ± 0.6	1.7 ± 0.4	1.5 ± 0.6	1.2 ± 0.3
C_{dl} (nF)	0.07 ± 0.01	4.2 ± 1.0	2.3 ± 0.6	0.9 ± 0.3	0.8 ± 0.2	1.0 ± 0.3
R_{en} (KΩ)	7.2 ± 0.3	11.5 ± 0.4	15.8 ± 0.7	13.2 ± 0.6	12.3 ± 0.6	12.1 ± 0.7
R_t (KΩ)	N/A	80.2 ± 7.9	252.5 ± 41.5	190.1 ± 28.7	188.2 ± 20.5	167.5 ± 13.5
C_t (pF)	N/A	49.3 ± 1.4	58.1 ± 3.3	59.6 ± 4.2	62.7 ± 4.8	55.8 ± 3.7

In this period, the swelling around the probe may occur such that microglia and reactive astrocytes begin to accumulate around the probe. Our findings show the number of microelectrodes with two or more units were higher for PEDOT-TFB microelectrodes (compared to Au) only for the first 4 weeks. Similarly, when compared to Au, the PEDOT-TFB microelectrodes had more unit with high SNR only for the first two weeks. This observation suggests that although low-impedance microelectrodes could potentially improve the neural recordings, for the long-term applications, other factors such as brain-tissue response could mask the long-term benefits of microelectrode coating.

Recently there has been an interest to utilize polymer-based approaches to develop neural probes with minimal brain-tissue response [217–219]. Examples include neural probes covered with biodegradable polymers or polymer-based probes with mechanical properties similar to the brain tissue [129, 131]. Conductive polymers such as PEDOT-TFB could be well integrated in such new designs as suitable materials for the microelectrodes.

Interestingly, we observed that the impedance of the PEDOT-TFB microelectrodes at 1 KHz was significantly smaller for those that showed neuronal activity compared to those coated microelectrodes that did not. Our circuit modeling revealed that PEDOT-TFB microelectrodes with minimal changes in their surface structure (R_{poly} and C_{dl}), had higher

97

Table 7.2: The fitted parameters for the equivalent circuit model for Au microelectrode-tissue interface. For the pre-implant, the R_{en} is the resistance of the electrolyte.

	Pre-implant	Day 2	Day 7	Day 28	Day 56	Day 77
Q_{gold} (nF.cm^{-2}.s^{n-1})	180.1 ± 54.9	1.1 ± 0.2	1.2 ± 0.1	1.4 ± 0.2	2.5 ± 0.4	3.60 ± 0.7
n ($0<n<1$)	0.61 ± 0.04	0.79 ± 0.01	0.8 ± 0.01	0.78 ± 0.02	0.74 ± 0.01	0.73 ± 0.01
R_{gold} (MΩ)	204 ± 67	412 ± 76	480 ± 82	411 ± 77	430 ± 82	525 ± 86
R_{en} (KΩ)	10.4 ± 0.6	14.4 ± 1.3	16.4 ± 0.8	14.2 ± 0.9	17.0 ± 1.8	13.3 ± 2.1
R_t (MΩ)	N/A	1.6 ± 4.1	1.9 ± 3.6	2.7 ± 4.2	3.1 ± 0.7	1.9 ± 4.8
C_t (pF)	N/A	300.7 ± 56	82 ± 9	96 ± 17	103 ± 23	73.7 ± 36

chance of registering units. In our circuit model, C_{dl} represents the effective surface area of at the microelectrode-tissue interface. The reduction in C_{dl} value points to the changes in the porous surface of the film. Similarly, the increase in the R_{poly} for the PEDOT-TFB microelectrodes without activity could be due to the absorption of non-conductive species such as proteins in the pores of the polymer films [189, 220].

Our findings from the EIS measurements and the equivalent circuit modeling suggests an overall stability for the PEDOT-TFB microelectrodes by maintaining lower impedance over time compared to the control Au microelectrodes. Such long-term stability in the PEDOT-TFB coatings could be attributed to the small TFB counter ions. In comparison to macromolecular poly anions such as PSS, the smaller counter ions cause the sheets of deposited PEDOT chains to remain closer to each other [221] reducing the chance of the polymer detachment from the substrate. The small counter ions also result in high order crystallinity in the PEDOT structure which may be mechanically more stable [222].

7.5 Conclusions

Designing new probes with smaller dimension and reduced brain-tissue response seems necessary for the next generation brain-machine interface devices. Our findings suggests that the PEDOT-TFB is a chronically stable coating for neural recording microelectrodes.

Compared to metal microelectrodes, it provides a larger effective surface area and a better coupling between microelectrode and the brain tissue. As such, PEDOT-TFB could facilitate the chronic recordings with ultra-small and high-density neural arrays.

Citation & Contributions:

This work is submitted to the Acta Biomaterialia as a full-length article:

- **H.Charkhkar**, G.L.Knaack, D.G.McHail, H.S.Mandal, N.Peixoto, J.F.Rubinson, T.C.Dumas, J.J.Pancrazio. Chronic intracortical neural recordings using microelectrode arrays coated with a new variant of PEDOT. Acta Biomater. (*submitted*)

HC wrote the paper and generated all the figures. HC, GLK, and DGM analyzed the neural recordings. HC analyzed the impedance data and developed the equivalent circuit model. DGM performed the surgeries and neural data collections. HSM modified the probes. JFR developed and provided the PEDOT variant. JJP, TCD, and NP designed the study. JJP revised the manuscript and provided feedback on data visualization and analysis.

Chapter 8: Summary and future directions

In this thesis, we demonstrated new techniques to improve the utility of MEAs for both *in vitro* and *in vivo* neural recordings. In addition, we showed the suitability of neuronal cultures on MEAs as a functional assay for new applications related to brain-machine interface (BMI) and Alzheimer's disease research.

The disposable low-cost *in vitro* MEAs presented in chapter 2 could facilitate the use of MEA-based testings for large-scale screening purposes. Compared to conventional cell-based assays, the MEA-based approach provides functional endpoints and high-content screening capability. Such features make the neuronal cultures on MEA a versatile platform for a variety of applications.

For the first time, we utilized this platform to assess the functional toxicity of materials for neural implants. Our results showed an enhanced sensitivity of the MEA approach, compared to the live/dead assay, to positive control materials. We also demonstrated that *in vitro* neuronal cultures could serve as a high-content and adaptable tool to advance the development of new therapeutics for AD.

The small implantable probes with the capability of chronically stable recordings are desirable for the next generation of BMI technology. In this work, we demonstrated the successful use of PEDOT-TFB as a novel material for long-term intracortical recordings in rat models. The PEDOT polymer doped with a small counter ion, TFB showed stable unit recordings with marked lower impedance over time suggesting an increase in the effective surface area while the geometrical area of the microelectrode remained unchanged.

For the future work, we aim to extend the ideas explored in this thesis and address their shortcomings. Some of the possible future directions are as follows:

- To ascertain the consistent functionality between the low-cost disposable MEAs and the commercially-available ones, a comparison between the performance of the two

array types seems necessary. Although the new design has several advantages over the conventional glass-based MEAs, the substrate of the new MEAs is less transparent than glass. Considering the growing interest in use of optical recording and stimulation techniques in neuroscience research, it is important to make the MEA surface optically accessible through an inverted microscope. Alternative substrate materials, which can be readily substituted in the manufacturing process, would allow easy integration of optical techniques to the new MEAs.

- Microfluidic technology based on polydimethylsiloxane (PDMS) material and soft lithography has brought novel and easy-to-fabricate *in vitro* platforms. The microfluidic devices allow creation of distinct spatially separated microenviroments. Integration of microfluidic technology to the MEAs would provide a large room for developing new *in vitro* models of neuronal systems. The new MEAs presented in chapter 2 are well positioned for such integration considering their plastic-based substrate and their low fabrication costs.

- The MEA approach could be adapted to achieve more specific *in vitro* models of AD. Recent studies suggest a strong interplay between $A\beta_{42}$ oligomer effects and another protein marker associated with AD, tau protein. The modulatory effect of $A\beta_{42}$ and its dependence on tau could be validated by MEAs using harvested tissue from tau-knockout mice. The toxic effects of $A\beta_{42}$ oligomers have been reported for wide range of concentrations, it is important to minimize the variation between the $A\beta_{42}$ synthesis and the peptide structure.

- The species-specific differences between animals and humans make it difficult to accurately simulate the human phenotypes of the disease in currently available models. Considerable effort has been directed in developing human-based models by using human stem cells. Such cells could be differentiated into distinctive neuronal cells e.g. motor neurons or dopaminergic neurons. Use of these cell on MEAs would provide more realistic *in vitro* disease models and allow for patient-specific drug testing and

101

drug discovery. However, established protocols are yet required to effectively control the proliferation and differentiation of these cells on MEAs.

- The extracellular recordings of populations of neurons via MEAs contain rich and complex information on dynamics of the network and interactions between different recorded units. However, the data from the MEA recordings present important analysis challenges. The current methods such as CC or TE are designed to study the interactions between pairs of neurons. Novel multivariate methods that could incorporate multiple spike train analysis might expand our ability to understand how specific patterns of activity are generated and change over time in neuronal networks.

- The validation of the connectivity methods has so far been limited to the synthesized neuronal models. New techniques such as microfluidic barriers or optical stimulation offer controlled growth or selective activation of neurons in the dish, respectively. When integrated with MEAs, these techniques provide the possibility to validate the performance of available computational methods for network connectivity analysis using real data.

- With the growing interest to develop polymer-based *in vivo* neural MEAs, PEDOT-TFB is well suited to be utilized as a coating material for the mircoelectrodes. Different biomolecules could be linked to PEDOT-TFB to promote the electrode-tissue coupling or reduce the brain tissue response.

102

Bibliography

Bibliography

[1] P. R. Huttenlocher, "Evoked and Spontaneous Activity in Single Units of Medial Brain Stem During Natural Sleep and Waking," *Journal of Neurophysiology*, vol. 24, no. 5, pp. 451–468, Sep. 1961.

[2] J. Buchwald, S. Holstein, and D. Weber, "Multiple unit recording: technique, interpretation, and experimental applications," in *Bioelectric recording techniques*. Academic Press New York, 1973, vol. 1, pp. 201–242.

[3] R. A. Maue and V. E. Dionne, "Patch-clamp studies of isolated mouse olfactory receptor neurons." *The Journal of General Physiology*, vol. 90, no. 1, pp. 95–125, Jul. 1987.

[4] W. L. C. Rutten, "Selective Electrical Interfaces with the Nervous System," *Annual Review of Biomedical Engineering*, vol. 4, no. 1, pp. 407–452, 2002.

[5] G. W. Gross, B. K. Rhoades, H. M. E. Azzazy, and M.-C. Wu, "The use of neuronal networks on multielectrode arrays as biosensors," *Biosensors and Bioelectronics*, vol. 10, pp. 553–567, 1995.

[6] J. J. Pancrazio, S. A. Gray, Y. S. Shubin, N. Kulagina, D. S. Cuttino, K. M. Shaffer, K. Eisemann, A. Curran, B. Zim, G. W. Gross, and T. J. O'Shaughnessy, "A portable microelectrode array recording system incorporating cultured neuronal networks for neurotoxin detection," *Biosensors and Bioelectronics*, vol. 18, no. 11, pp. 1339–1347, Oct. 2003.

[7] S. Martinoia, L. Bonzano, M. Chiappalone, M. Tedesco, M. Marcoli, and G. Maura, "In vitro cortical neuronal networks as a new high-sensitive system for biosensing applications," *Biosensors and Bioelectronics*, vol. 20, no. 10, pp. 2071–2078, Apr. 2005.

[8] A. B. Schwartz, "Cortical neural prosthetics," *Annual Review of Neuroscience*, vol. 27, pp. 487–507, 2004.

[9] S. Musallam, B. D. Corneil, B. Greger, H. Scherberger, and R. A. Andersen, "Cognitive control signals for neural prosthetics," *Science (New York, N.Y.)*, vol. 305, no. 5681, pp. 258–262, Jul. 2004.

[10] L. R. Hochberg, M. D. Serruya, G. M. Friehs, J. A. Mukand, M. Saleh, A. H. Caplan, A. Branner, D. Chen, R. D. Penn, and J. P. Donoghue, "Neuronal ensemble control of prosthetic devices by a human with tetraplegia," *Nature*, vol. 442, no. 7099, pp. 164–171, Jul. 2006.

104

[11] J. J. Pancrazio, "Neural interfaces at the nanoscale," *Nanomedicine (London, England)*, vol. 3, no. 6, pp. 823–830, Dec. 2008.

[12] G. W. Gross, A. Harsch, B. K. Rhoades, and W. Gpel, "Odor, drug and toxin analysis with neuronal networks in vitro: extracellular array recording of network responses," *Biosensors and Bioelectronics*, vol. 12, no. 5, pp. 373–393, 1997.

[13] E. W. Keefer, A. Gramowski, D. A. Stenger, J. J. Pancrazio, and G. W. Gross, "Characterization of acute neurotoxic effects of trimethylolpropane phosphate via neuronal network biosensors," *Biosensors and Bioelectronics*, vol. 16, pp. 513–525, Sep. 2001.

[14] J. J. Pancrazio, J. P. Whelan, D. A. Borkholder, W. Ma, and D. A. Stenger, "Development and Application of Cell-Based Biosensors," *Annals of Biomedical Engineering*, vol. 27, no. 6, pp. 697–711, Nov. 1999.

[15] D. A. Stenger, G. W. Gross, E. W. Keefer, K. M. Shaffer, J. D. Andreadis, W. Ma, and J. J. Pancrazio, "Detection of physiologically active compounds using cell-based biosensors," *Trends in Biotechnology*, vol. 19, no. 8, pp. 304–309, Aug. 2001.

[16] S. A. Gray, J. K. Kusel, K. M. Shaffer, Y. S. Shubin, D. A. Stenger, and J. J. Pancrazio, "Design and demonstration of an automated cell-based biosensor," *Biosensors and Bioelectronics*, vol. 16, pp. 535–542, Sep. 2001.

[17] G. W. Gross, B. Rhoades, and R. Jordan, "Neuronal networks for biochemical sensing," *Sensors and Actuators B: Chemical*, vol. 6, pp. 1–8, Jan. 1992.

[18] S. M. Potter, "Chapter 4 Distributed processing in cultured neuronal networks," in *Progress in Brain Research*, M. A. L. Nicolelis, Ed. Elsevier, 2001, vol. 130, pp. 49–62.

[19] Y. Jimbo, A. Kawana, P. Parodi, and V. Torre, "The dynamics of a neuronal culture of dissociated cortical neurons of neonatal rats," *Biological Cybernetics*, vol. 83, no. 1, pp. 1–20, Jun. 2000.

[20] G. W. Gross, E. Rieske, G. W. Kreutzberg, and A. Meyer, "A new fixed-array multi-microelectrode system designed for long-term monitoring of extracellular single unit neuronal activity in vitro," *Neuroscience Letters*, vol. 6, no. 2-3, pp. 101–105, Nov. 1977.

[21] G. W. Gross, "Simultaneous Single Unit Recording in vitro with a Photoetched Laser Deinsulated Gold Multimicroelectrode Surface," *IEEE Transactions on Biomedical Engineering*, vol. BME-26, no. 5, pp. 273–279, May 1979.

[22] G. W. Gross, W. Y. Wen, and J. W. Lin, "Transparent indium-tin oxide electrode patterns for extracellular, multisite recording in neuronal cultures," *Journal of Neuroscience Methods*, vol. 15, no. 3, pp. 243–252, Nov. 1985.

[23] A. Gramowski, K. Jgelt, D. G. Weiss, and G. W. Gross, "Substance identification by quantitative characterization of oscillatory activity in murine spinal cord networks on microelectrode arrays," *The European Journal of Neuroscience*, vol. 19, no. 10, pp. 2815–2825, May 2004.

105

[24] "Microelectrode Array (MEA) Manual," 2011. [Online]. Available: www.multichannelsystems.com

[25] F. Heer, W. Franks, A. Blau, S. Taschini, C. Ziegler, A. Hierlemann, and H. Baltes, "CMOS microelectrode array for the monitoring of electrogenic cells," *Biosensors and Bioelectronics*, vol. 20, no. 2, pp. 358–366, Sep. 2004.

[26] Q. Bai and K. Wise, "Single-unit neural recording with active microelectrode arrays," *IEEE Transactions on Biomedical Engineering*, vol. 48, no. 8, pp. 911–920, Aug. 2001.

[27] E. M. Schmidt, J. S. Mcintosh, and M. J. Bak, "Long-term implants of Parylene-C coated microelectrodes," *Medical and Biological Engineering and Computing*, vol. 26, no. 1, pp. 96–101, Jan. 1988.

[28] J. R. Webster, M. A. Burns, D. T. Burke, and C. H. Mastrangelo, "Monolithic Capillary Electrophoresis Device with Integrated Fluorescence Detector," *Analytical Chemistry*, vol. 73, no. 7, pp. 1622–1626, Apr. 2001.

[29] S. Takeuchi, D. Ziegler, Y. Yoshida, K. Mabuchi, and T. Suzuki, "Parylene flexible neural probes integrated with microfluidic channels," *Lab on a Chip*, vol. 5, no. 5, pp. 519–523, May 2005.

[30] W. Li, D. Rodger, J. Weiland, M. Humayun, and Y. Tai, "Integrated flexible ocular coil for power and data transfer in retinal prostheses," vol. 1, 2005, pp. 1028–1031.

[31] A. J. Spence, K. B. Neeves, D. Murphy, S. Sponberg, B. R. Land, R. R. Hoy, and M. S. Isaacson, "Flexible multielectrodes can resolve multiple muscles in an insect appendage," *Journal of Neuroscience Methods*, vol. 159, no. 1, pp. 116–124, Jan. 2007.

[32] S. Kim, R. Bhandari, M. Klein, S. Negi, L. Rieth, P. Tathireddy, M. Toepper, H. Oppermann, and F. Solzbacher, "Integrated wireless neural interface based on the Utah electrode array," *Biomedical Microdevices*, vol. 11, no. 2, pp. 453–466, Apr. 2009.

[33] G. E. Loeb, M. J. Bak, M. Salcman, and E. M. Schmidt, "Parylene as a chronically stable, reproducible microelectrode insulator," *IEEE transactions on bio-medical engineering*, vol. 24, no. 2, pp. 121–128, Mar. 1977.

[34] J. E. Hansen, K. Osakada, and M. J. Myers, "Container and method of making container from polyethylene naphthalate and copolymers thereof," USA Patent US5 780 130 A, 1998.

[35] E. Lewis, "Using electronic circuits to model simple neuroelectric interactions," *Proceedings of the IEEE*, vol. 56, no. 6, pp. 931–949, Jun. 1968.

[36] Z. F. Mainen, J. Joerges, J. R. Huguenard, and T. J. Sejnowski, "A model of spike initiation in neocortical pyramidal neurons," *Neuron*, vol. 15, no. 6, pp. 1427–1439, Dec. 1995.

106

[37] H. Haug, "Brain sizes, surfaces, and neuronal sizes of the cortex cerebri: A stereological investigation of man and his variability and a comparison with some mammals (primates, whales, marsupials, insectivores, and one elephant)," *American Journal of Anatomy*, vol. 180, no. 2, pp. 126–142, Oct. 1987.

[38] R. Lind, P. Connolly, C. D. W. Wilkinson, and R. D. Thomson, "Finite-element analysis applied to extracellular microelectrode design," *Sensors and Actuators B: Chemical*, vol. 3, no. 1, pp. 23–30, Jan. 1991.

[39] C. Moulin, A. Gliere, D. Barbier, S. Joucla, B. Yvert, P. Mailley, and R. Guillemaud, "A New 3-D Finite-Element Model Based on Thin-Film Approximation for Microelectrode Array Recording of Extracellular Action Potential," *IEEE Transactions on Biomedical Engineering*, vol. 55, no. 2, pp. 683–692, Feb. 2008.

[40] S. F. Cogan, "Neural Stimulation and Recording Electrodes," *Annual Review of Biomedical Engineering*, vol. 10, no. 1, pp. 275–309, 2008.

[41] L. Giovangrandi, K. H. Gilchrist, R. H. Whittington, and G. T.A. Kovacs, "Low-cost microelectrode array with integrated heater for extracellular recording of cardiomyocyte cultures using commercial flexible printed circuit technology," *Sensors and Actuators B: Chemical*, vol. 113, no. 1, pp. 545–554, Jan. 2006.

[42] D. Robinson, "The electrical properties of metal microelectrodes," *Proceedings of the IEEE*, vol. 56, no. 6, pp. 1065–1071, Jun. 1968.

[43] J. P. Seymour, N. B. Langhals, D. J. Anderson, and D. R. Kipke, "Novel multi-sided, microelectrode arrays for implantable neural applications," *Biomedical Microdevices*, vol. 13, no. 3, pp. 441–451, Jun. 2011.

[44] M. L. Roy and T. Narahashi, "Differential properties of tetrodotoxin-sensitive and tetrodotoxin-resistant sodium channels in rat dorsal root ganglion neurons," *The Journal of Neuroscience: The Official Journal of the Society for Neuroscience*, vol. 12, no. 6, pp. 2104–2111, Jun. 1992.

[45] T. Y. Chang, V. G. Yadav, S. De Leo, A. Mohedas, B. Rajalingam, C.-L. Chen, S. Selvarasah, M. R. Dokmeci, and A. Khademhosseini, "Cell and Protein Compatibility of Parylene-C Surfaces," *Langmuir*, vol. 23, no. 23, pp. 11 718–11 725, Nov. 2007.

[46] J. S. Song, S. Lee, S. H. Jung, G. C. Cha, and M. S. Mun, "Improved biocompatibility of parylene-C films prepared by chemical vapor deposition and the subsequent plasma treatment," *Journal of Applied Polymer Science*, vol. 112, no. 6, pp. 3677–3685, Jun. 2009.

[47] A. L. Lublin and S. Gandy, "Amyloid-beta oligomers: possible roles as key neurotoxins in Alzheimer's Disease," *The Mount Sinai Journal of Medicine, New York*, vol. 77, no. 1, pp. 43–49, Feb. 2010.

[48] I. Benilova, E. Karran, and B. De Strooper, "The toxic Aβ oligomer and Alzheimer's disease: an emperor in need of clothes," *Nature Neuroscience*, vol. 15, no. 3, pp. 349–357, Mar. 2012.

107

[49] L. N. Zhao, H. Long, Y. Mu, and L. Y. Chew, "The Toxicity of Amyloid β Oligomers," *International Journal of Molecular Sciences*, vol. 13, no. 6, pp. 7303–7327, 2012.

[50] J. Gotz, A. Eckert, M. Matamales, L. M. Ittner, and X. Liu, "Modes of Aβ toxicity in Alzheimer's disease," *Cellular and molecular life sciences: CMLS*, vol. 68, no. 20, pp. 3359–3375, Oct. 2011.

[51] M. Citron, "Alzheimer's disease: strategies for disease modification," *Nature Reviews. Drug Discovery*, vol. 9, no. 5, pp. 387–398, May 2010.

[52] G. Mairet-Coello, J. Courchet, S. Pieraut, V. Courchet, A. Maximov, and F. Polleux, "The CAMKK2-AMPK kinase pathway mediates the synaptotoxic effects of Aβ oligomers through Tau phosphorylation," *Neuron*, vol. 78, no. 1, pp. 94–108, Apr. 2013.

[53] M. Bucciantini, E. Giannoni, F. Chiti, F. Baroni, L. Formigli, J. Zurdo, N. Taddei, G. Ramponi, C. M. Dobson, and M. Stefani, "Inherent toxicity of aggregates implies a common mechanism for protein misfolding diseases," *Nature*, vol. 416, no. 6880, pp. 507–511, Apr. 2002.

[54] M. D. Kirkitadze, G. Bitan, and D. B. Teplow, "Paradigm shifts in Alzheimer's disease and other neurodegenerative disorders: the emerging role of oligomeric assemblies," *Journal of Neuroscience Research*, vol. 69, no. 5, pp. 567–577, Sep. 2002.

[55] M. J. Rowan, I. Klyubin, W. K. Cullen, and R. Anwyl, "Synaptic plasticity in animal models of early Alzheimer's disease." *Philosophical Transactions of the Royal Society B: Biological Sciences*, vol. 358, no. 1432, pp. 821–828, Apr. 2003.

[56] J. M. Alarcon, J. A. Brito, T. Hermosilla, I. Atwater, D. Mears, and E. Rojas, "Ion channel formation by Alzheimer's disease amyloid β-peptide (Aβ40) in unilamellar liposomes is determined by anionic phospholipids," *Peptides*, vol. 27, no. 1, pp. 95–104, Jan. 2006.

[57] A. Nunomura, T. Tamaoki, K. Tanaka, N. Motohashi, M. Nakamura, T. Hayashi, H. Yamaguchi, S. Shimohama, H.-g. Lee, X. Zhu, M. A. Smith, and G. Perry, "Intra-neuronal amyloid β accumulation and oxidative damage to nucleic acids in Alzheimer disease," *Neurobiology of Disease*, vol. 37, no. 3, pp. 731–737, Mar. 2010.

[58] M. E. Seward, E. Swanson, A. Norambuena, A. Reimann, J. N. Cochran, R. Li, E. D. Roberson, and G. S. Bloom, "Amyloid-β signals through tau to drive ectopic neuronal cell cycle re-entry in Alzheimer's disease," *Journal of Cell Science*, vol. 126, no. Pt 5, pp. 1278–1286, Mar. 2013.

[59] C. Lazzari, M. J. Kipanyula, M. Agostini, T. Pozzan, and C. Fasolato, "Aβ42 oligomers selectively disrupt neuronal calcium release," *Neurobiology of Aging*, vol. 36, no. 2, pp. 877–885, Oct. 2014.

[60] A. Eckert, S. Hauptmann, I. Scherping, J. Meinhardt, V. Rhein, S. Drse, U. Brandt, M. Fndrich, W. E. Mller, and J. Gtz, "Oligomeric and fibrillar species of β-amyloid (Aβ42) both impair mitochondrial function in P301l tau transgenic mice," *Journal of Molecular Medicine*, vol. 86, no. 11, pp. 1255–1267, Nov. 2008.

108

[61] X. Cheng, J. Wu, M. Geng, and J. Xiong, "The role of synaptic activity in the regulation of amyloid beta levels in Alzheimer's disease," *Neurobiology of Aging*, vol. 35, no. 6, pp. 1217–1232, Jun. 2014.

[62] L. Mucke and D. J. Selkoe, "Neurotoxicity of Amyloid β-Protein: Synaptic and Network Dysfunction," *Cold Spring Harbor Perspectives in Medicine*, vol. 2, no. 7, Jul. 2012.

[63] Y. Deng, Z. Xiong, P. Chen, J. Wei, S. Chen, and Z. Yan, "β-Amyloid impairs the regulation of N-methyl-D-aspartate receptors by glycogen synthase kinase 3," *Neurobiology of Aging*, vol. 35, no. 3, pp. 449–459, Mar. 2014.

[64] I. L. Ferreira, L. M. Bajouco, S. I. Mota, Y. P. Auberson, C. R. Oliveira, and A. C. Rego, "Amyloid beta peptide 1-42 disturbs intracellular calcium homeostasis through activation of GluN2b-containing N-methyl-d-aspartate receptors in cortical cultures," *Cell Calcium*, vol. 51, no. 2, pp. 95–106, Feb. 2012.

[65] L. Texido, M. Martn-Satu, E. Alberdi, C. Solsona, and C. Matute, "Amyloid β peptide oligomers directly activate NMDA receptors," *Cell Calcium*, vol. 49, no. 3, pp. 184–190, Mar. 2011.

[66] G. Yamin, "NMDA receptor-dependent signaling pathways that underlie amyloid beta-protein disruption of LTP in the hippocampus," *Journal of Neuroscience Research*, vol. 87, no. 8, pp. 1729–1736, Jun. 2009.

[67] L. Gravitz, "Drugs: A tangled web of targets," *Nature*, vol. 475, no. 7355, pp. S9–S11, Jul. 2011.

[68] G. McColl, B. R. Roberts, T. L. Pukala, V. B. Kenche, C. M. Roberts, C. D. Link, T. M. Ryan, C. L. Masters, K. J. Barnham, A. I. Bush, and R. A. Cherny, "Utility of an improved model of amyloid-beta (Aβ 1-42) toxicity in Caenorhabditis elegans for drug screening for Alzheimer's disease," *Molecular Neurodegeneration*, vol. 7, p. 57, Nov. 2012.

[69] D. M. Wilcock, "The usefulness and challenges of transgenic mouse models in the study of Alzheimer's disease," *CNS & neurological disorders drug targets*, vol. 9, no. 4, pp. 386–394, Aug. 2010.

[70] G. J. Harry, M. Billingsley, A. Bruinink, I. L. Campbell, W. Classen, D. C. Dorman, C. Galli, D. Ray, R. A. Smith, and H. A. Tilson, "In vitro techniques for the assessment of neurotoxicity." *Environmental Health Perspectives*, vol. 106, no. Suppl 1, pp. 131–158, Feb. 1998.

[71] S. J. Haugabook, D. M. Yager, E. A. Eckman, T. E. Golde, S. G. Younkin, and C. B. Eckman, "High throughput screens for the identification of compounds that alter the accumulation of the Alzheimer's amyloid beta peptide (Aβ)," *Journal of Neuroscience Methods*, vol. 108, no. 2, pp. 171–179, Jul. 2001.

[72] N. Yahata, M. Asai, S. Kitaoka, K. Takahashi, I. Asaka, H. Hioki, T. Kaneko, K. Maruyama, T. C. Saido, T. Nakahata, T. Asada, S. Yamanaka, N. Iwata, and

H. Inoue, "Anti-Aβ Drug Screening Platform Using Human iPS Cell-Derived Neurons for the Treatment of Alzheimer's Disease," *PLoS ONE*, vol. 6, no. 9, p. e25788, Sep. 2011.

[73] A. Tamburri, A. Dudilot, S. Licea, C. Bourgeois, and J. Boehm, "NMDA-Receptor Activation but Not Ion Flux Is Required for Amyloid-Beta Induced Synaptic Depression," *PLoS ONE*, vol. 8, no. 6, p. e65350, Jun. 2013.

[74] A. F. M. Johnstone, G. W. Gross, D. G. Weiss, O. H. U. Schroeder, A. Gramowski, and T. J. Shafer, "Microelectrode arrays: A physiologically based neurotoxicity testing platform for the 21st century," *NeuroToxicology*, vol. 31, no. 4, pp. 331–350, Aug. 2010.

[75] S. I. Morefield, E. W. Keefer, K. D. Chapman, and G. W. Gross, "Drug evaluations using neuronal networks cultured on microelectrode arrays," *Biosensors and Bioelectronics*, vol. 15, pp. 383–396, Oct. 2000.

[76] G. Xiang, L. Pan, L. Huang, Z. Yu, X. Song, J. Cheng, W. Xing, and Y. Zhou, "Microelectrode array-based system for neuropharmacological applications with cortical neurons cultured in vitro," *Biosensors and Bioelectronics*, vol. 22, no. 11, pp. 2478–2484, May 2007.

[77] H. Charkhkar, C. Frewin, M. Nezafati, G. L. Knaack, N. Peixoto, S. E. Saddow, and J. J. Pancrazio, "Use of cortical neuronal networks for in vitro material biocompatibility testing," *Biosensors and Bioelectronics*, vol. 53, pp. 316–323, Mar. 2014.

[78] D. J. Bakkum, Z. C. Chao, and S. M. Potter, "Long-Term Activity-Dependent Plasticity of Action Potential Propagation Delay and Amplitude in Cortical Networks," *PLoS ONE*, vol. 3, no. 5, p. e2088, May 2008.

[79] F. Hamilton, T. Berry, N. Peixoto, and T. Sauer, "Real-time tracking of neuronal network structure using data assimilation," *Physical Review E*, vol. 88, no. 5, p. 052715, Nov. 2013.

[80] D. A. Wagenaar, R. Madhavan, J. Pine, and S. M. Potter, "Controlling Bursting in Cortical Cultures with Closed-Loop Multi-Electrode Stimulation," *The Journal of Neuroscience*, vol. 25, no. 3, pp. 680–688, Jan. 2005.

[81] A. Novellino, B. Scelfo, T. Palosaari, A. Price, T. Sobanski, T. J. Shafer, A. F. M. Johnstone, G. W. Gross, A. Gramowski, O. Schroeder, K. Jgelt, M. Chiappalone, F. Benfenati, S. Martinoia, M. T. Tedesco, E. Defranchi, P. D'Angelo, and M. Whelan, "Development of micro-electrode array based tests for neurotoxicity: assessment of interlaboratory reproducibility with neuroactive chemicals," *Frontiers in Neuroengineering*, vol. 4, p. 4, 2011.

[82] S. Barghorn, V. Nimmrich, A. Striebinger, C. Krantz, P. Keller, B. Janson, M. Bahr, M. Schmidt, R. S. Bitner, J. Harlan, E. Barlow, U. Ebert, and H. Hillen, "Globular amyloid beta-peptide oligomer - a homogenous and stable neuropathological protein in Alzheimer's disease," *Journal of Neurochemistry*, vol. 95, no. 3, pp. 834–847, Nov. 2005.

[83] E. G. Matveeva, A. Rudolph, J. R. Moll, and R. B. Thompson, "Structure-Selective Anisotropy Assay for Amyloid Beta Oligomers," *ACS Chemical Neuroscience*, vol. 3, no. 11, pp. 982–987, Nov. 2012.

[84] R. C. Davis, I. T. Marsden, M. T. Maloney, L. S. Minamide, M. Podlisny, D. J. Selkoe, and J. R. Bamburg, "Amyloid beta dimers/trimers potently induce cofilin-actin rods that are inhibited by maintaining cofilin-phosphorylation," *Molecular Neurodegeneration*, vol. 6, p. 10, 2011.

[85] G. L. Knaack, H. Charkhkar, F. W. Hamilton, N. Peixoto, T. J. O'Shaughnessy, and J. J. Pancrazio, "Differential responses to ω-agatoxin IVA in murine frontal cortex and spinal cord derived neuronal networks," *NeuroToxicology*, vol. 37, pp. 19–25, Jul. 2013.

[86] T. J. Shafer, S. O. Rijal, and G. W. Gross, "Complete inhibition of spontaneous activity in neuronal networks in vitro by deltamethrin and permethrin," *Neurotoxicology*, vol. 29, no. 2, pp. 203–212, Mar. 2008.

[87] K. Varghese, P. Molnar, M. Das, N. Bhargava, S. Lambert, M. S. Kindy, and J. J. Hickman, "A New Target for Amyloid Beta Toxicity Validated by Standard and High-Throughput Electrophysiology," *PLoS ONE*, vol. 5, no. 1, p. e8643, Jan. 2010.

[88] M. Chiappalone, M. Bove, A. Vato, M. Tedesco, and S. Martinoia, "Dissociated cortical networks show spontaneously correlated activity patterns during in vitro development," *Brain Research*, vol. 1093, no. 1, pp. 41–53, Jun. 2006.

[89] S. A. Lipton, "Paradigm shift in neuroprotection by NMDA receptor blockade: Memantine and beyond," *Nature Reviews Drug Discovery*, vol. 5, no. 2, pp. 160–170, Feb. 2006.

[90] R. Netzer and H. Bigalke, "Memantine reduces repetitive action potential firing in spinal cord nerve cell cultures," *European Journal of Pharmacology*, vol. 186, no. 2-3, pp. 149–155, Sep. 1990.

[91] I. Kuperstein, K. Broersen, I. Benilova, J. Rozenski, W. Jonckheere, M. Debulpaep, A. Vandersteen, I. Segers-Nolten, K. Van Der Werf, V. Subramaniam, D. Braeken, G. Callewaert, C. Bartic, R. D'Hooge, I. C. Martins, F. Rousseau, J. Schymkowitz, and B. De Strooper, "Neurotoxicity of Alzheimer's disease Aβ peptides is induced by small changes in the Aβ42 to Aβ40 ratio," *The EMBO journal*, vol. 29, no. 19, pp. 3408–3420, Oct. 2010.

[92] K. Murakami, T. Shimizu, and K. Irie, "Formation of the 42-mer Amyloid β Radical and the Therapeutic Role of Superoxide Dismutase in Alzheimer's Disease." *Journal of Amino Acids*, vol. 2011, p. e654207, Jan. 2011.

[93] R. Roychaudhuri, M. Yang, M. M. Hoshi, and D. B. Teplow, "Amyloid β-Protein Assembly and Alzheimer Disease," *Journal of Biological Chemistry*, vol. 284, no. 8, pp. 4749–4753, Feb. 2009.

111

[94] K. Ono, M. M. Condron, and D. B. Teplow, "Structure-neurotoxicity relationships of amyloid β-protein oligomers," *Proceedings of the National Academy of Sciences of the United States of America*, vol. 106, no. 35, pp. 14 745–14 750, Sep. 2009.

[95] M. Sakono and T. Zako, "Amyloid oligomers: formation and toxicity of Aβ oligomers," *The FEBS journal*, vol. 277, no. 6, pp. 1348–1358, Mar. 2010.

[96] J. Hardy and D. J. Selkoe, "The Amyloid Hypothesis of Alzheimer's Disease: Progress and Problems on the Road to Therapeutics," *Science*, vol. 297, no. 5580, pp. 353–356, Jul. 2002.

[97] D. J. Selkoe, "Alzheimer's Disease Is a Synaptic Failure," *Science*, vol. 298, no. 5594, pp. 789–791, Oct. 2002.

[98] D. M. Walsh, I. Klyubin, J. V. Fadeeva, W. K. Cullen, R. Anwyl, M. S. Wolfe, M. J. Rowan, and D. J. Selkoe, "Naturally secreted oligomers of amyloid beta protein potently inhibit hippocampal long-term potentiation in vivo," *Nature*, vol. 416, no. 6880, pp. 535–539, Apr. 2002.

[99] P. Gortz, J. Opatz, M. Siebler, S. A. Funke, D. Willbold, and C. Lange-Asschenfeldt, "Transient reduction of spontaneous neuronal network activity by sublethal amyloid beta (1-42) peptide concentrations," *Journal of Neural Transmission (Vienna, Austria: 1996)*, vol. 116, no. 3, pp. 351–355, Mar. 2009.

[100] E. K. Ludmil Kirazov, "Amyloid Beta 1-42 Monomers but not High Oligomers Induce an Inhibition of Electrical Activity of Cultured Neuronal Network," *Comptes rendus de l'Academie Bulgare des Sciences*, vol. 63, no. 7, pp. 1023–1028, 2010.

[101] K. Parameshwaran, C. Sims, P. Kanju, T. Vaithianathan, B. C. Shonesy, M. Dhanasekaran, B. A. Bahr, and V. Suppiramaniam, "Amyloid beta-peptide Aβ(1-42) but not Aβ(1-40) attenuates synaptic AMPA receptor function," *Synapse (New York, N.Y.)*, vol. 61, no. 6, pp. 367–374, Jun. 2007.

[102] T. Gura, "Hope in Alzheimer's fight emerges from unexpected places," *Nature Medicine*, vol. 14, no. 9, pp. 894–894, Sep. 2008.

[103] S. N. Ozudogru and C. F. Lippa, "Disease modifying drugs targeting β-amyloid," *American Journal of Alzheimer's Disease and Other Dementias*, vol. 27, no. 5, pp. 296–300, Aug. 2012.

[104] R. H. Schirmer, H. Adler, M. Pickhardt, and E. Mandelkow, "Lest we forget you — methylene blue," *Neurobiology of Aging*, vol. 32, no. 12, pp. 2325.e7–2325.e16, Dec. 2011.

[105] R. McShane, A. Areosa Sastre, and N. Minakaran, "Memantine for dementia," *The Cochrane Database of Systematic Reviews*, no. 2, p. 3154, 2006.

[106] W. Danysz and C. G. Parsons, "Alzheimer's disease, β-amyloid, glutamate, NMDA receptors and memantine - searching for the connections," *British Journal of Pharmacology*, vol. 167, no. 2, pp. 324–352, 2012.

[107] M. Hu, M. E. Schurdak, P. S. Puttfarcken, R. El Kouhen, M. Gopalakrishnan, and J. Li, "High content screen microscopy analysis of A beta 1-42-induced neurite outgrowth reduction in rat primary cortical neurons: neuroprotective effects of alpha 7 neuronal nicotinic acetylcholine receptor ligands," *Brain Research*, vol. 1151, pp. 227–235, Jun. 2007.

[108] M. S. Song, G. Rauw, G. B. Baker, and S. Kar, "Memantine protects rat cortical cultured neurons against beta-amyloid-induced toxicity by attenuating tau phosphorylation," *The European Journal of Neuroscience*, vol. 28, no. 10, pp. 1989–2002, Nov. 2008.

[109] G. P. Eckert, K. Renner, S. H. Eckert, J. Eckmann, S. Hagl, R. M. Abdel-Kader, C. Kurz, K. Leuner, and W. E. Muller, "Mitochondrial Dysfunction-A Pharmacological Target in Alzheimer's Disease," *Molecular Neurobiology*, vol. 46, no. 1, pp. 136–150, Aug. 2012.

[110] A.-L. Lin, E. Poteet, F. Du, R. C. Gourav, R. Liu, Y. Wen, A. Bresnen, S. Huang, P. T. Fox, S.-H. Yang, and T. Q. Duong, "Methylene Blue as a Cerebral Metabolic and Hemodynamic Enhancer," *PLoS ONE*, vol. 7, no. 10, p. e46585, Oct. 2012.

[111] H. Atamna, A. Nguyen, C. Schultz, K. Boyle, J. Newberry, H. Kato, and B. N. Ames, "Methylene blue delays cellular senescence and enhances key mitochondrial biochemical pathways," *The FASEB Journal*, vol. 22, no. 3, pp. 703–712, Mar. 2008.

[112] J. Neugroschl and M. Sano, "An update on treatment and prevention strategies for Alzheimer's disease," *Current Neurology and Neuroscience Reports*, vol. 9, no. 5, pp. 368–376, Sep. 2009.

[113] K. Chiang and E. H. Koo, "Emerging Therapeutics for Alzheimer's Disease," *Annual Review of Pharmacology and Toxicology*, vol. 54, no. 1, pp. 381–405, 2014.

[114] J. M. Nussbaum, S. Schilling, H. Cynis, A. Silva, E. Swanson, T. Wangsanut, K. Tayler, B. Wiltgen, A. Hatami, R. Rnicke, K. Reymann, B. Hutter-Paier, A. Alexandru, W. Jagla, S. Graubner, C. G. Glabe, H.-U. Demuth, and G. S. Bloom, "Prion-like behaviour and tau-dependent cytotoxicity of pyroglutamylated amyloid-β," *Nature*, vol. 485, no. 7400, pp. 651–655, May 2012.

[115] R. A. Quintanilla, P. J. Dolan, Y. N. Jin, and G. V. W. Johnson, "Truncated tau and Aβ cooperatively impair mitochondria in primary neurons," *Neurobiology of Aging*, vol. 33, no. 3, pp. 619.e25–619.e35, Mar. 2012.

[116] T. Hedden, K. R. A. V. Dijk, J. A. Becker, A. Mehta, R. A. Sperling, K. A. Johnson, and R. L. Buckner, "Disruption of Functional Connectivity in Clinically Normal Older Adults Harboring Amyloid Burden," *The Journal of Neuroscience*, vol. 29, no. 40, pp. 12 686–12 694, Oct. 2009.

[117] Y. I. Sheline, M. E. Raichle, A. Z. Snyder, J. C. Morris, D. Head, S. Wang, and M. A. Mintun, "Amyloid Plaques Disrupt Resting State Default Mode Network Connectivity in Cognitively Normal Elderly," *Biological Psychiatry*, vol. 67, no. 6, pp. 584–587, Mar. 2010.

113

[118] E. Biffi, A. Menegon, G. Regalia, S. Maida, G. Ferrigno, and A. Pedrocchi, "A new cross-correlation algorithm for the analysis of in vitro neuronal network activity aimed at pharmacological studies," *Journal of Neuroscience Methods*, vol. 199, no. 2, pp. 321–327, Aug. 2011.

[119] X. Li, W. Zhou, S. Zeng, M. Liu, and Q. Luo, "Long-term recording on multi-electrode array reveals degraded inhibitory connection in neuronal network development," *Biosensors and Bioelectronics*, vol. 22, no. 7, pp. 1538–1543, Feb. 2007.

[120] M. Garofalo, T. Nieus, P. Massobrio, and S. Martinoia, "Evaluation of the Performance of Information Theory-Based Methods and Cross-Correlation to Estimate the Functional Connectivity in Cortical Networks," *PLoS ONE*, vol. 4, no. 8, p. e6482, Aug. 2009.

[121] R. Vicente, M. Wibral, M. Lindner, and G. Pipa, "Transfer entropy–a model-free measure of effective connectivity for the neurosciences," *Journal of Computational Neuroscience*, vol. 30, no. 1, pp. 45–67, Feb. 2011.

[122] S. Ito, M. E. Hansen, R. Heiland, A. Lumsdaine, A. M. Litke, and J. M. Beggs, "Extending Transfer Entropy Improves Identification of Effective Connectivity in a Spiking Cortical Network Model," *PLoS ONE*, vol. 6, no. 11, p. e27431, Nov. 2011.

[123] M. Lungarella, A. Pitti, and Y. Kuniyoshi, "Information transfer at multiple scales," *Physical Review. E, Statistical, Nonlinear, and Soft Matter Physics*, vol. 76, no. 5 Pt 2, p. 056117, Nov. 2007.

[124] E. M. Izhikevich, "Simple model of spiking neurons," *IEEE transactions on neural networks / a publication of the IEEE Neural Networks Council*, vol. 14, no. 6, pp. 1569–1572, 2003.

[125] ——, "Which model to use for cortical spiking neurons?" *IEEE transactions on neural networks / a publication of the IEEE Neural Networks Council*, vol. 15, no. 5, pp. 1063–1070, Sep. 2004.

[126] T. Berry, F. Hamilton, N. Peixoto, and T. Sauer, "Detecting connectivity changes in neuronal networks," *Journal of Neuroscience Methods*, vol. 209, no. 2, pp. 388–397, Aug. 2012.

[127] A. P. Bradley, "The use of the area under the ROC curve in the evaluation of machine learning algorithms," *Pattern Recognition*, vol. 30, no. 7, pp. 1145–1159, Jul. 1997.

[128] E. N. Brown, R. E. Kass, and P. P. Mitra, "Multiple neural spike train data analysis: state-of-the-art and future challenges," *Nature Neuroscience*, vol. 7, no. 5, pp. 456–461, May 2004.

[129] T. D. Y. Kozai, N. B. Langhals, P. R. Patel, X. Deng, H. Zhang, K. L. Smith, J. Lahann, N. A. Kotov, and D. R. Kipke, "Ultrasmall implantable composite microelectrodes with bioactive surfaces for chronic neural interfaces," *Nature Materials*, vol. 11, no. 12, pp. 1065–1073, Dec. 2012.

114

[130] D. Lewitus, K. L. Smith, W. Shain, and J. Kohn, "Ultrafast resorbing polymers for use as carriers for cortical neural probes," *Acta Biomaterialia*, vol. 7, no. 6, pp. 2483–2491, Jun. 2011.

[131] T. Ware, D. Simon, C. Liu, T. Musa, S. Vasudevan, A. Sloan, E. W. Keefer, R. L. Rennaker, and W. Voit, "Thiol-ene/acrylate substrates for softening intracortical electrodes," *Journal of Biomedical Materials Research. Part B, Applied Biomaterials*, vol. 102, no. 1, pp. 1–11, Jan. 2014.

[132] E. Defranchi, A. Novellino, M. Whelan, S. Vogel, T. Ramirez, B. van Ravenzwaay, and R. Landsiedel, "Feasibility Assessment of Micro-Electrode Chip Assay as a Method of Detecting Neurotoxicity in vitro," *Frontiers in Neuroengineering*, vol. 4, p. 6, 2011.

[133] T. J. O'Shaughnessy, S. A. Gray, and J. J. Pancrazio, "Cultured neuronal networks as environmental biosensors," *Journal of Applied Toxicology*, vol. 24, no. 5, pp. 379–385, Sep. 2004.

[134] J. J. Pancrazio, E. W. Keefer, W. Ma, D. A. Stenger, and G. W. Gross, "Neurophysiologic Effects of Chemical Agent Hydrolysis Products on Cortical Neurons In Vitro," *NeuroToxicology*, vol. 22, no. 3, pp. 393–400, Jun. 2001.

[135] E. R. Hascup, K. N. Hascup, M. Stephens, F. Pomerleau, P. Huettl, A. Gratton, and G. A. Gerhardt, "Rapid microelectrode measurements and the origin and regulation of extracellular glutamate in rat prefrontal cortex," *Journal of Neurochemistry*, vol. 115, no. 6, pp. 1608–1620, Dec. 2010.

[136] N. V. Kulagina, T. J. O'Shaughnessy, W. Ma, J. S. Ramsdell, and J. J. Pancrazio, "Pharmacological effects of the marine toxins, brevetoxin and saxitoxin, on murine frontal cortex neuronal networks," *Toxicon*, vol. 44, no. 6, pp. 669–676, Nov. 2004.

[137] J. V. Selinger, J. J. Pancrazio, and G. W. Gross, "Measuring synchronization in neuronal networks for biosensor applications," *Biosensors and Bioelectronics*, vol. 19, no. 7, pp. 675–683, Feb. 2004.

[138] S. Hooper and T. Cameron, "Neurotoxicity screening test for deep brain stimulation leads," *Journal of Biomaterials Science, Polymer Edition*, vol. 18, no. 10, pp. 1309–1320, Jan. 2007.

[139] W. Kern and D. Puotinen, "Cleaning solutions based on hydrogen peroxide for use in silicon semiconductor technology," *RCA Rev.*, vol. 31, pp. 187–206, 1970.

[140] X. Cui and D. Zhou, "Poly (3,4-Ethylenedioxythiophene) for Chronic Neural Stimulation," *IEEE Transactions on Neural Systems and Rehabilitation Engineering*, vol. 15, no. 4, pp. 502–508, Dec. 2007.

[141] D.-H. Kim, J. A. Wiler, D. J. Anderson, D. R. Kipke, and D. C. Martin, "Conducting polymers on hydrogel-coated neural electrode provide sensitive neural recordings in auditory cortex," *Acta Biomaterialia*, vol. 6, no. 1, pp. 57–62, Jan. 2010.

[142] E. R. McConnell, M. A. McClain, J. Ross, W. R. LeFew, and T. J. Shafer, "Evaluation of multi-well microelectrode arrays for neurotoxicity screening using a chemical training set," *NeuroToxicology*, vol. 33, no. 5, pp. 1048–1057, Oct. 2012.

[143] J. J. Pancrazio, G. L. Kamatchi, A. K. Roscoe, and C. Lynch, "Inhibition of neuronal Na+ channels by antidepressant drugs," *The Journal of Pharmacology and Experimental Therapeutics*, vol. 284, no. 1, pp. 208–214, Jan. 1998.

[144] A. R. White, A. I. Bush, K. Beyreuther, C. L. Masters, and R. Cappai, "Exacerbation of copper toxicity in primary neuronal cultures depleted of cellular glutathione," *Journal of Neurochemistry*, vol. 72, no. 5, pp. 2092–2098, May 1999.

[145] D. R. Brown, B. Schmidt, and H. A. Kretzschmar, "Effects of Copper on Survival of Prion Protein Knockout Neurons and Glia," *Journal of Neurochemistry*, vol. 70, no. 4, pp. 1686–1693, Apr. 1998.

[146] J. Kuhn, E. Shaffer, J. Mena, B. Breton, J. Parent, B. Rappaz, M. Chambon, Y. Emery, P. Magistretti, C. Depeursinge, P. Marquet, and G. Turcatti, "Label-Free Cytotoxicity Screening Assay by Digital Holographic Microscopy," *ASSAY and Drug Development Technologies*, vol. 11, no. 2, pp. 101–107, Oct. 2012.

[147] J.-H. Zhang, T. D. Y. Chung, and K. R. Oldenburg, "A Simple Statistical Parameter for Use in Evaluation and Validation of High Throughput Screening Assays," *Journal of Biomolecular Screening*, vol. 4, no. 2, pp. 67–73, Apr. 1999.

[148] J. D. Kralik, D. F. Dimitrov, D. J. Krupa, D. B. Katz, D. Cohen, and M. A. L. Nicolelis, "Techniques for Chronic, Multisite Neuronal Ensemble Recordings in Behaving Animals," *Methods*, vol. 25, no. 2, pp. 121–150, Oct. 2001.

[149] M. A. L. Nicolelis, D. Dimitrov, J. M. Carmena, R. Crist, G. Lehew, J. D. Kralik, and S. P. Wise, "Chronic, multisite, multielectrode recordings in macaque monkeys," *Proceedings of the National Academy of Sciences*, vol. 100, no. 19, pp. 11 041–11 046, Sep. 2003.

[150] A. Prasad, Q.-S. Xue, V. Sankar, T. Nishida, G. Shaw, W. J. Streit, and J. C. Sanchez, "Comprehensive characterization and failure modes of tungsten microwire arrays in chronic neural implants," *Journal of Neural Engineering*, vol. 9, no. 5, p. 056015, Oct. 2012.

[151] E. W. Keefer, B. R. Botterman, M. I. Romero, A. F. Rossi, and G. W. Gross, "Carbon nanotube coating improves neuronal recordings," *Nature Nanotechnology*, vol. 3, no. 7, pp. 434–439, Jul. 2008.

[152] A. R. Harris, S. J. Morgan, J. Chen, R. M. I. Kapsa, G. G. Wallace, and A. G. Paolini, "Conducting polymer coated neural recording electrodes," *Journal of Neural Engineering*, vol. 10, no. 1, p. 016004, Feb. 2013.

[153] R. A. Green, P. B. Matteucci, R. T. Hassarati, B. Giraud, C. W. D. Dodds, S. Chen, P. J. Byrnes-Preston, G. J. Suaning, L. A. Poole-Warren, and N. H. Lovell, "Performance of conducting polymer electrodes for stimulating neuroprosthetics," *Journal of Neural Engineering*, vol. 10, no. 1, p. 016009, Feb. 2013.

[154] R. Franco, R. Sanchez-Olea, E. M. Reyes-Reyes, and M. I. Panayiotidis, "Environmental toxicity, oxidative stress and apoptosis: Menage a Trois," *Mutation Research/Genetic Toxicology and Environmental Mutagenesis*, vol. 674, pp. 3–22, Mar. 2009.

116

[155] M. Asplund, E. Thaning, J. Lundberg, A. C. Sandberg-Nordqvist, B. Kostyszyn, O. Inganas, and H. v. Holst, "Toxicity evaluation of PEDOT/biomolecular composites intended for neural communication electrodes," *Biomedical Materials*, vol. 4, no. 4, p. 045009, Aug. 2009.

[156] R. M. Miriani, M. Abidian, and D. Kipke, "Cytotoxic analysis of the conducting polymer PEDOT using myocytes," in *30th Annual International Conference of the IEEE Engineering in Medicine and Biology Society, 2008. EMBS 2008*, Aug. 2008, pp. 1841–1844.

[157] X. Luo, C. L. Weaver, D. D. Zhou, R. Greenberg, and X. T. Cui, "Highly stable carbon nanotube doped poly(3,4-ethylenedioxythiophene) for chronic neural stimulation," *Biomaterials*, vol. 32, no. 24, pp. 5551–5557, Aug. 2011.

[158] R. Verma, X. Xu, M. K. Jaiswal, C. Olsen, D. Mears, G. Caretti, and Z. Galdzicki, "In vitro profiling of epigenetic modifications underlying heavy metal toxicity of tungsten-alloy and its components," *Toxicology and Applied Pharmacology*, vol. 253, no. 3, pp. 178–187, Jun. 2011.

[159] E. Patrick, M. E. Orazem, J. C. Sanchez, and T. Nishida, "Corrosion of tungsten microelectrodes used in neural recording applications," *Journal of Neuroscience Methods*, vol. 198, no. 2, pp. 158–171, Jun. 2011.

[160] S. Jain, A. Sharma, and B. Basu, "In vitro cytocompatibility assessment of amorphous carbon structures using neuroblastoma and Schwann cells," *Journal of Biomedical Materials Research Part B: Applied Biomaterials*, vol. 101B, no. 4, pp. 520–531, May 2013.

[161] Q. He, T. Zhang, Y. Yang, and F. Ding, "In vitro biocompatibility of chitosan-based materials to primary culture of hippocampal neurons," *Journal of Materials Science: Materials in Medicine*, vol. 20, no. 7, pp. 1457–1466, Mar. 2009.

[162] G. Bardi, M. A. Malvindi, L. Gherardini, M. Costa, P. P. Pompa, R. Cingolani, and T. Pizzorusso, "The biocompatibility of amino functionalized CdSe/ZnS quantum-dot-Doped SiO2 nanoparticles with primary neural cells and their gene carrying performance," *Biomaterials*, vol. 31, no. 25, pp. 6555–6566, Sep. 2010.

[163] H. Charkhkar, G. L. Knaack, B. E. Gnade, E. W. Keefer, and J. J. Pancrazio, "Development and demonstration of a disposable low-cost microelectrode array for cultured neuronal network recording," *Sensors and Actuators B: Chemical*, vol. 161, no. 1, pp. 655–660, Jan. 2012.

[164] W. Nisch, J. Bck, U. Egert, H. Hmmerle, and A. Mohr, "A thin film microelectrode array for monitoring extracellular neuronal activity in vitro," *Biosensors and Bioelectronics*, vol. 9, no. 9, pp. 737–741, 1994.

[165] M. C. T. Denyer, M. Riehle, S. T. Britland, and A. Offenhauser, "Preliminary study on the suitability of a pharmacological bio-assay based on cardiac myocytes cultured over microfabricated microelectrode arrays," *Medical and Biological Engineering and Computing*, vol. 36, no. 5, pp. 638–644, 1998-09-01.

117

[166] Y. Nam and B. C. Wheeler, "In vitro microelectrode array technology and neural recordings," *Critical reviews in Biomedical Engineering*, vol. 39, no. 1, pp. 45–61, 2011.

[167] T. J. O'Shaughnessy, B. Zim, W. Ma, K. M. Shaffer, D. A. Stenger, K. Zamani, G. W. Gross, and J. J. Pancrazio, "Acute neuropharmacologic action of chloroquine on cortical neurons in vitro," *Brain Research*, vol. 959, no. 2, pp. 280–286, Jan. 2003.

[168] J. Du, I. H. Riedel-Kruse, J. C. Nawroth, M. L. Roukes, G. Laurent, and S. C. Masmanidis, "High-resolution three-dimensional extracellular recording of neuronal activity with microfabricated electrode arrays," *Journal of Neurophysiology*, vol. 101, no. 3, pp. 1671–1678, 2009-03-01.

[169] M. Heim, B. Yvert, and A. Kuhn, "Nanostructuration strategies to enhance micro-electrode array (MEA) performance for neuronal recording and stimulation," *Journal of Physiology-Paris*, vol. 106, no. 3, pp. 137–145, 2012-05.

[170] M. O. Heuschkel, M. Fejtl, M. Raggenbass, D. Bertrand, and P. Renaud, "A three-dimensional multi-electrode array for multi-site stimulation and recording in acute brain slices," *Journal of Neuroscience Methods*, vol. 114, no. 2, pp. 135–148, 2002-03-15.

[171] K. A. Ludwig, J. D. Uram, J. Yang, D. C. Martin, and D. R. Kipke, "Chronic neural recordings using silicon microelectrode arrays electrochemically deposited with a poly(3,4-ethylenedioxythiophene) (PEDOT) film," *Journal of Neural Engineering*, vol. 3, no. 1, pp. 59–70, 2006-03.

[172] E. Ben-Jacob and Y. Hanein, "Carbon nanotube micro-electrodes for neuronal interfacing," *Journal of Materials Chemistry*, vol. 18, no. 43, pp. 5181–5186, Oct. 2008.

[173] G. Cellot, F. M. Toma, Z. K. Varley, J. Laishram, A. Villari, M. Quintana, S. Cipollone, M. Prato, and L. Ballerini, "Carbon nanotube scaffolds tune synaptic strength in cultured neural circuits: novel frontiers in nanomaterial-tissue interactions," *The Journal of Neuroscience*, vol. 31, no. 36, pp. 12 945–12 953, Sep. 2011.

[174] G. Krause, S. Lehmann, M. Lehmann, I. Freund, E. Schreiber, and W. Baumann, "Measurement of electrical activity of long-term mammalian neuronal networks on semiconductor neurosensor chips and comparison with conventional microelectrode arrays," *Biosensors and Bioelectronics*, vol. 21, no. 7, pp. 1272–1282, 2006.

[175] P. S. Mangan and J. Kapur, "Factors underlying bursting behavior in a network of cultured hippocampal neurons exposed to zero magnesium," *Journal of Neurophysiology*, vol. 91, no. 2, pp. 946–957, 2004-02-01.

[176] S. Chen, W. Pei, Q. Gui, R. Tang, Y. Chen, S. Zhao, H. Wang, and H. Chen, "PEDOT/MWCNT composite film coated microelectrode arrays for neural interface improvement," *Sensors and Actuators A: Physical*, vol. 193, pp. 141–148, 2013-04-15.

[177] R. Gerwig, K. Fuchsberger, B. Schroeppel, G. S. Link, G. Heusel, U. Kraushaar, W. Schuhmann, A. Stett, and M. Stelzle, "PEDOT-CNT composite microelectrodes

118

for recording and electrostimulation applications: Fabrication, morphology, and electrical properties," *Frontiers in Neuroengineering*, vol. 5, 2012-05-04.

[178] A. Stett, U. Egert, E. Guenther, F. Hofmann, T. Meyer, W. Nisch, and H. Haemmerle, "Biological application of microelectrode arrays in drug discovery and basic research," *Analytical and Bioanalytical Chemistry*, vol. 377, no. 3, pp. 486–495, 2003-10-01.

[179] G. Cellot, E. Cilia, S. Cipollone, V. Rancic, A. Sucapane, S. Giordani, L. Gambazzi, H. Markram, M. Grandolfo, D. Scaini, F. Gelain, L. Casalis, M. Prato, M. Giugliano, and L. Ballerini, "Carbon nanotubes might improve neuronal performance by favouring electrical shortcuts," *Nature Nanotechnology*, vol. 4, no. 2, pp. 126–133, Feb. 2009.

[180] A. Mazzatenta, M. Giugliano, S. Campidelli, L. Gambazzi, L. Businaro, H. Markram, M. Prato, and L. Ballerini, "Interfacing neurons with carbon nanotubes: Electrical signal transfer and synaptic stimulation in cultured brain circuits," *The Journal of Neuroscience*, vol. 27, no. 26, pp. 6931–6936, Jun. 2007.

[181] G. Baranauskas, E. Maggiolini, E. Castagnola, A. Ansaldo, A. Mazzoni, G. N. Angotzi, A. Vato, D. Ricci, S. Panzeri, and L. Fadiga, "Carbon nanotube composite coating of neural microelectrodes preferentially improves the multiunit signal-to-noise ratio," *Journal of Neural Engineering*, vol. 8, no. 6, p. 066013, Oct. 2011.

[182] M. R. Abidian, J. M. Corey, D. R. Kipke, and D. C. Martin, "Conducting-polymer nanotubes improve electrical properties, mechanical adhesion, neural attachment, and neurite outgrowth of neural electrodes," *Small*, vol. 6, no. 3, pp. 421–429, 2010.

[183] M. R. Abidian, K. A. Ludwig, T. C. Marzullo, D. C. Martin, and D. R. Kipke, "Interfacing Conducting Polymer Nanotubes with the Central Nervous System: Chronic Neural Recording using Poly(3,4-ethylenedioxythiophene) Nanotubes," *Advanced Materials*, vol. 21, no. 37, pp. 3764–3770, Oct. 2009.

[184] M. v. Gerven, J. Farquhar, R. Schaefer, R. Vlek, J. Geuze, A. Nijholt, N. Ramsey, P. Haselager, L. Vuurpijl, S. Gielen, and P. Desain, "The brain-computer interface cycle," *Journal of Neural Engineering*, vol. 6, no. 4, p. 041001, Aug. 2009.

[185] M. A. Lebedev and M. A. L. Nicolelis, "Brain-machine interfaces: past, present and future," *Trends in Neurosciences*, vol. 29, no. 9, pp. 536–546, Jan. 2006.

[186] A. B. Schwartz, X. T. Cui, D. J. Weber, and D. W. Moran, "Brain-Controlled Interfaces: Movement Restoration with Neural Prosthetics," *Neuron*, vol. 52, no. 1, pp. 205–220, May 2006.

[187] K. Najafi, J. Ji, and K. Wise, "Scaling limitations of silicon multichannel recording probes," *IEEE Transactions on Biomedical Engineering*, vol. 37, no. 1, pp. 1–11, Jan. 1990.

[188] X. Cui and D. C. Martin, "Electrochemical deposition and characterization of poly(3,4-ethylenedioxythiophene) on neural microelectrode arrays," *Sensors and Actuators B: Chemical*, vol. 89, no. 12, pp. 92–102, Mar. 2003.

119

[189] S. M. Richardson-Burns, J. L. Hendricks, B. Foster, L. K. Povlich, D.-H. Kim, and D. C. Martin, "Polymerization of the conducting polymer poly(3,4-ethylenedioxythiophene) (PEDOT) around living neural cells," *Biomaterials*, vol. 28, no. 8, pp. 1539–1552, Mar. 2007.

[190] M. R. Abidian and D. C. Martin, "Multifunctional Nanobiomaterials for Neural Interfaces," *Advanced Functional Materials*, vol. 19, no. 4, pp. 573–585, Feb. 2009.

[191] U. A. Aregueta-Robles, A. J. Woolley, L. A. Poole-Warren, N. H. Lovell, and R. A. Green, "Organic electrode coatings for next-generation neural interfaces," *Frontiers in Neuroengineering*, vol. 7, May 2014.

[192] H. Yamato, M. Ohwa, and W. Wernet, "Stability of polypyrrole and poly(3,4-ethylenedioxythiophene) for biosensor application," *Journal of Electroanalytical Chemistry*, vol. 397, no. 12, pp. 163–170, Nov. 1995.

[193] R. A. Green, N. H. Lovell, G. G. Wallace, and L. A. Poole-Warren, "Conducting polymers for neural interfaces: Challenges in developing an effective long-term implant," *Biomaterials*, vol. 29, no. 2425, pp. 3393–3399, Aug. 2008.

[194] K. A. Ludwig, N. B. Langhals, M. D. Joseph, S. M. Richardson-Burns, J. L. Hendricks, and D. R. Kipke, "Poly(3,4-ethylenedioxythiophene) (PEDOT) polymer coatings facilitate smaller neural recording electrodes," *Journal of Neural Engineering*, vol. 8, no. 1, p. 014001, Feb. 2011.

[195] S. Venkatraman, J. Hendricks, Z. King, A. Sereno, S. Richardson-Burns, D. Martin, and J. Carmena, "In Vitro and In Vivo Evaluation of PEDOT Microelectrodes for Neural Stimulation and Recording," *IEEE Transactions on Neural Systems and Rehabilitation Engineering*, vol. 19, no. 3, pp. 307–316, Jun. 2011.

[196] Z. A. King, C. M. Shaw, S. A. Spanninga, and D. C. Martin, "Structural, chemical and electrochemical characterization of poly(3,4-Ethylenedioxythiophene) (PEDOT) prepared with various counter-ions and heat treatments," *Polymer*, vol. 52, no. 5, pp. 1302–1308, Mar. 2011.

[197] J. Yang and D. C. Martin, "Microporous conducting polymers on neural microelectrode arrays: II. Physical characterization," *Sensors and Actuators A: Physical*, vol. 113, no. 2, pp. 204–211, Jul. 2004.

[198] T. Nyberg, O. Ingans, and H. Jerregrd, "Polymer Hydrogel Microelectrodes for Neural Communication," *Biomedical Microdevices*, vol. 4, no. 1, pp. 43–52, Mar. 2002.

[199] Y. P. Kayinamura, M. Ovadia, D. Zavitz, and J. F. Rubinson, "Investigation of Near Ohmic Behavior for Poly(3,4-ethylenedioxythiophene): A Model Consistent with Systematic Variations in Polymerization Conditions," *ACS Applied Materials & Interfaces*, vol. 2, no. 9, pp. 2653–2662, Sep. 2010.

[200] H. S. Mandal, G. L. Knaack, H. Charkhkar, D. G. McHail, J. S. Kastee, T. C. Dumas, N. Peixoto, J. F. Rubinson, and J. J. Pancrazio, "Improving the performance of poly(3,4-ethylenedioxythiophene) for brain-machine interface applications," *Acta Biomaterialia*, vol. 10, no. 6, pp. 2446–2454, Jun. 2014.

120

[201] K. A. Ludwig, R. M. Miriani, N. B. Langhals, M. D. Joseph, D. J. Anderson, and D. R. Kipke, "Using a Common Average Reference to Improve Cortical Neuron Recordings From Microelectrode Arrays," *Journal of Neurophysiology*, vol. 101, no. 3, pp. 1679–1689, Mar. 2009.

[202] S. Suner, M. Fellows, C. Vargas-Irwin, G. Nakata, and J. Donoghue, "Reliability of signals from a chronically implanted, silicon-based electrode array in non-human primate primary motor cortex," *IEEE Transactions on Neural Systems and Rehabilitation Engineering*, vol. 13, no. 4, pp. 524–541, Dec. 2005.

[203] X. Cui and D. C. Martin, "Fuzzy gold electrodes for lowering impedance and improving adhesion with electrodeposited conducting polymer films," *Sensors and Actuators A: Physical*, vol. 103, no. 3, pp. 384–394, Feb. 2003.

[204] Y. Xiao, X. Cui, and D. C. Martin, "Electrochemical polymerization and properties of PEDOT/S-EDOT on neural microelectrode arrays," *Journal of Electroanalytical Chemistry*, vol. 573, no. 1, pp. 43–48, Nov. 2004.

[205] D. H. Szarowski, M. D. Andersen, S. Retterer, A. J. Spence, M. Isaacson, H. G. Craighead, J. N. Turner, and W. Shain, "Brain responses to micro-machined silicon devices," *Brain Research*, vol. 983, no. 12, pp. 23–35, Sep. 2003.

[206] Z. Yang, Q. Zhao, E. Keefer, W. Liu, Y. Bengio, D. Schuurmans, J. Lafferty, C. Williams, and A. Culotta, "Noise characterization, modeling, and reduction for in vivo neural recording," in *Advances in Neural Information Processing Systems 22*, 2009, pp. 2160–2168.

[207] R. J. Vetter, J. C. Williams, J. F. Hetke, E. A. Nunamaker, and D. R. Kipke, "Chronic neural recording using silicon-substrate microelectrode arrays implanted in cerebral cortex," *IEEE Transactions on Biomedical Engineering*, vol. 51, no. 6, pp. 896–904, Jun. 2004.

[208] S. Minnikanti, G. Diao, J. J. Pancrazio, X. Xie, L. Rieth, F. Solzbacher, and N. Peixoto, "Lifetime assessment of atomic-layer-deposited Al_2o_3-Parylene C bilayer coating for neural interfaces using accelerated age testing and electrochemical characterization," *Acta Biomaterialia*, vol. 10, no. 2, pp. 960–967, Feb. 2014.

[209] A. Bozkurt, R. Gilmour, and A. Lal, "In Vivo Electrochemical Characterization of a Tissue-Electrode Interface During Metamorphic Growth," *IEEE Transactions on Biomedical Engineering*, vol. 58, no. 8, pp. 2401–2406, Aug. 2011.

[210] X. Cui, J. Wiler, M. Dzaman, R. A. Altschuler, and D. C. Martin, "In vivo studies of polypyrrole/peptide coated neural probes," *Biomaterials*, vol. 24, no. 5, pp. 777–787, Feb. 2003.

[211] M. Johnson, K. Otto, and D. Kipke, "Repeated voltage biasing improves unit recordings by reducing resistive tissue impedances," *IEEE Transactions on Neural Systems and Rehabilitation Engineering*, vol. 13, no. 2, pp. 160–165, Jun. 2005.

121

[212] G. C. McConnell, R. J. Butera, and R. V. Bellamkonda, "Bioimpedance modeling to monitor astrocytic response to chronically implanted electrodes," *Journal of Neural Engineering*, vol. 6, no. 5, p. 055005, Oct. 2009.

[213] W. Franks, I. Schenker, P. Schmutz, and A. Hierlemann, "Impedance characterization and modeling of electrodes for biomedical applications," *IEEE Transactions on Biomedical Engineering*, vol. 52, no. 7, pp. 1295–1302, Jul. 2005.

[214] Y. Lu, Y. Li, J. Pan, P. Wei, N. Liu, B. Wu, J. Cheng, C. Lu, and L. Wang, "Poly(3,4-ethylenedioxythiophene)/poly(styrenesulfonate)-poly(vinyl alcohol)/poly(acrylic acid) interpenetrating polymer networks for improving optrode-neural tissue interface in optogenetics," *Biomaterials*, vol. 33, no. 2, pp. 378–394, Jan. 2012.

[215] V. S. Polikov, P. A. Tresco, and W. M. Reichert, "Response of brain tissue to chronically implanted neural electrodes," *Journal of Neuroscience Methods*, vol. 148, no. 1, pp. 1–18, Oct. 2005.

[216] M. P. Ward, P. Rajdev, C. Ellison, and P. P. Irazoqui, "Toward a comparison of microelectrodes for acute and chronic recordings," *Brain Research*, vol. 1282, pp. 183–200, Jul. 2009.

[217] S. M. Gutowski, J. T. Shoemaker, K. L. Templeman, Y. Wei, R. A. Latour Jr., R. V. Bellamkonda, M. C. LaPlaca, and A. J. Garca, "Protease-degradable PEG-maleimide coating with on-demand release of IL-1ra to improve tissue response to neural electrodes," *Biomaterials*, vol. 44, pp. 55–70, Mar. 2015.

[218] T. D. Y. Kozai, Z. Gugel, X. Li, P. J. Gilgunn, R. Khilwani, O. B. Ozdoganlar, G. K. Fedder, D. J. Weber, and X. T. Cui, "Chronic tissue response to carboxymethyl cellulose based dissolvable insertion needle for ultra-small neural probes," *Biomaterials*, vol. 35, no. 34, pp. 9255–9268, Nov. 2014.

[219] J. K. Nguyen, D. J. Park, J. L. Skousen, A. E. Hess-Dunning, D. J. Tyler, S. J. Rowan, C. Weder, and J. R. Capadona, "Mechanically-compliant intracortical implants reduce the neuroinflammatory response," *Journal of Neural Engineering*, vol. 11, no. 5, p. 056014, Oct. 2014.

[220] H. S. Mandal, J. S. Kastee, D. G. McHail, J. F. Rubinson, J. J. Pancrazio, and T. C. Dumas, "Improved Poly(3,4-Ethylenedioxythiophene) (PEDOT) for Neural Stimulation," *Neuromodulation: Technology at the Neural Interface*, pp. n/a–n/a, Apr. 2015.

[221] D. C. Martin, J. Wu, C. M. Shaw, Z. King, S. A. Spanninga, S. Richardson-Burns, J. Hendricks, and J. Yang, "The Morphology of Poly(3,4-Ethylenedioxythiophene)," *Polymer Reviews*, vol. 50, no. 3, pp. 340–384, Jul. 2010.

[222] T. Takano, H. Masunaga, A. Fujiwara, H. Okuzaki, and T. Sasaki, "PEDOT Nanocrystal in Highly Conductive PEDOT:PSS Polymer Films," *Macromolecules*, vol. 45, no. 9, pp. 3859–3865, May 2012.

122

Curriculum Vitae

Hamid Charkhkar received his B.Sc. degree in Electrical and Computer Engineering from Ferdowsi University of Mashhad, Mashhad, Iran. After spending few years working in industry, he started his graduate studies in Department of Electrical and Computer Engineering at George Mason University (GMU) in 2009. He has been a graduate research assistant in Neural Engineering lab at GMU since fall 2010 under the supervision of professor Joseph J. Pancrazio. His research projects include 1) assessing the biocompatibility of advanced materials for brain-computer interface and 2) developing functional neuron-based assays to study the effects of neurotoxins and biomarkers associated with neurodegenerative diseases. In most of the projects during his PhD, he has worked closely with multidisciplinary teams in government, academia, and industry. These include the Food and Drug Administration (FDA), University of Southern Florida, University of Texas at Dallas, Plexon Inc. and Adlyfe Inc.

His peer-reviewed publications during his graduate studies at GMU are:

- **H.Charkhkar**, G.L.Knaack, D.G.McHail, H.S.Mandal, N.Peixoto, J.F.Rubinson, T.C.Dumas, J.J.Pancrazio. Chronic intracortical neural recordings using microelectrode arrays coated with a new variant of PEDOT. Acta Biomaterialia. *Submitted*

- D.M.Simon, **H.Charkhkar**, C.St.John, T.Kang, R.Reit, D. Arreaga-Salas, D.G.McHail, G.L.Knaack, J.Kastee, A.Sloan, D.Grasse, T.C.Dumas, R.Rennaker, W.Voit, J.J.Pancrazio. Long-term cortical recordings from modulus changing polymer probes. *In preparation*

- **H.Charkhkar**, S.Meyyappan, E.Matveeva, D.G. McHail, N.Peixoto, R.O.Cliff, J.J.Pancrazio. Amyloid beta modulation of neuronal network activity *in vitro*. Brain Research. *Under review*

- H.S.Mandal, G.L.Knaack, **H.Charkhkar**, D.G.McHail, J.Kastee, T.C.Dumas, N.Peixoto, J.F.Rubinson, J.J.Pancrazio. Improving the performance of poly(3,4- ethylenedioxythiophene) (PEDOT) for brain machine interface applications. Acta Biomaterialia. 10(6), 2014.

- **H.Charkhkar**, C.Frewin, M.Nezafati, G.L.Knaack, N.Peixoto, S.E.Saddow, J.J.Pancrazio. Use of cortical networks for *in vitro* material biocompatibility testing. Biosensors and Bioelectronics. vol. 53, 2013.

- G.L.Knaack, **H.Charkhkar**, F.W.Hamilton, N.Peixoto, T.J.O'Shaughnessy, J.J.Pancrazio. Differential responses to ω-Agatoxin IVA in murine frontal cortex and spinal cord derived neuronal networks. Neurotoxicology. vol. 37, 2013.

- N.Peixoto, H.G.Nik, **H.Charkhkar**. Voice controlled wheelchairs: Fine control by humming. Computer Methods and Programs in Biomedicine. vol. 112, 2013.

- **H.Charkhkar**, G.L.Knaack, B.E.Gnade, E.W.Keefer, J.J.Pancrazio. Development and demonstration of a disposable low-cost microelectrode array for cultured neuronal network recording. J. Sensors and Actuators. B vol. 161, 2012.

- E.Cohen, A.Agrawal, M.Connors, B.Hansen, **H.Charkhkar**, J.Pfefer. Optical coherence tomography imaging of retinal damage in real-time under a stimulus electrode. Journal of Neural Engineering. vol. 8, 2011.

- **H.Charkhkar**, G.L.Knaack, H.S.Mandal, E.W.Keefer, J.J.Pancrazio. Effects of carbon nanotube and conducting polymer coated microelectrodes on single-unit recordings *in vitro*. Proceedings of 36th Annual International Conference of the IEEE, Engineering in Medicine and Biology Society (EMBC'14), Chicago, IL, Aug. 2014, pp. 469-473.

- F.W.Hamilton, A.Akhavian, G.L.Knaack, **H.Charkhkar**, S.Minnikanti, WJ.Kim, J.S.Kastee, N.Peixoto. Dynamic steering of *in vitro* cortical neurons using field stimulation. Proceedings of 36th Annual International Conference of the IEEE, Engineering in Medicine and Biology Society (EMBC'14), Chicago, IL, Aug. 2014, pp. 6577-6580.